

THESIS FOR THE DEGREE OF DOCTOR OF PHILOSOPHY

**Thermal Modelling and Evaluation of  
Borehole Heat Transfer**

SAQIB JAVED

Building Services Engineering  
Department of Energy and Environment  
CHALMERS UNIVERSITY OF TECHNOLOGY  
Göteborg, Sweden 2012

# **Thermal Modelling and Evaluation of Borehole Heat Transfer**

**Saqib Javed**

© SAQIB JAVED, 2012

ISBN 978-91-7385-623-2

Doktorsavhandlingar vid Chalmers tekniska högskola

Ny serie nr 3304

ISSN 0346-718X

Technical report D2012:01  
Building Services Engineering  
Department of Energy and Environment  
Chalmers University of Technology  
SE-412 96 Göteborg  
Sweden  
Telephone +46 (0)31 772 1000

Printed by  
Chalmers Reproservice  
Göteborg, 2012

# Thermal modelling and evaluation of borehole heat transfer

Saqib Javed  
Building Services Engineering  
Chalmers University of Technology

## Abstract

The use of ground source heat pump systems to provide heating and cooling in buildings has increased greatly in the last decade or so. These systems have a high potential for energy efficiency, which has environmental and economic advantages. Moreover, the energy efficiency of the ground source heat pump systems can be further enhanced by optimizing the performance of the system. However, a key obstacle to the performance optimization of ground source heat pump systems is the scarcity of mathematical models that can rapidly, yet accurately, simulate the dynamic thermal response of the borehole system.

This study aims to develop analytical models and methods that can simulate the thermal response of a borehole system in time scales from minutes to years. An analytical solution to model the short-time response of the borehole system is presented. The solution studies the heat transfer problem in the Laplace domain and provides an exact solution to the radial heat transfer problem in the borehole. A finite-length line-source solution to determine the long-term response of the borehole system is also presented. The line-source solution can be used for modelling both single and multiple borehole systems. The analytical and finite-length line-source solutions were combined to obtain step-response functions for various configurations of borehole systems. The step-response functions are valid from short (hours) to long (years) periods. A load aggregation method is also presented to speed up the simulations of the borehole systems. All the proposed models and methods can be easily implemented in any building energy simulation software to optimize the overall performance of ground source heat pump systems.

The study also analyzes various aspects of the thermal response testing and evaluation of borehole systems. A ground source heat pump test facility with nine boreholes was used for the experimental investigations. Several thermal response tests were conducted for issues that include random variations between tests, sensitivity of system design to uncertainties in test results, convective heat transport in boreholes, and recovery times after a test. The evaluations of multi-injection rate tests on groundwater-filled boreholes were also extensively studied. Recommendations regarding each of these issues are suggested to improve the testing and evaluation procedure of borehole systems.

**Keywords:** ground source heat pump, ground-coupled, ground heat exchanger, borehole, short-term, long-term, step-response, load aggregation, groundwater-filled, fluid temperature, thermal response test, recovery times, design, simulation, optimization

---

This study has been funded by the Swedish Energy Agency through their national research program EFFSYS2 and EFFSYS+ in corporation with our research partners Akademiska Hus, Andersson & Hultmark, Carrier, CTC, Donghua University, Equa Solutions, Fastighetsägarna, Geotec, Grundfos, IFLA, IVT, Lafor, NCC, Nibe, Oklahoma State University, Palne Mogensen, Sweco, Schneider Electric (TAC), SP, Thermia, Uponor, Vänersborgsbostäder, Wilo and ÅF-Infrastruktur.

---

# Acknowledgements

*One can pay back the loan of gold, but one dies forever in debt to those who are kind.*

Malayan Proverb.

Although my name is the only one to appear on the cover of this thesis, I did not make this journey alone. This thesis would not have been possible if it were not for the support and contributions of many individuals and organizations.

I would like to thank my supervisors, Professor Per Fahlén and Professor Johan Claesson, for their unfailing support and guidance. Per, without your thoughtful recommendations and constructive critiques, this thesis would not have been the same. Johan, I am forever indebted to you for your time, expertise and patience.

I am grateful to the Swedish Energy Agency and the participating companies for funding the research and also for their cooperation and valuable insights during the project meetings. I thank Professor Jeffrey Spitler and Professor Richard Beier from Oklahoma State University and Heiko Liebel from the Norwegian University of Science and Technology for their very fruitful research collaborations. I would like to extend my sincere gratitude to Professor Spitler, who has been an unwavering source of support and inspiration throughout this endeavour.

I express my acknowledgements to all my colleagues in the Division of Building Services Engineering. Special thanks to Håkan Larsson, Jan-Olof Dalenbäck, Tommy Sundström and Torbjörn Lindholm. How can I ever thank Katarina Bergkvist enough for helping me with everyday problems at Chalmers? Take a bow Katarina; indeed, take several!

I owe enormous gratitude to my parents for their lifelong tolerance and support. Finally, my greatest appreciation is reserved for my wife, Mona, and my children, Baasil and baby Shanza.

Göteborg, January 2012

*Saqib Javed*



# List of publications

This thesis is based on the following peer-reviewed publications.

- I. Javed, S, Fahlén, P, Claesson, J, 2009. Vertical ground heat exchangers – A review of heat flow models. Proceedings of 11th International Conference on Thermal Energy Storage (Effstock 2009), Stockholm, Sweden.
- II. Javed, S, Claesson, J, 2011. New analytical and numerical solutions for the short-term analysis of vertical ground heat exchangers. ASHRAE Transactions, vol. 117(1), pp. 3-12.
- III. Javed, S, Spitler, J, Fahlén, P, 2011. An experimental investigation of the accuracy of thermal response tests used to measure ground thermal properties. ASHRAE Transactions, vol. 117(1), pp. 13-21.
- IV. Javed, S, Fahlén, P, 2011. Thermal response testing of a multiple borehole ground heat exchanger. International Journal of Low Carbon Technologies, vol. 6(3), pp. 141-148.
- V. Claesson, J, Javed, S, 2011. An analytical method to calculate borehole fluid temperatures for time-scales from minutes to decades. ASHRAE Transactions, vol. 117(2), pp. 279-288.
- VI. Javed, S, Claesson, J, Beier, R, 2011. Recovery times after thermal response tests on vertical borehole heat exchangers. Proceedings of 23rd IIR International Congress of Refrigeration (ICR2011), Prague, Czech Republic.
- VII. Javed, S, Nakos, H, Claesson, J, 2012. A method to evaluate thermal response tests on groundwater-filled boreholes. Accepted for publication in ASHRAE Transactions.

Additional publications not included in this thesis are:

1. Javed, S, Fahlén, P, Holmberg, H, 2009. Modelling for optimization of brine temperature in ground source heat pump systems. Proceedings of 8th International Conference on Sustainable Energy Technologies (SET 2009), Aachen, Germany.
2. Javed, S, Claesson, J, Fahlén, P, 2010. Analytical modelling of short-term response of ground heat exchangers in ground source heat pump systems. Proceedings of 10th REHVA World Congress (Clima 2010), Antalya, Turkey.
3. Javed, S, Fahlén, P, 2010. Development and planned operation of a ground source heat pump test facility. Newsletter IEA heat pump centre, vol. 28(1), pp. 32-35.

4. Javed, S, Fahlén, P, 2010. Thermal response testing of a multiple borehole ground heat exchanger. Proceedings of 9th International Conference on Sustainable Energy Technologies (SET 2010), Shanghai, China.
5. Javed, S, 2010. Design of ground source heat pump systems - Thermal modelling and evaluation of boreholes. Licentiate Thesis, (Chalmers University of Technology.) Sweden.
6. Javed, S, Fahlén, P, 2011. Termisk modellering och utvärdering av borrhållssystem. Energi & Miljö, No. 6-7/11: 51-54.
7. Claesson, J, Javed, S, (Unpublished). A load-aggregation method to calculate extraction temperatures of borehole heat exchangers. Accepted for publication in ASHRAE Transactions.
8. Liebel, H, Javed, S, Vistnes, G, (Unpublished). Multi-injection rate thermal response test with forced convection in a groundwaterfilled borehole in hard rock. Submitted to Renewable Energy.

# Contents

|  | <b>Page</b> |
|--|-------------|
|--|-------------|

|   | <b>Page</b> |
|---|-------------|
| <b>Abstract</b>   | <b>iii</b>  |
| <b>Foreword</b>   | <b>v</b>    |
| <b>List of publications</b>   | <b>vii</b>  |
| <b>Symbols and abbreviations</b>  | <b>xi</b>   |
| <b>1 Introduction</b>   | <b>1</b>    |
| 1.1 Previous work   | 1           |
| 1.2 Research objectives   | 3           |
| 1.3 Research methodology and limitations  | 3           |
| 1.4 Thesis outline  | 4           |
| <b>2 Analytical solution</b>  | <b>5</b>    |
| 2.1 Introduction  | 5           |
| 2.2 Mathematical background   | 6           |
| 2.3 Validation of the analytical solution   | 13          |
| 2.4 Conclusions   | 22          |
| <b>3 Multi-year Simulations</b>   | <b>23</b>   |
| 3.1 Background  | 23          |
| 3.2 Step-response functions   | 26          |
| 3.3 Load aggregation scheme for multi-year simulations  | 35          |
| 3.4 Examples of multi-year simulations  | 37          |
| 3.5 Conclusions   | 45          |
| <b>4 Thermal response testing and analysis</b>  | <b>47</b>   |
| 4.1 Test facility   | 47          |
| 4.2 Response testing and evaluation of the test facility boreholes  | 49          |
| 4.3 Sensitivity of borehole system design to uncertainties in TRT results   | 54          |
| 4.4 Convection in groundwater-filled boreholes  | 57          |
| 4.5 Recovery times after a TRT  | 62          |
| 4.6 New TRT evaluation method   | 65          |
| 4.7 Conclusions   | 70          |
| <b>5 Concluding remarks</b>   | <b>71</b>   |
| 5.1 Summary and conclusions   | 71          |
| 5.2 Future work   | 72          |
| <b>References</b>   | <b>75</b>   |
| <b>Papers</b>   |             |
| I. Vertical ground heat exchangers – A review of heat flow models.  |             |
| II. New analytical and numerical solutions for the short-term analysis of vertical ground heat exchangers.              |             |
| III. An experimental investigation of the accuracy of thermal response tests used to measure ground thermal properties. |             |

- IV. Thermal response testing of a multiple borehole ground heat exchanger.
- V. An analytical method to calculate borehole fluid temperatures for time-scales from minutes to decades.
- VI. Recovery times after thermal response tests on vertical borehole heat exchangers.
- VII. A method to evaluate thermal response tests on groundwater-filled boreholes.

# Symbols and abbreviations

## Symbols

### Latin letters

|                       |  |                         |
|-----------------------|--|-------------------------|
| $a$                   | thermal diffusivity; $a = \frac{\lambda}{\rho \cdot c}$  | [m <sup>2</sup> /s]     |
| $B$                   | spacing between boreholes in Chapter 3   | [m]                     |
| $C$                   | thermal capacity per unit length   | [J/(m·K)]               |
| $c$                   | specific heat capacity   | [J/(kg·K)]              |
| $H$                   | height   | [m]                     |
| $h$                   | convective heat transfer coefficient, Eq. 2.5  | [W/(m <sup>2</sup> ·K)] |
| $h$                   | variable of substitution in Section 3.2.1, Eq. 3.14  | [-]                     |
| $h$                   | time step in Section 3.3   | [hour]                  |
| $I_n$                 | nth-order modified Bessel function of first kind   | [-]                     |
| $J_n$                 | nth-order Bessel function of first kind  | [-]                     |
| $K$                   | thermal conductance  | [W/(m·K)]               |
| $K_n$                 | nth-order modified Bessel function of second kind  | [-]                     |
| $\bar{K}$             | thermal conductance in Laplace domain  | [W/(m·K)]               |
| $N$                   | number of cells in the numerical model of Chapter 2  | [-]                     |
| $N$                   | number of boreholes in Chapter 3   | [-]                     |
| $n$                   | enumeration of the time step in Section 3.3  | [-]                     |
| $p$                   | cell numbers on level $q$ in Chapter 3   | [-]                     |
| $P_q$                 | number of aggregated cells on level $q$ in Chapter 3   | [-]                     |
| $Q$                   | heating or cooling load  | [W]                     |
| $Q_{in}(\tau)$        | prescribed heat injection in Chapter 3   | [W]                     |
| $Q_{step}$            | amplitude of heat injection step   | [W]                     |
| $Q_v^{(n)}$           | heat injection pulse $v$ at time step $n$ in Chapter 3, Eq. 3.4  | [W]                     |
| $\bar{Q}_{q,p}^{(n)}$ | heat injection for aggregated cell $q,p$ in Chapter 3  | [W]                     |
| $q$                   | rate of heat transfer per unit length  | [W/m]                   |
| $q$                   | level of aggregation in Section 3.3  | [-]                     |
| $R$                   | thermal resistance   | [(m·K)/W]               |
| $\bar{R}$             | thermal resistance in Laplace domain   | [(m·K)/W]               |
| $r$                   | radius   | [m]                     |
| $r_q$                 | number of cells in lumped cells of level $q$ in Chapter 3  | [-]                     |
| $s$                   | Laplace transform variable in short-term response;<br>$= 1/\sqrt{4a(\tau - \tau')}$ in long-term response, Eq. 3.9 | [1/s]                   |
| $T$                   | temperature  | [K or °C]               |
| $T_{step}$            | step-response temperature  | [K]                     |

|              |   |             |
|--------------|---|-------------|
| $\bar{T}$    | mean temperature in Chapter 3                       | [K]         |
| $\bar{T}(s)$ | Laplace transform of $T(\tau)$                      | [K·s]       |
| $u$          | variable of integration                             | [ $\cdot$ ] |
| $u$          | dimensionless coordinate in Section 2.3.1, Eq. 2.50 | [ $\cdot$ ] |
| $Y_n$        | nth-order Bessel function of second kind            | [ $\cdot$ ] |
| $z$          | axial coordinate                                    | [m]         |

## Greek letters

|                      |  |                      |
|----------------------|--|----------------------|
| $\kappa_v$           | weighting factors in Chapter 3                           | [ $\cdot$ ]          |
| $\bar{\kappa}_{q,p}$ | weighting factors for aggregated cell $q,p$ in Chapter 3 | [ $\cdot$ ]          |
| $\lambda$            | thermal conductivity                                     | [W/(m·K)]            |
| $v$                  | enumeration of the time step in Section 2.3.1            | [ $\cdot$ ]          |
| $v$                  | enumeration of loads backward in time in Chapter 3       | [ $\cdot$ ]          |
| $v_{q,p}$            | last $v$ -value in cell $q,p$ in Chapter 3               | [ $\cdot$ ]          |
| $\rho$               | density  | [kg/m <sup>3</sup> ] |
| $\tau$               | time   | [hours or s]         |

## Subscripts

|    |               |
|----|---------------|
| b  | borehole      |
| bw | borehole wall |
| f  | fluid         |
| g  | grout         |
| i  | in / inner    |
| ls | line-source   |
| o  | out / outer   |
| p  | pipe          |
| s  | soil (ground) |
| ss | steady-state  |
| t  | transmittive  |

## Abbreviations

|         |  |
|---------|--|
| ASHRAE  | American Society of Heating, Refrigerating, and Air-Conditioning Engineers |
| EED     | Earth Energy Designer Program  |
| GLHEPro | Ground Loop Heat Exchanger Program   |
| GPM     | Geothermal Properties Measurement Program                                  |
| GSHP    | Ground Source Heat Pump  |
| SBM     | Superposition Borehole Model   |
| TRT     | Thermal Response Test  |

# 1 Introduction

The use of ground source heat pump (GSHP) systems to provide heating and cooling in buildings has increased greatly in the last decade or so. During this period, the worldwide installed capacities of GSHP systems have increased from approximately 5,300 MW in 2000 to over 33,000 MW in 2010, at a compound annual rate of 20 %. At present, the total energy use of GSHP systems exceeds 200,000 TJ/year. Sweden now stands third behind the USA and China in having the largest installed capacities of GSHP systems. The energy use of the GSHP systems installed in Sweden is also behind only those of China and the USA<sup>[38]</sup>.

The most common application of a GSHP system is with vertical borehole heat exchangers. The current focus of vertical GSHP systems-related research is on the performance optimization of these systems. A key prerequisite for this optimization process is the accurate knowledge of the temperature of the circulating fluid that exits the borehole heat exchanger. The borehole exit fluid temperatures are determined using either numerical or analytical solutions. Numerical solutions are more accurate but have extended computational time requirements and limited flexibility, especially when analyzing multiple borehole systems. On the other hand, analytical solutions have better flexibility and are more efficient in terms of superior computational time. However, existing analytical solutions are less accurate and their ability to analyze multiple borehole systems remains largely untested.

In Sweden, there are approximately 250,000 installations of vertical GSHP systems, and this number is increasing at a steady rate of about 10 % a year<sup>[5]</sup>. Sweden is unique in the respect that it uses groundwater-filled boreholes. In much of the country, the underground structure is solid bedrock, which allows the boreholes to be filled naturally with groundwater, eliminating the need for grouting. Casing is used only at the very top of the borehole, where sediments overlay the bedrock, to avoid intrusion of the surface water. Heat transfer between the borehole and the surrounding ground is by conduction and buoyancy-driven natural convection, which is sometimes assisted by advection (horizontal water currents in fractured bedrock). Analysis and evaluation of groundwater-filled boreholes presents challenges that are somewhat different to those of grouted boreholes.

## 1.1 Previous work

Various analytical, semi-analytical and numerical models have been developed for the modelling and simulation of borehole heat transfer. A detailed review of these models has been provided in Paper 1. This section provides an overview of several of the most significant mathematical models and methods used for modelling and simulation of borehole heat transfer.

Classical analytical models for determining the thermal response of a borehole system include the line-source<sup>[28]</sup> and the cylindrical-source<sup>[19]</sup> solutions. The line-source solution treats the radial heat transfer in a plane perpendicular to the vertical borehole, which is assumed to be a line source of constant heat output and infinite length, and is surrounded by an infinite homogeneous ground. On the

other hand, the cylindrical-source solution models the borehole as a cylinder surrounded by homogeneous ground and having constant heat-flux across its outer boundary. Both the classical line-source and cylindrical-source solutions oversimplify the geometry of a borehole and thus have limited application for short-time analysis of the borehole heat transfer. The issue of the accuracy of line-source and cylindrical-source solutions has been addressed by many researchers. The solution proposed by Lamarche and Beauchamp<sup>[35]</sup> assumes a steady heat-flux condition across a concentric hollow pipe instead of the borehole outer boundary considered by the classical cylindrical-source solution. The authors also proposed a finite-length line-source solution<sup>[34]</sup> based on the integral mean temperature along the borehole. Gu and Neal<sup>[25]</sup> developed an analytical solution assuming a cylindrical source in an infinite composite region. They solved the transient heat transfer problem of the borehole heat exchanger using the generalized orthogonal expansion technique, which requires calculation of multiple Eigen-values. Young<sup>[53]</sup> modified the classical buried electric cable solution to develop his borehole fluid thermal mass solution. The solution is based on an analogy between a buried electric cable and a vertical borehole. Bandyopadhyay et al.<sup>[9]</sup> adapted the classical Blackwell solution<sup>[17]</sup> in their ‘virtual solid’ solution, which was developed for thermal analysis of boreholes backfilled with the borehole cuttings.

Beier and Smith<sup>[12]</sup> and Bandyopadhyay et al.<sup>[9]</sup> presented semi-analytical solutions that first solve the heat transfer problem of a borehole heat exchanger in the Laplace domain and then use numerical inversion methods to obtain the solution in the time domain.

In his superposition borehole model (SBM), Eskilson<sup>[22]</sup> used a numerical approach that considered the transient radial-axial heat transfer in the borehole to develop non-dimensional thermal response solutions, also known as *g-functions*. The SBM also determines thermal interactions between boreholes using an intricate superposition of numerical solutions for each borehole. Yavuzturk and Spitler<sup>[52]</sup> extended the work of Eskilson and developed the so-called short time step *g-functions* using a numerical approach. Austin<sup>[7]</sup> and Shonter and Beck<sup>[44]</sup> also developed solutions that numerically solve the heat transfer in the borehole heat exchanger. However, these solutions are aimed at the evaluation of thermal response tests (TRTs). Other significant numerical solutions include the work of Muraya<sup>[41]</sup>, Zeng et al.<sup>[54]</sup>, Al-Khoury et al.<sup>[3, 4]</sup>, Xu and Spitler<sup>[50]</sup> and He et al.<sup>[27]</sup>, among others.

The principal applications of the above mathematical models include evaluating a TRT conducted on a borehole, designing a borehole system, and performing simulations of a borehole system<sup>[27]</sup>. The models extensively used for evaluation of TRTs include the line-source solution and the numerical models of Austin<sup>[7]</sup> and Shonter and Beck<sup>[44]</sup>. Gehlin<sup>[23]</sup> developed a simple and straightforward approach to evaluate TRTs using an approximation of the line-source solution. Shonter and Beck’s model was implemented in the Geothermal Properties Measurement<sup>[43]</sup> (GPM) computer program to evaluate TRTs using a parameter estimation approach. Austin’s numerical model was also implemented in the Vertical Borehole Analysis and Parameter Estimation Program<sup>[7]</sup>. The design of a borehole system is generally carried out using commercial software, such as Earth Energy Designer (EED)<sup>[18]</sup> and the Ground Loop Heat Exchanger Program

(GLHEPRO)<sup>[47]</sup>, among others. These programs are based on the *g-functions* developed by Eskilson<sup>[22]</sup>. Monthly aggregated values of heating and cooling loads are used, and the peak loads are superimposed on the aggregated values. Simulations of a borehole system can be performed using any of the above-mentioned models. However, each model has both merits and demerits with regard to issues such as accuracy of short- and long-term response, thermal interactions between boreholes, and computational time requirements when performing a simulation. To perform rapid multi-year simulations, load aggregation techniques have been presented by Yavuzturk and Spitler<sup>[52]</sup>, Bernier et al.<sup>[16]</sup>, Liu<sup>[37]</sup>, and Marcotte and Pasquier<sup>[39]</sup>, among others.

## 1.2 Research objectives

The main objective of this research is the development of analytical models and methods to perform multi-year simulations of borehole systems. The aim is to develop analytical solutions for both single and multiple borehole systems, which can model the heat transfer in borehole systems from short periods (minutes) to long periods (years or longer).

Another objective is to contribute to the already existing range of research in the area of thermal response testing. The goal is to increase the knowledge of testing and evaluation of vertical borehole systems in general and groundwater-filled boreholes in particular.

## 1.3 Research methodology and limitations

This study started with an extensive survey of literature to gain insight into and understanding of the state-of-the-art modelling and simulation of GSHP systems in general and of borehole systems in particular. The emphasis of the literature review was on the analytical modelling of heat transfer in borehole systems, which is the primary area of focus in this research.

Next, mathematical modelling was used to develop analytical models and methods for the simulation of borehole systems. Mathematical modelling was utilized to develop analytical solutions for single and multiple borehole systems. A method to perform multi-year simulations of borehole systems was also developed through mathematical modelling.

Simulation and experimental studies were used for validation of the proposed models and methods. Simulations were performed using state-of-the-art research and commercial tools. Experiments were performed mostly in a carefully controlled experimental setup that was designed and built in the initial phase of this study. Experimental investigations to study various other aspects of heat transfer in borehole systems were also designed and conducted. Issues pertaining to thermal response of borehole heat exchangers, convective heat transfer in groundwater-filled boreholes, and recovery times of a borehole system were all comprehensively studied through a systematic series of experiments.

The method presented in this thesis to develop step-response functions was tested for small- to medium-sized borehole fields. Its application to determine the step-response functions for large-sized borehole fields requires further testing and validation. Another limitation is that the experimental investigations reported in this thesis were carried out on groundwater-filled borehole systems. Hence, some of results reported and conclusions drawn in this thesis hold true only for groundwater-filled boreholes.

## 1.4 Thesis outline

This thesis is divided into five chapters, of which Chapters 2, 3 and 4 comprise the main body. The chapters are organized as follows.

Chapter 1 provides an overview of the research context with a description of the motivations, perspectives, and methods of research. The chapter also includes a brief literature review of the models and methods used for modelling and simulations of borehole systems.

In Chapter 2, an analytical solution to model the radial heat transfer problem in a borehole is presented. The chapter describes the background, the mathematical formulation and the validation of the analytical solution in considerable detail. Chapter 2 is an extended version of Paper II.

Chapter 3 deals with the simulations of borehole systems. The chapter first presents the development of step-response functions for single and multiple borehole systems by combining the analytical solution of Chapter 2 with a finite line-source solution. A load aggregation scheme is then presented to perform rapid, yet accurate, multi-year simulations of borehole systems. Chapter 3 extends Paper V.

In Chapter 4, several key aspects of thermal response testing and evaluation are investigated. The chapter first reports the thermal response testing of nine adjacent boreholes. Case studies are used to analyze the effects of the uncertainties in TRT results on the design of a borehole system. Next, the chapter examines issues of convective heat transfer in a borehole system and the recovery times after a thermal response test. Finally, a method to evaluate thermal response tests on groundwater-filled boreholes is presented. Chapter 4 draws from Papers III, IV, VI and VII.

Chapter 5 concludes the thesis with a summary of research findings and suggestions for continued research on this topic.

## 2 Analytical solution

*This chapter is based on Paper II.*

An analytical solution has been developed to enable modelling and simulation of borehole systems. The emphasis of the new solution is very much on short-term modelling of borehole heat transfer. The analytical solution accounts for thermal conductivities, thermal resistances, thermal capacities and thermal properties of all borehole elements. One limitation is that the solution considers only radial heat transfer in the borehole and the surrounding ground. The development and validation of the analytical solution were summarized in Paper II and reported in detail in other publications<sup>[20, 29]</sup>.

### 2.1 Introduction

The analytical solution studies the radial heat transfer and the related boundary conditions in the Laplace domain. To meet the radial heat transfer requirement, an equivalent-diameter pipe is used to model the U-tube. The model considers a constant heat flux  $q_{inj}$  injected to the circulating fluid at temperature  $T_f(\tau)$  starting from time  $\tau = 0$ . The thermal capacity  $C_p$  of the circulating fluid in the equivalent-diameter pipe is kept equal to that in the U-tube. A resistance value of  $R_p$  is introduced to account for fluid and pipe resistances. The resulting outer boundary temperature of the equivalent-diameter pipe is  $T_p(\tau)$ . A grout region of thermal conductivity  $\lambda_g$  and thermal diffusivity  $a_g$  surrounds the equivalent-diameter pipe. The borehole is surrounded by infinite homogeneous ground (soil) of thermal conductivity  $\lambda_s$  and thermal diffusivity  $a_s$ . The heat flux from the fluid to the grout region through the pipe wall is  $q_p(\tau)$ . Similarly, the heat flux from the grout region to the surrounding ground through the borehole radius is  $q_b(\tau)$ . The resulting radial heat transfer problem is shown in Figure 2.1.

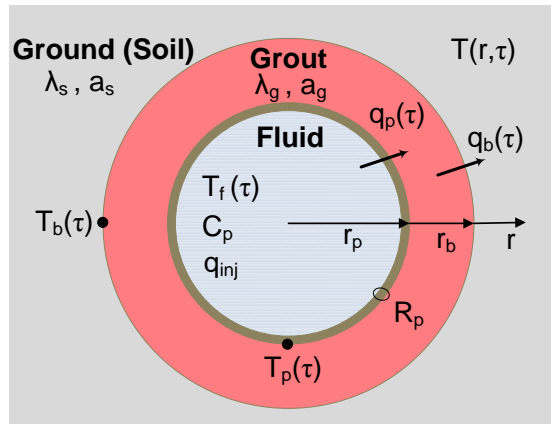


**Figure 2.1** The geometry and the thermal properties of the borehole

## 2.2 Mathematical background

For the heat transfer problem shown in Figure 2.1, the temperature distribution  $T(r, \tau)$  must satisfy the following radial heat conduction equation in both the grout and the ground (soil) regions.

$$\frac{1}{a(r)} \cdot \frac{\partial T}{\partial \tau} = \frac{\partial^2 T}{\partial r^2} + \frac{1}{r} \cdot \frac{\partial T}{\partial r}, \quad a(r) = \begin{cases} a_g, & r_p < r < r_b \\ a_s, & r > r_b \end{cases}. \quad (2.1)$$

The radial heat flux in the grout and the soil regions is

$$q(r, \tau) = 2\pi r [-\lambda(r)] \cdot \frac{\partial T}{\partial r}, \quad \lambda(r) = \begin{cases} \lambda_g, & r_p < r < r_b \\ \lambda_s, & r > r_b \end{cases}. \quad (2.2)$$

The heat flux at the grout-soil interface is continuous, and hence the boundary condition from Equation 2.2 at  $r=r_b$  is

$$\lambda_g \cdot \frac{\partial T}{\partial r} \Big|_{r=r_b-0} = \lambda_s \cdot \frac{\partial T}{\partial r} \Big|_{r=r_b+0}. \quad (2.3)$$

The pipe is filled with a heat transfer fluid at temperature  $T_f(\tau)$ . A thermal resistance  $R_p$  exists over the pipe periphery between the fluid in the pipe and the grout just outside the pipe. This resistance accounts for the pipe wall and the fluid boundary layer. The heat flux over this thermal resistance is equal to the radial heat flux in the grout just outside the pipe. The boundary condition at the pipe-grout interface then is

$$T_f(\tau) - T(r_p, \tau) = R_p \cdot q(r_p, \tau). \quad (2.4)$$

Here, the thermal resistance  $R_p$  is defined as

$$R_p = \frac{1}{K_p} = \frac{1}{2 \pi \cdot \lambda_p} \cdot \ln \left( \frac{r_{p,o}}{r_{p,i}} \right) + \frac{1}{2 \pi r_p \cdot h_p}. \quad (2.5)$$

The first part of Equation 2.5 refers to the conductive resistance of the pipe, and the second part refers to the fluid convective resistance.

The heat balance of the fluid in the pipe with the injected heat  $q_{inj}$  is

$$q_{inj} = C_p \cdot \frac{dT_f}{d\tau} + q(r_p, \tau). \quad (2.6)$$

The initial temperatures in the pipe, the grout and the ground (soil) are all taken as zero.

$$T_f(0) = 0, \quad T(r, 0) = 0, \quad r > r_p. \quad (2.7)$$

## 2.2.1 Laplace transform for the pipe region

Taking Laplace transforms of Equations 2.4 and 2.6 give

$$\bar{T}_f(s) - \bar{T}_p(s) = R_p \cdot \bar{q}_p(s) \quad (2.8)$$

and

$$\frac{q_{inj}}{s} = C_p \cdot s \cdot [\bar{T}_f(s) - 0] + \bar{q}_p(s). \quad (2.9)$$

Here,  $\bar{T}_p(s)$  and  $\bar{q}_p(s)$  are temperature and heat flux in the borehole at the pipe wall and  $s$  is the complex-valued argument of the Laplace transform.

## 2.2.2 Laplace transform for the annular region

The Laplace transform of the radial heat equation for the annular region gives

$$\frac{\partial^2 \bar{T}}{\partial r^2} + \frac{1}{r} \cdot \frac{\partial \bar{T}}{\partial r} = \frac{s}{a_g} \cdot \bar{T}(r, s) = \left( \sqrt{\frac{s}{a_g}} \right)^2 \cdot \bar{T}(r, s). \quad (2.10)$$

We can scale  $r$  together with  $\sqrt{s/a_g}$  to have

$$z = r \sqrt{\frac{s}{a_g}}, \quad \bar{T}(r, s) = g(z). \quad (2.11)$$

Now Equation 2.10 can be written as an ordinary differential equation as

$$\frac{d^2 g}{dz^2} + \frac{1}{z} \cdot \frac{dg}{dz} - g(z) = 0. \quad (2.12)$$

The solutions of Equation 2.12 are  $I_0(z)$  and  $K_0(z)$ , which are modified Bessel functions of zero order<sup>[1]</sup>. Using these functions to get a general solution of Equation 2.10 gives

$$\bar{T}(r, s) = A(s) \cdot I_0\left(r \sqrt{\frac{s}{a_g}}\right) + B(s) \cdot K_0\left(r \sqrt{\frac{s}{a_g}}\right), \quad r_p \leq r \leq r_b. \quad (2.13)$$

Let us define:

$$\sigma_p = r_p \sqrt{\frac{s}{a_g}}, \quad \sigma_b = r_b \sqrt{\frac{s}{a_g}}. \quad (2.14)$$

Now Equation 2.13 can be written as the following two equations for the temperatures at the two boundaries (i.e.  $r_p$  and  $r_b$ ) of the annular region.

$$\bar{T}_p(s) = A(s) \cdot I_0(\sigma_p) + B(s) \cdot K_0(\sigma_p) \quad (2.15)$$

and

$$\bar{T}_b(s) = A(s) \cdot I_0(\sigma_b) + B(s) \cdot K_0(\sigma_b). \quad (2.16)$$

Another set of equations can be obtained for the boundary fluxes by taking the Laplace transform of the radial heat flux (Equation 2.2) and inserting the Laplace transforms from Equation 2.13 and taking  $r = r_p$  and  $r = r_b$ .

$$\bar{q}_p(s) = 2\pi \cdot \lambda_g \cdot \sigma_p [-A(s) \cdot I_1(\sigma_p) + B(s) \cdot K_1(\sigma_p)] \quad (2.17)$$

and

$$\bar{q}_b(s) = 2\pi \cdot \lambda_g \cdot \sigma_b [-A(s) \cdot I_1(\sigma_b) + B(s) \cdot K_1(\sigma_b)]. \quad (2.18)$$

$A(s)$  and  $B(s)$  may be eliminated from Equations 2.15 to 2.18, and thus two equations between the Laplace transforms of the boundary temperatures and boundary fluxes are obtained. These equations may be written as follows:

$$\bar{q}_p(s) = \bar{K}_p(s) \cdot (\bar{T}_p(s) - 0) + \bar{K}_t(s) \cdot (\bar{T}_p(s) - \bar{T}_b(s)) \quad (2.19)$$

and

$$-\bar{q}_b(s) = \bar{K}_b(s) \cdot (\bar{T}_b(s) - 0) + \bar{K}_t(s) \cdot (\bar{T}_b(s) - \bar{T}_p(s)). \quad (2.20)$$

Equations 2.19 and 2.20 can be represented in the form of a thermal network for the borehole annulus as shown in Figure 2.2.

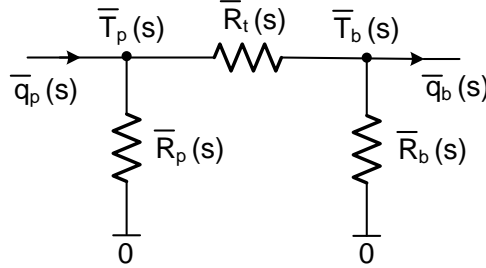


**Figure 2.2** Thermal network for the borehole annular region

The values of one transmittive and two absorptive conductances (and their inverse, the resistances) used in Equations 2.19 and 2.20 and in the thermal network for the annular region are as follows:

$$\bar{K}_t(s) = \frac{1}{\bar{R}_t(s)} = \frac{2\pi\lambda_g}{K_0(\sigma_p) \cdot I_0(\sigma_b) - I_0(\sigma_p) \cdot K_0(\sigma_b)}, \quad (2.21)$$

$$\bar{K}_p(s) = \frac{1}{\bar{R}_p(s)} = \frac{\sigma_p [I_1(\sigma_p) \cdot K_0(\sigma_b) + K_1(\sigma_p) \cdot I_0(\sigma_b)] - 1}{\bar{R}_t(s)}, \quad (2.22)$$

and

$$\bar{K}_b(s) = \frac{1}{\bar{R}_b(s)} = \frac{\sigma_b [I_1(\sigma_b) \cdot K_0(\sigma_p) + K_1(\sigma_b) \cdot I_0(\sigma_p)] - 1}{\bar{R}_t(s)}. \quad (2.23)$$

### 2.2.3 The soil region

Regarding the soil region outside the borehole radius, a solution exists that is similar to the one given by Equation 2.13:

$$\bar{T}(r, s) = A(s) \cdot I_0\left(r \sqrt{\frac{s}{a_s}}\right) + B(s) \cdot K_0\left(r \sqrt{\frac{s}{a_s}}\right). \quad (2.24)$$

The function  $I_0$  in Equation 2.24 increases exponentially with  $r$  and is finite at  $r = 0$ . On the other hand, the function  $K_0$  decreases exponentially with  $r$  and is infinite at  $r = 0$ . Because the radius outside the borehole tends to infinity, the value of coefficient  $A(s)$  must be zero. This gives

$$\bar{T}(r, s) = B(s) \cdot K_0\left(r \sqrt{\frac{s}{a_s}}\right), \quad r \geq r_b. \quad (2.25)$$

The coefficient  $B(s)$  can be eliminated if the temperature in the ground outside the borehole is expressed in the following form:

$$\bar{T}(r, s) = \frac{K_0\left(r \sqrt{\frac{s}{a_s}}\right)}{K_0\left(r_b \sqrt{\frac{s}{a_s}}\right)} \cdot \bar{T}_b(s). \quad (2.26)$$

For the soil region, we define

$$\sigma_s = r_b \sqrt{\frac{s}{a_s}}. \quad (2.27)$$

Equation 2.26 can now be written as

$$\bar{T}(r, s) = \frac{K_0\left(r \sqrt{\frac{s}{a_s}}\right)}{K_0(\sigma_s)} \cdot \bar{T}_b(s). \quad (2.28)$$

Taking the Laplace transform of the radial heat flux (i.e., Equation 2.2) for the soil region (at  $r = r_b$ ) and using Equations 2.3 and 2.28, we obtain

$$\bar{q}_b(s) = 2\pi r_b (-\lambda_s) \cdot \frac{\sqrt{\frac{s}{a_s}} \cdot K'_0(\sigma_s)}{K_0(\sigma_s)} \cdot \bar{T}_b(s). \quad (2.29)$$

In Equation 2.29, the derivative  $K'_0(\sigma_s) = -K_1(\sigma_s)$ . Here,  $K_1$  is the first order modified Bessel function.

We obtain the following relations between the Laplace transforms of temperature and heat flux at boundary  $r = r_b$ .

$$\bar{T}_b(s) - 0 = \bar{R}_s(s) \cdot \bar{q}_b(s) \quad (2.30)$$

The following relation for the ground thermal resistance (and its inverse, the ground thermal conductance) is obtained from Equations 2.29 and 2.30:

$$\bar{R}_s(s) = \frac{1}{\bar{K}_s(s)} = \frac{1}{2\pi\lambda_s} \cdot \frac{K_0(\sigma_s)}{\rho_s \cdot K_1(\sigma_s)} \quad (2.31)$$

## 2.2.4 The whole thermal network

The whole network (Figure 2.3) for the equivalent-diameter pipe, the circulating fluid, the borehole annulus region and the infinite ground outside the borehole can now be drawn using Equations 2.8 and 2.9 for the pipe boundary, Equations 2.19 and 2.20 for the annular region, and Equation 2.30 for the soil region.

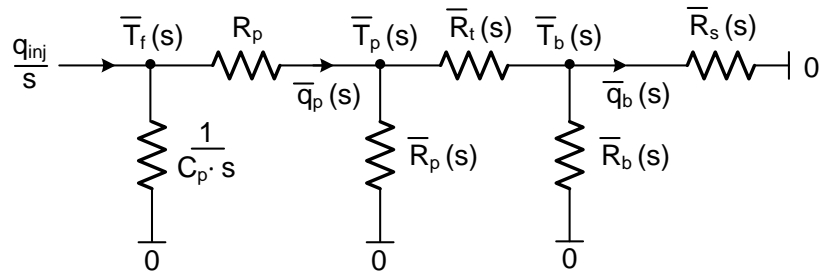


**Figure 2.3** The whole thermal network for a borehole in ground

The Laplace transform for the fluid temperature can be readily obtained from the thermal network.

$$\bar{T}_f(s) = \frac{q_{inj}}{s} \cdot \frac{1}{C_p \cdot s + \frac{1}{R_p + \frac{1}{\bar{K}_p(s) + \frac{1}{\bar{R}_t(s) + \frac{1}{\bar{K}_b(s) + \bar{K}_s(s)}}}}} \quad (2.32)$$

The network involves a sequence of composite resistances. We start from the right in Figure 2.3. The conductances  $\bar{K}_b(s)$  and  $\bar{K}_s(s)$  lie in parallel and are added. The inverse of this composite conductance is added to the resistance  $\bar{R}_t(s)$ . This composite resistance lies in parallel with  $\bar{R}_p(s) = 1/\bar{K}_p(s)$ , and their inverses are added. This composite resistance lies in series with the resistance of the pipe wall  $R_p$ . The total composite resistance from  $R_p$  towards the right lies in parallel with the thermal conductance  $C_p \cdot s$ .

## 2.2.5 Fluid temperature

In the type of problems considered here, the inversion formula to obtain  $f(\tau)$  from  $\bar{f}(s)$  is given by the integral:

$$f(\tau) = \frac{2}{\pi} \cdot \int_0^{\infty} \frac{1 - e^{-u^2 \cdot \frac{\tau}{\tau_0}}}{u} \cdot L(u) du. \quad (2.33)$$

The function  $L(u)$  in the above equations is given by

$$L(u) = \text{Im}[-s \cdot \bar{f}(s)]_{\Gamma}, \quad \Gamma: \tau_0 \cdot s = -u^2 + i \cdot 0, \quad (2.34)$$

$$\sqrt{\tau_0 \cdot s} = i \cdot u, \quad 0 < u < \infty.$$

Here,  $\text{Im}[\dots]$  denotes the imaginary part and  $\tau_0$  (in seconds) is an arbitrary time constant that makes both  $\tau_0 \cdot s$  and the integration variable  $u$  dimensionless. The first factor in the integral of Equation 2.33 is independent of the particular Laplace transform  $\bar{f}(s)$  and depends only on dimensionless time  $\tau/\tau_0$ . The second factor, the function  $L(u)$  in Equation 2.33, represents the particular Laplace transform for the considered case and is independent of time  $\tau$ . The inversion integral in Equation 2.33 is obtained by replacing the original integral along the vertical line  $\Gamma_0$  with an integral along the negative real axis  $\Gamma$ . A closed-loop integration path in the complex  $s$ -plane is used instead, as shown in Figure 2.4. The following conditions must be fulfilled:

$$f(0) = 0, \quad \frac{df}{d\tau} \rightarrow 0, \quad \tau \rightarrow \infty. \quad (2.35)$$

There is a pole at  $s = 0$  and a cut in the complex  $s$ -plane along the negative real axis to account for  $\sqrt{s}$ . A final requirement, which is fulfilled in our applications, is that no other poles lie inside the closed loop of Figure 2.4.

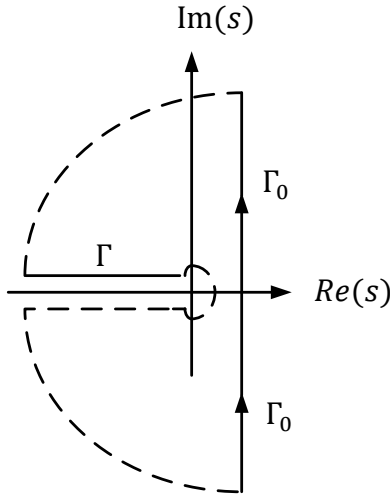


**Figure 2.4** Considered closed path for the inversion integral to get Equations 2.33 and 2.34

Using Equation 2.33, we can now write the fluid temperature  $T_f(\tau)$  as

$$T_f(\tau) = \frac{2}{\pi} \cdot \int_0^\infty \frac{1 - e^{-u^2 \cdot \frac{\tau}{\tau_0}}}{u} \cdot L(u) du. \quad (2.36)$$

The Laplace transform for the fluid temperature is given by Equation 2.32. When taken for  $s$  on the negative real axis  $\Gamma$ , we obtain

$$L(u) = \text{Im} \frac{-q_{inj}}{C_p \cdot \frac{-u^2}{\tau_0} + \frac{1}{R_p + \frac{1}{\bar{K}_p(u) + \frac{1}{\bar{R}_t(u) + \frac{1}{\bar{K}_b(u) + \bar{K}_s(u)}}}}} \quad (2.37)$$

The four thermal resistances (and the corresponding conductances) for the Laplace transforms are given by Equations 2.21 to 2.23 and Equation 2.31. On the negative real axis  $\Gamma$ , these become functions of the real variable  $u$ . From Equations 2.14, 2.27 and 2.34, we obtain

$$\sigma_p = i \cdot p_p \cdot u, \quad \sigma_b = i \cdot p_b \cdot u, \quad \sigma_s = i \cdot p_s \cdot u, \quad (2.38)$$

and

$$p_p = \frac{r_p}{\sqrt{a_g \cdot \tau_0}}, \quad p_b = \frac{r_b}{\sqrt{a_g \cdot \tau_0}}, \quad p_s = \frac{r_b}{\sqrt{a_s \cdot \tau_0}}. \quad (2.39)$$

The arguments in the formulas for the resistances are now imaginary numbers. In this case, the modified Bessel functions may be expressed as ordinary Bessel functions. The final formulas for the thermal resistances taken on the negative real axis  $\Gamma$  become

$$\bar{R}_s(u) = \frac{1}{2\pi\lambda_s} \cdot \frac{J_0(p_s u) - i \cdot Y_0(p_s u)}{p_s u \cdot [J_1(p_s u) - i \cdot Y_1(p_s u)]}, \quad 0 < u < \infty \quad (2.40)$$

$$\bar{R}_t(u) = \frac{J_0(p_p u) \cdot Y_0(p_b u) - Y_0(p_p u) \cdot J_0(p_b u)}{4\lambda_g}, \quad (2.41)$$

$$\bar{R}_p(u) = \frac{\bar{R}_t(u)}{0.5 \pi p_p u \cdot [J_1(p_p u) Y_0(p_b u) - Y_1(p_p u) J_0(p_b u)] - 1}, \quad (2.42)$$

and

$$\bar{R}_b(u) = \frac{\bar{R}_t(u)}{0.5 \pi p_b u \cdot [J_1(p_b u) Y_0(p_p u) - Y_1(p_b u) J_0(p_p u)] - 1}. \quad (2.43)$$

## 2.3 Validation of the analytical solution

The analytical solution has been validated using multiple approaches. The first approach involved development of a one-dimensional numerical solution to validate the results of the analytical solution. In the second approach, the analytical solution was validated against an existing semi-analytical solution<sup>[12]</sup>. The third approach validated the analytical method using the experimental results from a laboratory setup. The following sections provide further details on the validation of the analytical solution using these different approaches.

### 2.3.1 Validation using a numerical solution

A numerical solution has been developed to validate the results of the new analytical solution. For consistency with the analytical solution, which solves the radial heat transfer problem, the numerical solution has also been developed to solve the one-dimensional heat transfer problem in the borehole and the ground. The new numerical solution uses a special coordinate transformation for which the heat flux has the simplest possible form. The mathematical background of the numerical solution is given in detail in the following section.

#### 2.3.1.1 Mathematical background of numerical solution

The radial heat equation in its general form is

$$\rho(r) \cdot c(r) \cdot \frac{\partial T}{\partial r} = \frac{1}{r} \cdot \frac{\partial}{\partial r} \left[ r \cdot \lambda(r) \cdot \frac{\partial T}{\partial r} \right], \quad r \geq r_p. \quad (2.44)$$

In Equation 2.44, the thermal conductivity  $\lambda$ , the density  $\rho$  and the specific heat capacity  $c$  can be constant or any positive functions of radial distance  $r$ . The heat equation can also be rewritten as

$$\rho c \cdot 2\pi r \cdot \frac{\partial T}{\partial r} = -\frac{\partial q}{\partial r}, \quad q(r, t) = -2\pi r \cdot \lambda \cdot \frac{\partial T}{\partial r}, \quad r \geq r_p. \quad (2.45)$$

For steady-state condition the heat flux in a radial direction is constant:

$$T = T_{ss}(r): \quad \frac{\partial T}{\partial t} = 0, \quad \frac{\partial q}{\partial r} = 0 \Rightarrow q(r, t) = q_{ss}. \quad (2.46)$$

Equation 2.45, when written for steady-state conditions, is

$$q_{ss} = -2\pi r \cdot \lambda(r) \cdot \frac{dT_{ss}}{dr}, \quad -dT_{ss} = \frac{q_{ss}}{2\pi \cdot r \cdot \lambda(r)} dr. \quad (2.47)$$

The temperature difference over the annular region between pipe radius  $r_p$  and any radial distance  $r$  is equal to the heat flux times the thermal resistance of the annular region  $r_p \leq r < \infty$ :

$$T_{ss}(r_p) - T_{ss}(r) = q_{ss} \cdot R(r). \quad (2.48)$$

Comparing Equations 2.47 and 2.48 gives the thermal resistance  $R(r)$ :

$$R(r) = \int_{r_p}^r \frac{1}{\lambda(r') \cdot 2\pi r'} dr', \quad \frac{dR}{dr} = \frac{1}{\lambda(r) \cdot 2\pi r}, \quad r_p \leq r < \infty. \quad (2.49)$$

The transient heat conduction for variable thermal conductivity  $\lambda(r)$  may be simplified by using the steady-state thermal resistance of an annular region as a new dimensionless coordinate  $u = u(r)$ :

$$u(r) = \lambda_0 \cdot R(r) = \int_{r_p}^r \frac{\lambda_0}{\lambda(r')} \cdot 2\pi r' dr', \quad \frac{du}{dr} = \frac{\lambda_0}{\lambda(r) \cdot 2\pi r}. \quad (2.50)$$

Here,  $\lambda_0$  is a reference thermal conductivity the value of which can be chosen arbitrarily.

The radial heat flux of Equation 2.45 can now be written as

$$q(r, \tau) = -2\pi r \cdot \lambda(r) \cdot \frac{\partial T}{\partial r} = -2\pi r \cdot \lambda(r) \cdot \frac{\partial T}{\partial u} \cdot \frac{du}{dr} = -\lambda_0 \cdot \frac{\partial T}{\partial u}. \quad (2.51)$$

The heat flux as a function of  $u$  and  $\tau$  becomes

$$q_u(u, \tau) = -\lambda_0 \cdot \frac{\partial T_u}{\partial u}, \quad -\frac{\partial q_u}{\partial u} = \lambda_0 \cdot \frac{\partial^2 T_u}{\partial u^2}, \quad u \geq 0. \quad (2.52)$$

The heat balance of Equation 2.45 can now be written as

$$\rho c \cdot 2\pi r \cdot \frac{\partial T}{\partial \tau} \cdot \frac{dr}{du} = -\frac{\partial q}{\partial r} \cdot \frac{dr}{du} = -\frac{\partial q_u}{\partial u} = \lambda_0 \cdot \frac{\partial^2 T_u}{\partial u^2}. \quad (2.53)$$

Heat capacity for an annular region is the volumetric heat capacity times the area of the annular region. For the new coordinate  $u$  the heat capacity becomes

$$C_u(u) = \rho c \cdot 2\pi r \cdot \frac{dr}{du} = \rho c \cdot \pi \cdot \frac{d}{du} [(r(u))^2] = \frac{\lambda \rho c}{\lambda_0} \cdot [2\pi r(u)]^2. \quad (2.54)$$

In Equation 2.54, we used the expression for  $du/dr$  from Equation 2.50 to obtain the expression of capacity. The final expression for the heat equation with the new coordinate  $u$  is obtained by inserting  $C_u(u)$  from Equation 2.54 in Equation 2.53:

$$C_u(u) \cdot \frac{\partial T_u}{\partial \tau} = -\frac{\partial q_u}{\partial u}, \quad q_u(u, \tau) = -\lambda_0 \cdot \frac{\partial T_u}{\partial u}. \quad (2.55)$$

The new numerical solution is based on the one-dimensional heat conduction problem represented by Equation 2.55, using a constant thermal conductivity  $\lambda_0$ . We consider an equivalent-diameter pipe inside a borehole surrounded by homogeneous ground (soil). The two sets of thermal properties for the borehole and the ground (soil) region are

$$\lambda(r) = \begin{cases} \lambda_g & r_p \leq r < r_b \\ \lambda_s & r > r_b \end{cases}, \quad \rho(r)c(r) = \begin{cases} \rho_g c_g & r_p \leq r < r_b \\ \rho_s c_s & r > r_b \end{cases}, \quad a(r) = \begin{cases} \lambda_g / \rho_g c_g & r_p \leq r < r_b \\ \lambda_s / \rho_s c_s & r > r_b \end{cases}. \quad (2.56)$$

For the case of an equivalent diameter pipe in a borehole in the ground, the new coordinate  $u(r)$  from Equation 2.50 is

$$u(r) = \begin{cases} \frac{\lambda_0}{2\pi \cdot \lambda_g} \cdot \ln\left(\frac{r}{r_p}\right) & r_p \leq r \leq r_b \\ \frac{\lambda_0}{2\pi \cdot \lambda_g} \cdot \ln\left(\frac{r_b}{r_p}\right) + \frac{\lambda_0}{2\pi \cdot \lambda_s} \cdot \ln\left(\frac{r}{r_b}\right) & r > r_b \end{cases}. \quad (2.57)$$

We choose  $\lambda_0 = 2\pi \cdot \lambda_g$ . Equation 2.57 becomes

$$u(r) = \begin{cases} \ln\left(\frac{r}{r_p}\right) & r_p \leq r \leq r_b \\ \ln\left(\frac{r_b}{r_p}\right) + \frac{\lambda_g}{\lambda_s} \cdot \ln\left(\frac{r}{r_b}\right) & r > r_b \end{cases} \quad (2.58)$$

The  $u$ -coordinate at pipe and borehole radii become

$$u(r_p) = 0, \quad u_b = u(r_b) = \ln\left(\frac{r_b}{r_p}\right). \quad (2.59)$$

The radius as a function of  $u$  is obtained from Equation 2.57:

$$r(u) = \begin{cases} r_p \cdot \exp(u), & 0 \leq u \leq u_b \\ r_b \cdot \exp[(u - u_b) \cdot \lambda_s / \lambda_g], & u \geq u_b \end{cases}. \quad (2.60)$$

The borehole region and the soil outside the borehole are divided into  $N_b$  and  $N_s$  cells, respectively. The total number of cells is  $N = N_b + N_s$ . The temperature at the midpoint of cell  $n$  at time step  $v$  is  $T_{n,v}$  and the heat flux from cell  $n$  to  $n+1$  is  $q_{n,v}$  [W/m]. The initial temperatures for  $v=0$  are zero:  $T_{n,0}=0$ ,  $n=0,1,2,\dots,N$ .

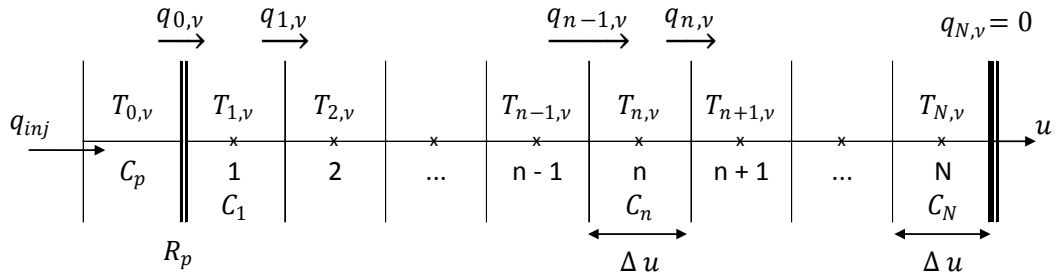


**Figure 2.5** Notations for the numerical solution

A constant cell width  $\Delta u$  and a time step of  $\Delta\tau$  are used for the heat transfer problem of Figure 2.5:

$$\Delta u = \frac{u_b}{N_b}, \quad N_s = 1 + \text{int}\left[\frac{\lambda_g}{\Delta u \cdot \lambda_s} \cdot \ln\left(\frac{\sqrt{p_{max} \cdot 4a_s \tau_{max}}}{r_b}\right)\right] \quad (2.61)$$

Here,  $\tau_{max}$  is the end time for the computations, and  $\text{int}[\dots]$  denotes the integer part. The number  $N_s$  is chosen so that the heat flux at the outer boundary is negligible for  $\tau \leq \tau_{max}$ . The particular expression is obtained from the line-source solution in soil. The criterion is that the heat flux at the outer boundary is smaller than  $(e^{-p_{max}} \cdot q_{inj})$  up to the maximum time  $\tau_{max}$ . The choice  $p_{max}=4$  is sufficient ( $e^{-4}=0.02$ ).

We use explicit forward differences to get the heat fluxes and the temperatures. The heat fluxes are

$$\begin{aligned} q_{0,v} &= K_0 \cdot (T_{0,v} - T_{1,v}), & q_{N,v} &= 0, \\ q_{n,v} &= K_u \cdot (T_{n,v} - T_{n+1,v}), & n &= 1, 2, \dots, N-1. \end{aligned} \quad (2.62)$$

The temperatures at the new time step,  $\tau = (v + I) \cdot \Delta\tau$ , are given by

$$\begin{aligned} T_{0,v+1} &= T_{0,v} + \frac{q_{inj} - q_{0,v}}{C_p} \cdot \Delta\tau, \\ T_{n,v+1} &= T_{n,v} + \frac{q_{n-1,v} - q_{n,v}}{C_n} \cdot \Delta\tau, & n &= 1, 2, \dots, N. \end{aligned} \quad (2.63)$$

The above set of Equations 2.62 and 2.63 gives the iterative numerical calculation procedure. The conductances  $K_0$  and  $K_u$ , the heat capacities  $C_n$  of all cells, and the time step  $\Delta\tau$  must be specified. The thermal conductances, in accordance with Equation 2.51 for  $\lambda_0 = 2\pi \cdot \lambda_g$ , are

$$K_u = \frac{2\pi \cdot \lambda_g}{\Delta u}, \quad K_0 = \frac{1}{R_p + 0.5 \Delta u / (2\pi \cdot \lambda_g)}. \quad (2.64)$$

Here,  $R_p$  is the pipe resistance and  $0.5 \cdot \Delta u / (2\pi \cdot \lambda_g)$  is the resistance from the pipe wall to the centre of the first cell. The heat capacity of cell  $n$  is equal to the area of the annular cell times the volumetric heat capacity:

$$C_n = \pi \{ [r(n \cdot \Delta u)]^2 - [r(n \cdot \Delta u - \Delta u)]^2 \} \cdot \begin{cases} \rho_g c_g & n = 1, \dots, N_b \\ \rho_s c_s & n = N_b + 1, \dots, N \end{cases} \quad (2.65)$$

To ensure numerical stability, the time step must satisfy the inequalities:

$$\Delta\tau \leq \min \left( \frac{C_{min}}{2K_u}, \frac{C_p}{K_0} \right), \quad C_{min} = \min_{1 \leq n \leq N} (C_n) \quad (2.66)$$

### 2.3.1.2 Comparison of analytical and numerical solutions

The analytical and numerical solutions were compared in a number of cases. The comparisons showed that the results from the analytical and numerical solutions are in complete agreement and that the deviations between the two solutions are smaller than 0.01 K in all cases. Figure 2.6 presents simulated fluid temperatures from both analytical and numerical solutions for one comparison. For this comparison, a heat injection rate of 50 W/m was used for 100 hours. The thermal properties of the fluid, pipe, grout and soil considered for the comparison are shown in Table 2.1. In this case, the response from the numerical solution was determined using 5 cells in the grout region and 38 cells in the soil region. Figure 2.7 shows the absolute difference in the predicted fluid temperatures from the analytical and numerical methods. The maximum absolute difference in fluid temperatures predicted by the two very different approaches is 0.004 K, while the average absolute difference is smaller than 0.002 K.

**Table 2.1** Thermal properties of the fluid, grout and soil considered for the comparison of the new models

| Element                        | Fluid + Pipe | Grout | Soil |
|--------------------------------|--------------|-------|------|
| Thermal conductivity (W/(m·K)) | 0.47 (pipe)  | 1.5   | 3.0  |
| Heat capacity (J/(kg·K))       | 4182 (fluid) | 2000  | 2500 |
| Density (kg/m <sup>3</sup> )   | 1000 (fluid) | 1550  | 750  |

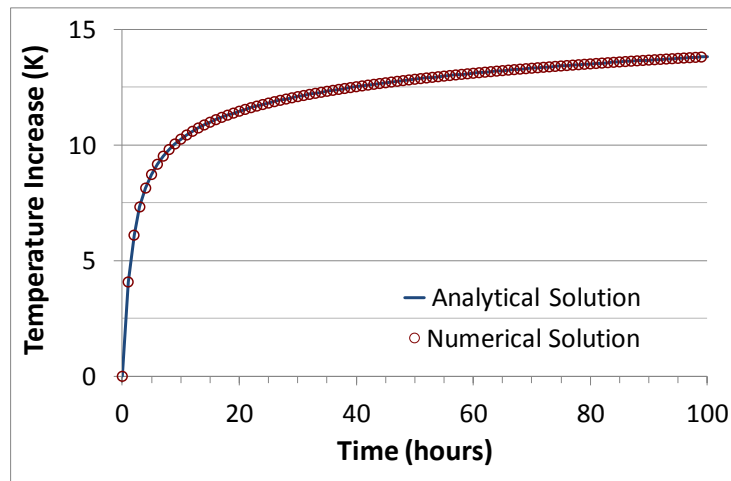


**Figure 2.6** Fluid temperature predicted by new analytical and numerical solutions for a test simulation

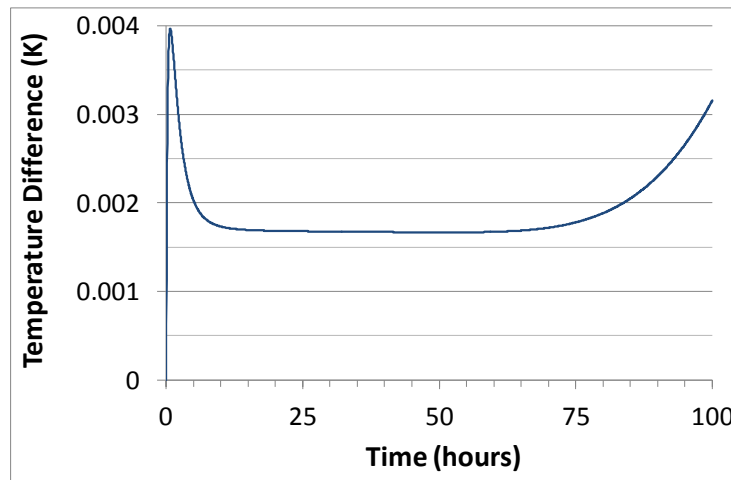


**Figure 2.7** Difference in fluid temperature predicted from analytical and numerical solutions for a test simulation

### 2.3.2 Validation using a semi-analytical solution

The analytical solution has also been validated against the composite model of Beier and Smith<sup>[12]</sup>. The composite model also uses the Laplace transformations approach to determine the borehole thermal response. The major difference between the composite model and the analytical solution is that the new solution is a fully analytical solution. The composite model, on the other hand, uses a numerical inversion technique<sup>[48]</sup> to invert the Laplace transforms in the real time and hence is semi-analytical. Another significant difference between the two solutions is that the composite model does not explicitly account for pipe and fluid resistances. Instead, the composite model accounts for the pipe and fluid resistances indirectly by adjusting the radius of the equivalent-diameter pipe or by adding the fluid temperature increase—because of the pipe and fluid resistances—to the predicted fluid temperature. On the contrary, the analytical solution directly considers all resistances, including those from the pipe and fluid when simulating the fluid temperatures.

Figure 2.8 shows the comparison of the analytical solution and the composite model for the test case of the previous section. The effects of fluid and pipe resistances were implicitly added to the fluid temperatures predicted from the composite model. As seen in Figure 2.8, the results from the analytical solution and the semi-analytical composite model are in very close agreement.

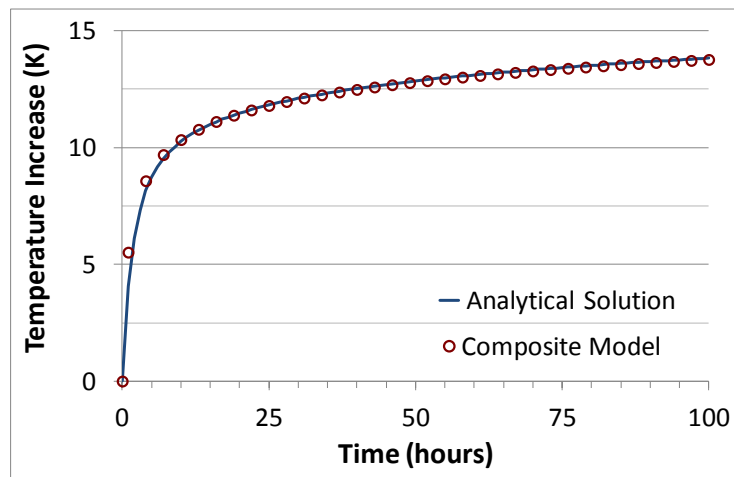


**Figure 2.8** Fluid temperatures from new solutions and the composite model

### 2.3.3 Validation using experimental data

The new analytical solution was also validated using the experimental data from a medium-scale laboratory setup. The sandbox setup has been used by various Oklahoma State University researchers<sup>[8, 12, 51]</sup> to simulate and validate their models under controlled conditions. Recently, Beier et al.<sup>[14]</sup> made reference data sets from the sandbox setup available for researchers to test and validate their borehole models. The sandbox setup is shown in Figure 2.9. The setup consists of a sandbox of dimensions 1.8 m x 1.8 m x 18 m. An aluminium pipe is centred horizontally along the length of the wooden box to simulate a borehole in the ground. The aluminium pipe contains a grouted U-tube, which is kept centred in

the aluminium pipe by means of spacers. Detailed specifications of aluminium pipe, U-tube, the grouting material and other sandbox elements can be found in the work of Beier et al.<sup>[14]</sup>



**Figure 2.9** Sandbox setup used to validate the new solution (Pictures courtesy of Professor Jeffrey Spangler<sup>[45]</sup>)

The sandbox was used to conduct the two different tests shown in Figure 2.10. The first test continued uninterrupted for approximately 50 hours. The power input used for the test had an average value and a standard deviation of approximately 1050 W and 4 W, respectively. The second test was also conducted for approximately 50 hours but with an input power interruption between 9 and 11 hours. The average value and the standard deviation of the input power used beyond the interruption period were approximately 595 W and 3 W, respectively. The supply and return temperatures of the fluid circulating in the U-tube were measured once a minute for both tests.

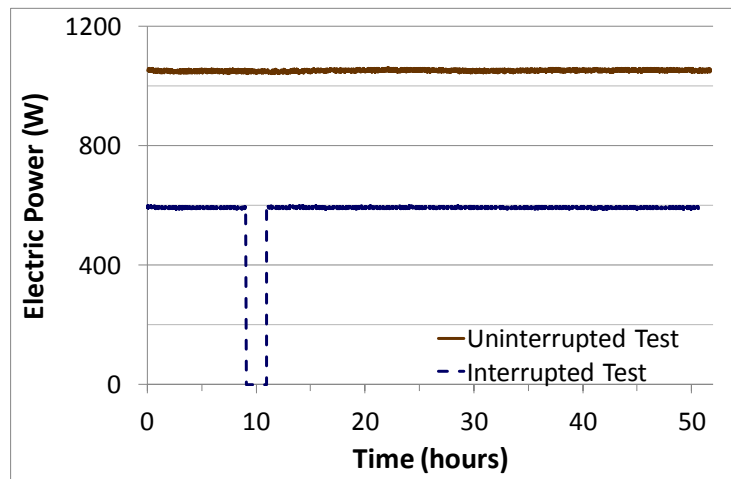


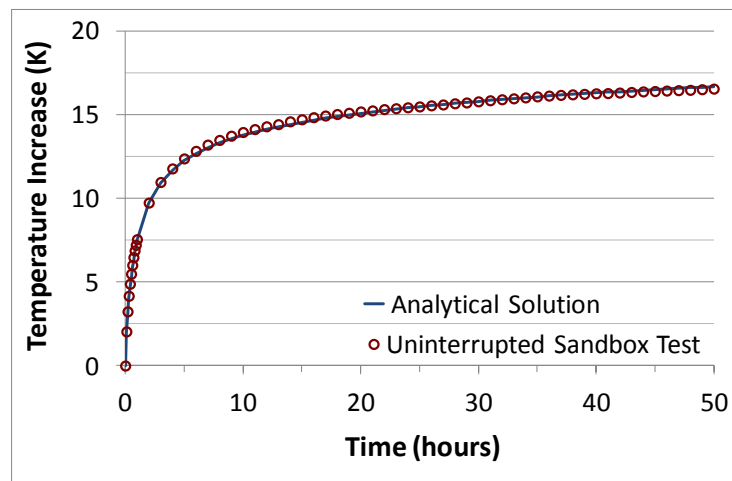
**Figure 2.10** Input powers for uninterrupted and interrupted sandbox tests

Before conducting the tests, independent measurements of the thermal properties of the sandbox elements were made. The independently measured thermal conductivity and volumetric heat capacity values of grouting material and soil are given in Table 2.2.

**Table 2.2** Independently measured thermal properties of the sandbox elements

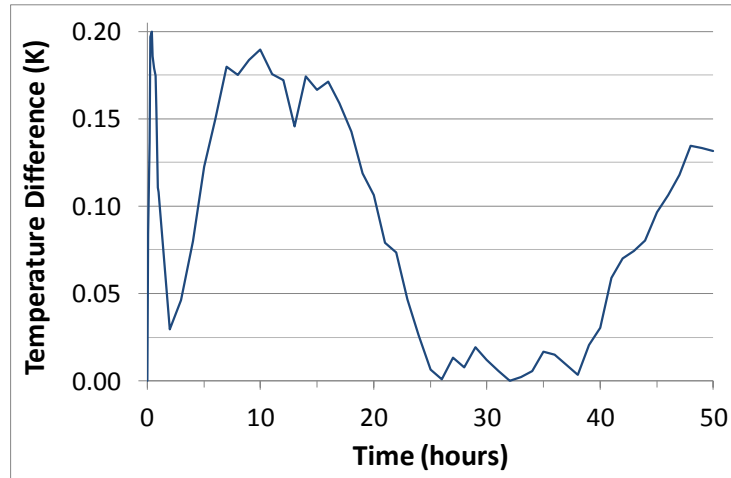
| Element  | Grout | Soil |
|--|-------|------|
| Thermal conductivity<br>(W/(m·K))                    | 0.73  | 2.82 |
| Volumetric Heat Capacity<br>(MJ/(m <sup>3</sup> ·K)) | 3.84  | 1.92 |

The new analytical solution was also validated against the two sandbox tests. The mean temperatures of the circulating fluid for the two sandbox tests were simulated by the analytical solution using independently measured thermal properties of Table 2.2 and average values of input powers used in the respective tests. The comparison of the simulated fluid temperatures in the new analytical solution and the experimentally measured temperatures for the uninterrupted sandbox test is presented in Figure 2.11. The mean fluid temperatures obtained in the new analytical method and experimental measurements are very similar.



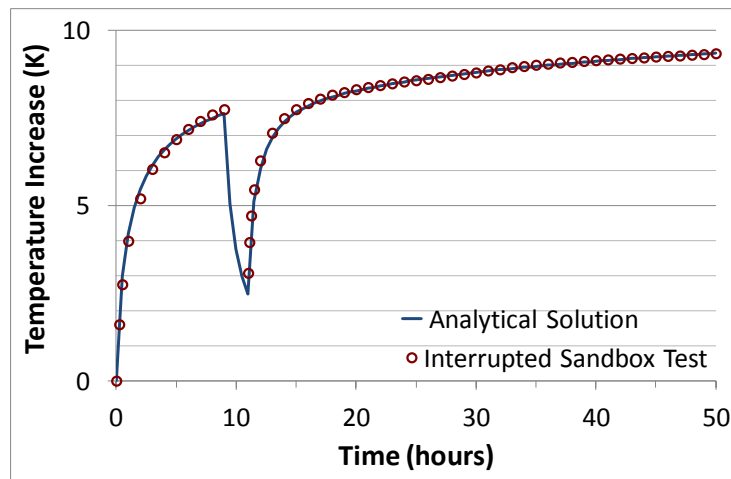
**Figure 2.11** Comparison of fluid temperatures from the analytical solution and the experimental data from the uninterrupted sandbox test

Figure 2.12 shows that the maximum absolute difference between the predicted and the measured temperatures is approximately 0.2 K, whereas the average absolute difference between the two data sets is less than 0.1 K. This difference is despite the fact that the variations in input power, though quite small, were not accounted for by the new analytical solution because an average value was used instead.



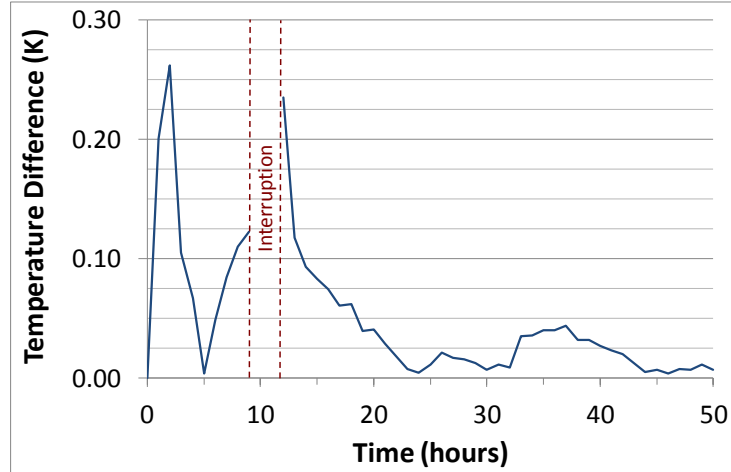
**Figure 2.12** Difference in fluid temperature from the new analytical solution and the experimental data from the uninterrupted sandbox test

Figure 2.13 presents the comparison of the mean fluid temperatures simulated in the analytical method and the experimentally measured temperatures for the interrupted test. The fluid temperature in the analytical solution is simulated by superposition of the temperature response on the average values of heat input levels used in the test.



**Figure 2.13** Comparison of fluid temperatures from the analytical solution and the experimental data from the interrupted sandbox test

Figure 2.14 shows the absolute difference between the simulated and the measured temperatures. The maximum absolute difference is approximately 0.26 K, whereas the average absolute difference is less than 0.1 K. Because the power to the circulation pump was also switched off during the interruption period, the fluid temperatures for 9-11 h were not measured.



**Figure 2.14** Difference in fluid temperature from the new analytical solution and the experimental data from the interrupted sandbox test

## 2.4 Conclusions

An analytical solution that is valid even for short periods has been developed. The solution was tested and validated using different approaches. Comparison of the analytical solution with a numerical solution shows that the results of the two solutions agree with a deviation less than 0.01 K. The results of the analytical solutions are also consistent with the results of an existing semi-analytical method adjusted for pipe and fluid resistances. The fluid temperatures predicted by the analytical solution are also in very good agreement with the experimental results of tests conducted under controlled laboratory conditions. A maximum difference of less than 0.3 K is observed between the simulated and the experimental results.

### 3 Multi-year Simulations

Accurate knowledge of the fluid temperatures exiting the borehole heat exchanger is necessary in order to optimize the design and performance of GSHP and ground storage systems. The fluid temperature exiting a borehole heat exchanger depends upon the thermal response of the borehole and the surrounding ground. For a multiple borehole heat exchanger, the exiting fluid temperature also depends upon the thermal interactions between the boreholes. The development of the thermal response of the ground surrounding the borehole field is a slow process because the thermal capacity of the ground surrounding a borehole field is very large. Hence, typically, a time resolution of months or years is used to study the temperature development of the ground. On the other hand, the borehole heat exchanger itself has limited thermal mass and capacity and, consequently, the heat transfer inside the borehole is more sensitive to any changes in the prescribed injection or extraction rates. As a result, the thermal response of the borehole is quite rapid and is, therefore, studied using a time resolution ranging from minutes to hours. The development of thermal interactions between different boreholes is again a slow and long-term process and thus requires monthly or yearly time resolution. Determining the accurate borehole fluid temperatures is an intricate procedure because it involves thermal processes that vary from short- to long-term intervals, with time resolutions ranging from minutes to years. At present, no single analytical model exists that can perform rapid simulations of single and multiple borehole heat exchangers—from short to long time durations—that accurately determine the extraction fluid temperatures. Another key challenge associated with multi-year simulations of borehole heat exchangers is the use of hourly load values. The heating and cooling demands of a building and the resulting loads on a borehole heat exchanger are presented typically as annual hourly values. Simulations using hourly borehole loads to determine extraction fluid temperatures—15–25 years forward in time—involve high computational effort and therefore are very time-consuming.

This chapter addresses the above issues and presents an analytical approach to compute step-response functions that are valid in short- to long-time scales. The step-response functions are then used together with a load aggregation scheme to conduct multi-year simulations. The presented approach can be used to calculate extraction fluid temperatures for both single and multiple borehole heat exchangers.

#### 3.1 Background

Let  $Q_{step}$ , as shown in Figure 3.1a, be a constant heat injection rate starting at  $\tau = 0$  for a single borehole or a system of multiple vertical boreholes. The required temperature of the heat carrier fluid in the pipes of the boreholes to sustain this injection rate is a basic tool in the analysis of the dynamic relations between heat injection/extraction and fluid temperatures. This step-response temperature  $T_{step}(\tau)$ , shown in Figure 3.1b, increases monotonously from zero at  $\tau = 0$  to a steady-state value  $T_{step}(\infty)$  at very large times.

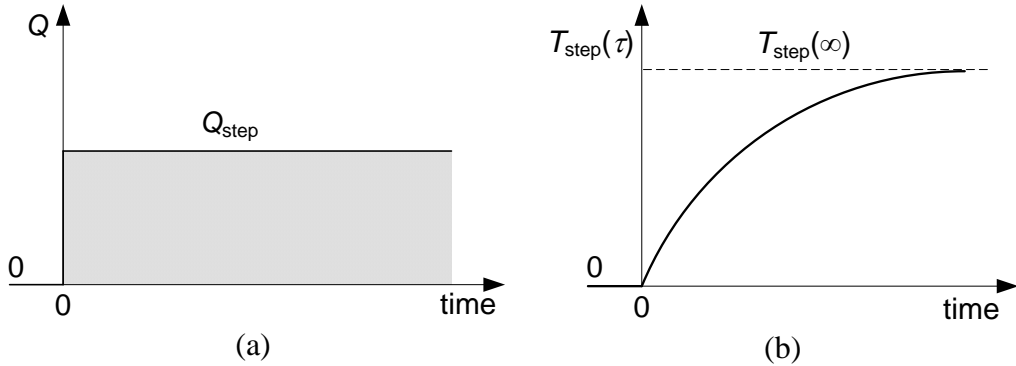


**Figure 3.1** Temperature response  $T_{step}(\tau)$  for a constant heat injection step  $Q_{step}$

The step-response solution for temperature concerns the excess temperature above undisturbed ground and borehole conditions. This means that the initial temperature of the ground and the borehole with the heat carrier fluid is zero for the step-response solution. The steady-state temperature defines the thermal resistance  $R_{ss}$  between the heat carrier fluid and the surrounding ground:

$$T_{step}(\infty) = R_{ss} \cdot Q_{step}, \quad R_{ss} = T_{step}(\infty)/Q_{step} \quad (3.1)$$

For time-varying heat loads, the prescribed heat injection rate can be treated as constant during each time step. Figure 3.2 shows an example of piece-wise constant heat injections for each time-step. The prescribed injection rate  $Q_{in}(\tau)$  can include any number of heat pulses  $Q_n$ . The heat injection to the ground is taken as positive, whereas the heat extraction from the ground is treated as negative. The length  $h$  (seconds or hours) of the time step may be chosen at will. The number of pulses  $n_{max}$  is very large to cover a calculation period of up to, for example,  $\tau_{max} = 20$  years.

$$\begin{aligned} Q_{in}(\tau) &= Q_n, & nh - h < \tau \leq nh, \\ n &= 1, n_{max}; \quad \tau_{max} = n_{max}. \end{aligned} \quad (3.2)$$

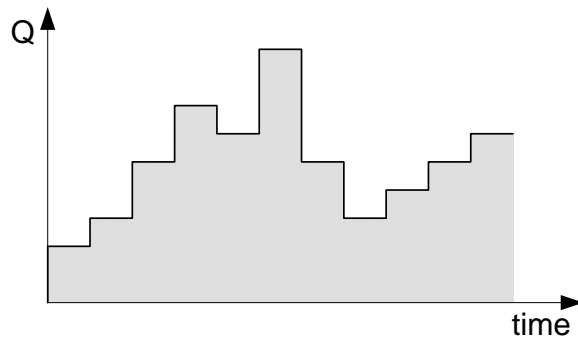


**Figure 3.2** Piece-wise constant heat injections for each time-step

Due to the preceding pulses, the fluid temperature,  $T_f(nh)$  at the end of pulse  $n$  may be obtained by superposition of the solution from each of the preceding pulses  $Q_{n+1-v}$ ,  $v=1, \dots, n$ :

$$T_f(nh) = \sum_{v=1}^n \frac{Q_{n+1-v}}{Q_{step}} \cdot [T_{step}(vh) - T_{step}(vh-h)]. \quad (3.3)$$

Here,  $v$  enumerates the pulses backwards in time. By superposition, pulse  $v$  may be considered a step that starts at the time  $vh$  before  $\tau = nh$  minus a second step that starts at the time  $vh-h$  before  $\tau = nh$ , as given by the expression within the brackets. Figure 3.3 provides further explanation of the super-positioning principle.

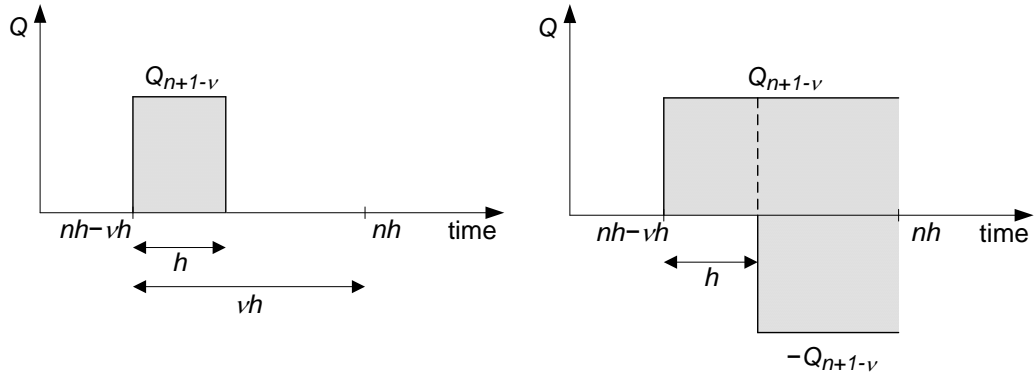


**Figure 3.3** Superposition of heat pulses

Alternatively, we can use a second notation for the injection values for a better representation:

$$Q_{n+1-v} = Q_v^{(n)} = Q_{in}((n+1-v)h), \quad v = 1, \dots n. \quad (3.4)$$

The fluid temperature at time step  $n$  is given by the sum (Equation 3.3) of the preceding injection rates times a factor that depends on  $v$ :

$$T_f(nh) = \sum_{v=1}^n Q_v^{(n)} \cdot R_v = R_{ss} \cdot \sum_{v=1}^n Q_v^{(n)} \cdot \kappa_v. \quad (3.5)$$

The thermal resistance factors  $R_v$  and the dimensionless factors  $\kappa_v$  are given by

$$R_v = \frac{T_{step}(vh) - T_{step}(vh-h)}{Q_{step}}, \quad (3.6)$$

$$\kappa_v = \frac{T_{step}(vh) - T_{step}(vh-h)}{T_{step}(\infty)} = \frac{R_v}{R_{ss}}.$$

An advantage of using the thermal resistance factors  $R_v$  is that the final steady-state value  $T_{step}(\infty)$  is not needed. However, the dimensionless weighting factors  $\kappa_v$  directly give the relative influence of the preceding injection rates. The weighting factor is determined by the increase of the step-response function over the time from  $vh-h$  to  $vh$  divided by the total increase of  $T_{step}(\tau)$  from zero to infinity, as shown in Figure 3.4. The sum of the weighting factors tends to 1 as  $v$  tends to infinity.

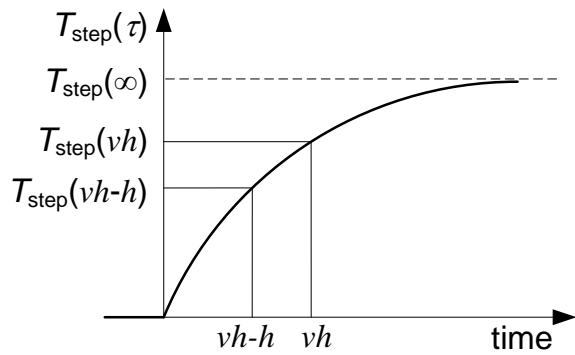


**Figure 3.4** Step-response fluid temperature over time step  $h$

The calculations are performed for consecutive time steps. The loads are shifted one step from time  $n-1$  to  $n$ :

$$Q_{v+1}^{(n)} = Q_v^{(n-1)}, \quad v = 1, \dots n-1, \quad Q_1^{(n)} = Q_{in}(nh). \quad (3.7)$$

The required number of terms in the summation of Equation 3.5 increases with the number of time steps. After 10 years, with  $h=1$  hour, a summation of 87,600 preceding values is required. The weighting factors decrease strongly with  $v$ , but the factors for larger  $v$  cannot be neglected since there are so many. The idea of a solution that uses some kind of aggregated values for preceding loads in suitable time intervals before the considered time is implemented later in this chapter.

## 3.2 Step-response functions

*This section is based on Paper V.*

Step-response is an important tool for the thermal analysis of borehole heat exchangers. The step-response solution gives the fluid temperature required for a *constant* injection rate  $q_0$  (W/m). The time derivative of the step-response shows how the preceding extraction rates influence the extraction fluid temperature. In other words, the time derivative of the step-response provides a weighting function for the preceding injection rates. The step-response functions may be computed using different approaches. They can be determined using analytical methods, such as classical line<sup>[28]</sup> and cylindrical<sup>[19]</sup> source solutions or numerical methods like superposition borehole model<sup>[22]</sup>. The step-response functions determined from these approaches are valid for medium- to large-periods. Yavuzturk<sup>[51]</sup> and Xu and Spitler<sup>[50]</sup> determined step-response functions for short times using numerical methods. This section provides a methodology to calculate the response function from very short periods (minutes) to very long periods (years or longer). For short times, up to 100 hours, the analytical radial solution presented in Chapter 2 is used. After this point, a finite line-source solution described in the following sections is used. The line-source response function for single boreholes and any configuration of vertical boreholes has been reduced to one integral only.

### 3.2.1 Finite line-source solution

We assume that the borehole acts as a continuous line heat source of strength  $q_0$  (W/m) at  $x = 0$ ,  $y = 0$ , and  $0 < z < H$ . If the initial ground temperature is zero and the heat emission starts at  $\tau = 0$ , the temperature distribution  $T(r, z, \tau)$  can be obtained by a double integration of the point heat source solution<sup>[19]</sup> in time from zero to  $\tau$  and along the borehole length from zero to  $H$ .

$$T(r, z, \tau) = \int_0^\tau d\tau' \int_0^H dz' \frac{q_0}{\rho c [4\pi a(\tau - \tau')]^{1.5}} \cdot e^{-\frac{r^2 + (z-z')^2}{4a(\tau - \tau')}} , \quad (3.8)$$

$$r = \sqrt{x^2 + y^2}, \quad q_0 = Q_{step}/H.$$

Equation 3.8 can be rewritten as

$$T(r, z, \tau) = \frac{q_0}{4\pi\lambda} \int_{1/\sqrt{4a\tau}}^\infty ds \cdot e^{-r^2 s^2} \cdot \frac{2}{\sqrt{\pi}} \int_0^H dz' \cdot e^{-s^2 (z-z')^2}, \quad (3.9)$$

$$s = 1/\sqrt{4a(\tau - \tau')}.$$

To achieve zero temperature at ground level  $z = 0$ , a mirror sink is introduced above the ground surface. The line-source solution corrected by the addition of a mirror sink is obtained by subtracting  $T(r, -z, \tau)$  from the above solution. In the following line-source solution, the last exponential in the second integral represents the mirror sink:

$$T_{ls}(r, z, \tau) = \frac{q_0}{4\pi\lambda} \int_{1/\sqrt{4a\tau}}^\infty ds \cdot e^{-r^2 s^2} \cdot$$

$$\frac{2}{\sqrt{\pi}} \int_0^H dz' [e^{-s^2 (z-z')^2} - e^{-s^2 (z+z')^2}]. \quad (3.10)$$

We are particularly interested in the mean temperature over the borehole length  $0 < z < H$  at any radial distance  $r$ :

$$\bar{T}_{ls}(r, \tau) = \frac{1}{H} \cdot \int_0^H T_{ls}(r, z, \tau) dz. \quad (3.11)$$

The integral mean temperature over the borehole length is obtained by substituting  $T_{ls}(r, z, \tau)$  from Equation 3.10 into Equation 3.11:

$$\bar{T}_{ls}(r, \tau) = \frac{q_0}{4\pi\lambda} \int_{1/\sqrt{4a\tau}}^\infty ds \cdot e^{-r^2 s^2} \cdot$$

$$\underbrace{\frac{2}{H\sqrt{\pi}} \cdot \int_0^H dz \int_0^H dz' [e^{-s^2 (z-z')^2} - e^{-s^2 (z+z')^2}]}_I. \quad (3.12)$$

The above expression of integral mean temperature is further simplified by evaluating the double integral  $I$ . Firstly, substitutions  $sz = u$  and  $sz' = v$  are made:

$$I = \frac{1}{Hs^2} \cdot \frac{2}{\sqrt{\pi}} \cdot \int_0^{Hs} du \int_0^{Hs} dv [e^{-(u-v)^2} - e^{-(u+v)^2}]. \quad (3.13)$$

Equation 3.13 can be rewritten as

$$I = \frac{1}{Hs^2} \cdot I_{ls}(h), \quad h = Hs. \quad (3.14)$$

We now evaluate the double integral  $I_{ls}(h)$ :

$$I_{ls}(h) = \frac{2}{\sqrt{\pi}} \cdot \int_0^h du \int_0^h dv [e^{-(u-v)^2} - e^{-(u+v)^2}]. \quad (3.15)$$

To solve the Equation 3.15 further, we define

$$F(X, Y) = \frac{2}{\sqrt{\pi}} \cdot \int_0^X du \int_0^Y dv \cdot e^{-(u-v)^2}. \quad (3.16)$$

The function  $F(X, -Y)$  becomes

$$F(X, -Y) = \frac{2}{\sqrt{\pi}} \cdot \int_0^X du \int_0^{-Y} dv \cdot e^{-(u-v)^2}. \quad (3.17)$$

Substituting  $v = -v'$  in Equation 3.17 gives

$$F(X, -Y) = \frac{2}{\sqrt{\pi}} \cdot \int_0^X du \int_0^Y (-)dv' \cdot e^{-(u+v')^2}, \quad (3.18)$$

$$= -\frac{2}{\sqrt{\pi}} \cdot \int_0^X du \int_0^Y dv \cdot e^{-(u+v)^2}. \quad (3.19)$$

Equation 3.15 can now be written as

$$I_{ls}(h) = F(h, h) + F(h, -h). \quad (3.20)$$

We now consider the second integral of Equation 3.16 and make the substitution  $u - v = v'$  in this integral:

$$\frac{2}{\sqrt{\pi}} \cdot \int_0^Y dv \cdot e^{-(u-v)^2} = \frac{2}{\sqrt{\pi}} \int_u^{u-Y} (-)dv' \cdot e^{-(v')^2} = \text{erf}(u) - \text{erf}(u - Y). \quad (3.21)$$

Here,  $\text{erf}(u)$  denotes the error function.

Equation 3.21 is used to rewrite Equation 3.16 as:

$$F(X, Y) = \int_0^X \text{erf}(u) du - \int_0^X \text{erf}(u - Y) du. \quad (3.22)$$

Substituting  $u - Y = u'$  in Equation 3.22 results in

$$F(X, Y) = \int_0^X \operatorname{erf}(u) du - \int_{-Y}^{X-Y} \operatorname{erf}(u') du'. \quad (3.23)$$

We have

$$\operatorname{i erf}(X) = \int_0^X \operatorname{erf}(u) du = X \cdot \operatorname{erf}(X) - \frac{1}{\sqrt{\pi}} (1 - e^{-X^2}). \quad (3.24)$$

We can now rewrite Equation 3.23 as

$$\begin{aligned} F(X, Y) &= \operatorname{i erf}(X) - \operatorname{i erf}(X - Y) + \operatorname{i erf}(-Y), \\ &= \operatorname{i erf}(X) - \operatorname{i erf}(X - Y) + \operatorname{i erf}(Y). \end{aligned} \quad (3.25)$$

Similarly,  $F(X, -Y)$  of Equation 3.19 is equal to:

$$F(X, -Y) = \operatorname{i erf}(X) - \operatorname{i erf}(X + Y) + \operatorname{i erf}(-Y). \quad (3.26)$$

Equations 3.25 and 3.26 can now be used to rewrite Equation 3.20 to give the final expression of the double integral:

$$I_{ls}(h) = 4 \cdot \operatorname{i erf}(h) - \operatorname{i erf}(2h). \quad (3.27)$$

The mean temperature (Equation 3.12) over the borehole length can now be represented as a single integral:

$$\bar{T}_{ls}(r, \tau) = \frac{q_0}{4\pi\lambda} \cdot \int_{1/\sqrt{4a\tau}}^{\infty} ds \cdot e^{-r^2 s^2} \cdot \frac{I_{ls}(Hs)}{Hs^2}. \quad (3.28)$$

The mean temperature at the borehole radius  $r_b$  gives the long-term response for a single borehole:

$$T_1(\tau) = \bar{T}_{ls}(r_b, \tau). \quad (3.29)$$

### 3.2.2 Finite line-source solution for multiple boreholes

The new line-source solution can also be extended to determine the long-term response of multiple borehole systems. Let us assume a field of  $N$  vertical and parallel boreholes, each of height  $H$ . The boreholes are taken to be at positions  $(x_j, y_j, z)$ ,  $0 < z < H$ ,  $j = 1, 2, \dots, N$ . The temperature distribution for the total field becomes

$$T(x, y, z, \tau) = \sum_{j=1}^N T_{ls} \left( \sqrt{(x - x_j)^2 + (y - y_j)^2}, z, \tau \right). \quad (3.30)$$

The mean temperature is needed along the borehole wall (bw) for any borehole  $i$ .

$$\bar{T}_{bw,i}(\tau) = \sum_{j=1}^N \bar{T}_{ls}(r_{i,j}, \tau). \quad (3.31)$$

Here  $r_{i,j}$  denotes the radial distance between borehole  $i$  and  $j$  ( $i \neq j$ ). The contribution from the internal heat source of the borehole  $i$  is obtained for the radial distance  $r_b$ :

$$r_{i,i} = r_b, \quad r_{i,j} = \sqrt{(x_i - x_j)^2 + (y_i - y_j)^2} \quad i \neq j. \quad (3.32)$$

The mean borehole wall temperature for the entire set of  $N$  boreholes is

$$\frac{1}{N} \sum_{i=1}^N \bar{T}_{bw,i}(\tau) = \frac{1}{N} \sum_{i=1}^N \sum_{j=1}^N \bar{T}_{ls}(r_{i,j}, \tau). \quad (3.33)$$

This mean temperature is used as the response function. Using Equation 3.28, the response function for  $N$  boreholes may now be written in the following way:

$$T_N(\tau) = \frac{q_0}{4\pi\lambda} \cdot \int_{1/\sqrt{4a\tau}}^{\infty} ds \cdot I_e(s) \cdot \frac{I_{ls}(Hs)}{Hs^2}, \quad q_0 = Q_{step}/N \cdot H. \quad (3.34)$$

Here, the function  $I_e(s)$  involves a double sum in the exponentials

$$I_e(s) = \frac{1}{N} \sum_{i=1}^N \sum_{j=1}^N e^{-r_{i,j}^2 s^2}. \quad (3.35)$$

For multiple borehole heat exchangers, the exponential function  $I_e(s)$  depends upon the size and the configuration of the borehole field. The following examples show how the exponential function  $I_e(s)$  can be obtained for different configurations of multiple borehole heat exchangers.

The first example considers three boreholes in a straight line (Figure 3.5), separated by the spacing  $B$ . The double sum in Equation 3.35 involves nine terms. The exponent involves the distances  $r_{i,j}$ . Three terms involve  $r_b$ , four terms involve  $B$ , and two terms involve  $2B$ . The exponential function  $I_e(s)$  for three boreholes in a line configuration is given by Equation 3.36. The sum of the factors before the exponentials is  $3+4+2=9$ .

$$I_e(s) = \frac{1}{3} [3 \cdot e^{-r_b^2 s^2} + 4 \cdot e^{-B^2 s^2} + 2 \cdot e^{-(2B)^2 s^2}]. \quad (3.36)$$

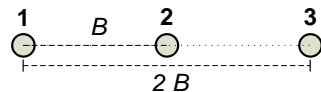


**Figure 3.5** Three boreholes in a  $1 \times 3$  line configuration

The second example considers four boreholes (Figure 3.6) in a  $2 \times 2$  square configuration with spacing  $B$ . The double sum (Equation 3.35) now involves  $4 \times 4 = 16$  terms. The exponent involves distances  $r_b$ ,  $B$ , and  $\sqrt{2}B$ . For example, in Figure 3.6, the distance  $B$  occurs eight times between boreholes: 1 to 2, 1 to 3, 2 to 1, 2 to 4, 3 to 1, 3 to 4, 4 to 2 and 4 to 3. Similarly, diagonal distance  $\sqrt{2}B$  occurs four times between boreholes: 1 to 4, 2 to 3, 3 to 2, and 4 to 1. Counting

the number of occurrences for each distance gives exponential function  $I_e(s)$  for four boreholes in a square configuration as

$$I_e(s) = \frac{1}{4} [4 \cdot e^{-r_b^2 s^2} + 8 \cdot e^{-B^2 s^2} + 4 \cdot e^{-(\sqrt{2}B)^2 s^2}]. \quad (3.37)$$

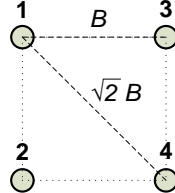


**Figure 3.6** Four boreholes in a  $2 \times 2$  square configuration.

The third example considers five boreholes in a  $3 \times 3$  L-configuration (Figure 3.7). For five boreholes, the double sum of Equation 3.35 involves 25 terms. The exponent involves the distances  $r_b$ ,  $B$ ,  $\sqrt{2}B$ ,  $2B$ ,  $\sqrt{5}B$ , and  $\sqrt{8}B$ . The exponential function  $I_e(s)$  for five boreholes in L-configuration is obtained by counting the number of occurrences for each distance.

$$I_e(s) = \frac{1}{5} [5 \cdot e^{-r_b^2 s^2} + 8 \cdot e^{-B^2 s^2} + 2 \cdot e^{-(\sqrt{2}B)^2 s^2} + 4 \cdot e^{-(2B)^2 s^2} + 4 \cdot e^{-(\sqrt{5}B)^2 s^2} + 2 \cdot e^{-(\sqrt{8}B)^2 s^2}]. \quad (3.38)$$

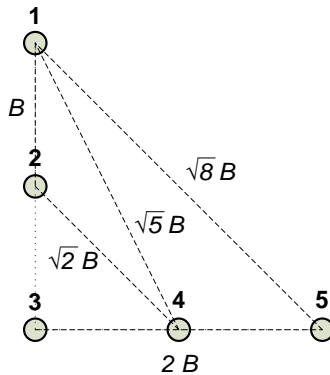


**Figure 3.7** Five boreholes in a  $3 \times 3$  L-configuration

In the fourth example, we consider six boreholes in a  $2 \times 3$  rectangular configuration with spacing  $B$  (Figure 3.8). The double sum (Equation 3.35) involve 36 terms. The exponent involves the distances  $r_b$ ,  $B$ ,  $\sqrt{2}B$ ,  $2B$ , and  $\sqrt{5}B$ . The exponential function  $I_e(s)$  for  $2 \times 3$  rectangular configuration becomes

$$I_e(s) = \frac{1}{6} [6 \cdot e^{-r_b^2 s^2} + 14 \cdot e^{-B^2 s^2} + 8 \cdot e^{-(\sqrt{2}B)^2 s^2} + 4 \cdot e^{-(2B)^2 s^2} + 4 \cdot e^{-(\sqrt{5}B)^2 s^2}]. \quad (3.39)$$

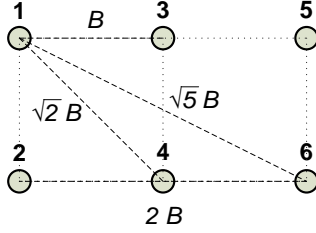


**Figure 3.8** Six boreholes in a  $2 \times 3$  rectangular configuration

The next example considers seven boreholes in a  $5 \times 2$  U-configuration (Figure 3.9). For seven boreholes, the double sum of Equation 3.35 involves  $7 \times 7 = 49$  terms. The exponent involves the distances  $r_b$ ,  $B$ ,  $\sqrt{2}B$ ,  $2B$ ,  $\sqrt{5}B$ ,  $3B$ ,  $\sqrt{10}B$ ,  $4B$ , and  $\sqrt{17}B$ . The exponential function  $I_e(s)$  for seven boreholes in a  $5 \times 2$  U-configuration is

$$I_e(s) = \frac{1}{7} \left[ 7 \cdot e^{-r_b^2 s^2} + 12 \cdot e^{-B^2 s^2} + 4 \cdot e^{-(\sqrt{2}B)^2 s^2} + 6 \cdot e^{-(2B)^2 s^2} + 4 \cdot e^{-(\sqrt{5}B)^2 s^2} + 4 \cdot e^{-(3B)^2 s^2} + 4 \cdot e^{-(\sqrt{10}B)^2 s^2} + 4 \cdot e^{-(4B)^2 s^2} + 4 \cdot e^{-(\sqrt{17}B)^2 s^2} \right]. \quad (3.40)$$

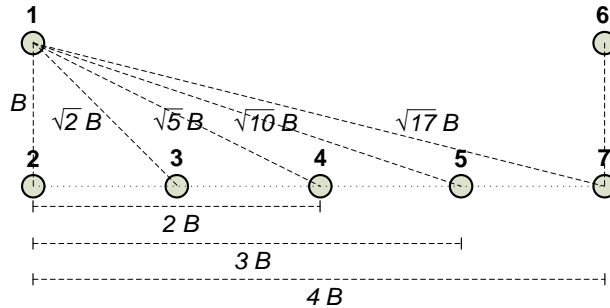


**Figure 3.9** Seven boreholes in a  $5 \times 2$  U-configuration

Next, we consider eight boreholes in a  $3 \times 3$  open rectangular configuration with spacing  $B$  (Figure 3.10). The double term (Equation 3.35) involves 64 terms. The exponent involves distances  $r_b$ ,  $B$ ,  $\sqrt{2}B$ ,  $2B$ ,  $\sqrt{5}B$ , and  $\sqrt{8}B$ . The exponential function  $I_e(s)$  for eight boreholes in open rectangular configuration becomes:

$$I_e(s) = \frac{1}{8} \left[ 8 \cdot e^{-r_b^2 s^2} + 16 \cdot e^{-B^2 s^2} + 8 \cdot e^{-(\sqrt{2}B)^2 s^2} + 12 \cdot e^{-(2B)^2 s^2} + 16 \cdot e^{-(\sqrt{5}B)^2 s^2} + 4 \cdot e^{-(\sqrt{8}B)^2 s^2} \right]. \quad (3.41)$$

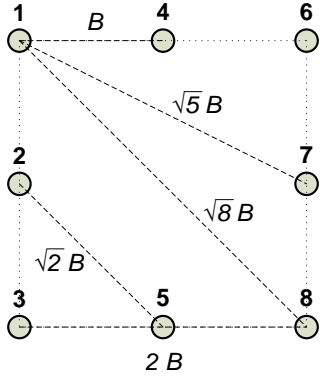


**Figure 3.10** Eight boreholes in a  $3 \times 3$  open rectangular configuration

Finally, we consider nine boreholes in a square configuration of Figure 3.11. The double sum of Equation 3.35 now involves  $9 \times 9 = 81$  terms. The exponent involves the distances  $r_b$ ,  $B$ ,  $\sqrt{2}B$ ,  $2B$ ,  $\sqrt{5}B$ , and  $\sqrt{8}B$ . Counting the number of occurrences for each distance yields

$$I_e(s) = \frac{1}{9} [9 \cdot e^{-r_b^2 s^2} + 24 \cdot e^{-B^2 s^2} + 16 \cdot e^{-(\sqrt{2}B)^2 s^2} + 12 \cdot e^{-(2B)^2 s^2} + 16 \cdot e^{-(\sqrt{5}B)^2 s^2} + 4 \cdot e^{-(\sqrt{8}B)^2 s^2}]. \quad (3.42)$$

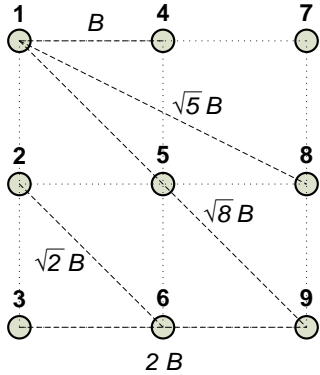


**Figure 3.11** Nine boreholes in a  $3 \times 3$  rectangular configuration

### 3.2.3 Combined step-response functions

The short-term solution presented in Chapter 2 and the finite line-source solution demonstrated in the previous sections are used together to obtain a combined step-response. In comparison with the finite line-source solution, the short-term analytical solution is computational heavy. Hence, it is used only up to a certain time to account for the short-term response. After that time, the finite line-source solution is used. However, the line-source solution needs to be adjusted for thermal processes inside the borehole because the line-source solution does not account for thermal resistances over the pipe and the grout. In order to obtain the circulating fluid temperatures, the effects of pipe and grout resistances are added

to the borehole wall temperatures obtained by the finite line-source solution. This adjustment is illustrated in Figure 3.12.

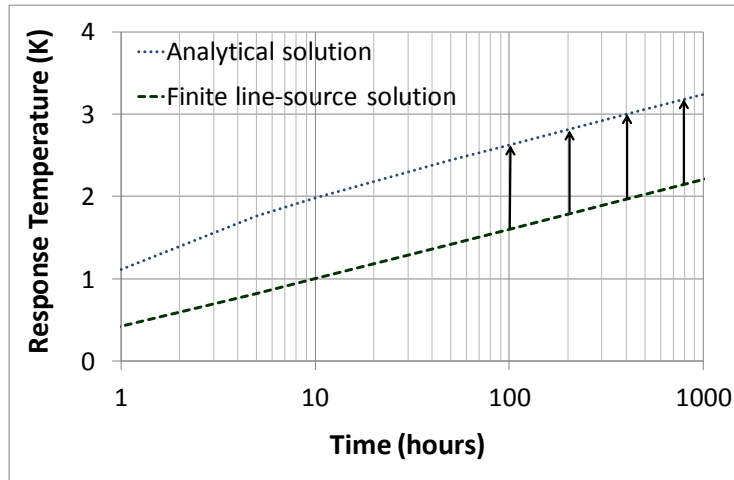


**Figure 3.12** Response temperatures from analytical and finite line-source solutions

The top curve in the figure shows the temperature response of a ground heat exchanger from the analytical solution, which accounts for the local thermal processes inside the borehole. The lower curve shows the corresponding response from the finite line-source solution, which does not consider the local thermal processes inside the borehole. The difference between the two curves after a certain time, which is 100 hours in this case, is due to the effects of the pipe and grout resistances on the temperature of the circulating fluid. In order to account for the temperature increase due to the pipe and grout resistances, the response of the finite line-source solution is shifted upwards so that the analytical and the line-source solutions coincide at a suitable breaking time. This adjustment results in a step-response function that uses the response from the analytical solution up to the breaking point in addition to the response, including the upward shift, from the finite line-source solution after the breaking point. The choice of the breaking time is not critical because the difference between the two curves is almost the same—between 10 and 1000 hours.

Figure 3.13 shows the combined response functions obtained for three example cases of a single borehole, three boreholes in a straight line (Figure 3.5) and nine boreholes in a square (Figure 3.11). The step-response functions were developed for a heat flux of 10 W/m injected into a 110 mm diameter borehole with a single equivalent-diameter pipe. The ground surrounding the borehole heat exchangers was assumed to have thermal conductivity, density and heat capacity values of 3 W/(m·K), 2500 kg/m<sup>3</sup> and 750 J/(kg·K), respectively. The considered values of these properties for the grout region were 1.5 W/(m·K), 1550 kg/m<sup>3</sup> and 2000 J/(kg·K), respectively.

The figure also compares the combined step-response functions to the fluid temperatures predicted by the Eskilson's *g-functions* approach<sup>[22]</sup>. The comparison is performed only for medium to large periods due to the limitations of the *g-function* approach for shorter time scales. It can be seen that, in all three cases,

the difference between the two approaches is reasonably small up to 25 years (2.2.E+05). The difference between the two approaches increases with time and with the number of boreholes. However, it should be noted that using a higher injection rate of 10 W/m for the considered cases, instead of unit injection rate, increased the differences shown in Figure 3.13 by a factor of ten.

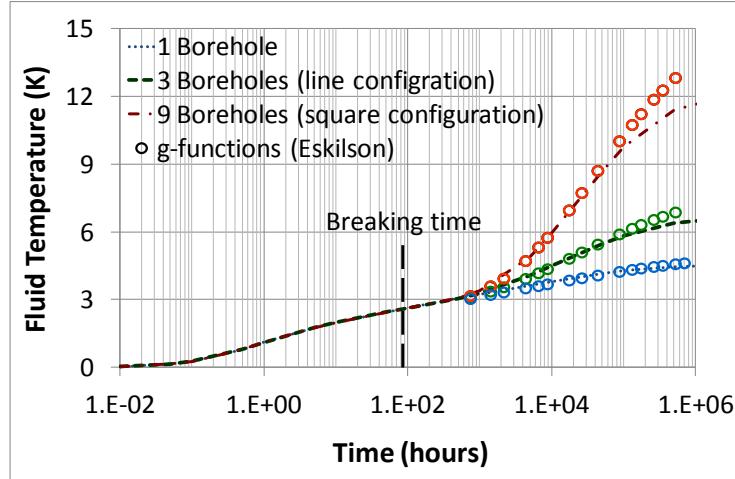


**Figure 3.13** Combined step-response functions for one, three and nine boreholes

### 3.3 Load aggregation scheme for multi-year simulations

*This section is based on one of the additional publications (Paper 7 on Page viii).*

Multi-year simulations of a borehole heat exchanger performed over a period from 20 to 25 years involve approximately 200,000 hourly load values. These values, if not aggregated, can lead to unacceptably long computational times. A load aggregation scheme is presented to perform rapid yet accurate multi-year simulations of borehole systems. The starting point is the step-response function for the considered borehole system and the annual hourly heating and cooling loads:

$$T_{step}(\tau), \quad 0 \leq \tau < \infty \text{ (or } 0 \leq \tau < \tau_{max}); \\ Q_{in}(nh), \quad n = 1, \dots n_{max}. \quad (3.43)$$

In this study, the combined step-response function approach discussed in the previous section is used. However, it is also possible to implement the load aggregation scheme using step-response functions or *g-functions* determined from other approaches. First, the thermal resistance between the circulating fluid and the surrounding ground is determined from Equation 3.1 by using the step-injection rate and the steady-state temperature. The time step  $h$  and the magnitude of the injection step are not critical and thus can be chosen at will.

Next, the loads to be aggregated are placed in a long sequence of “cells”. The original loads from cells  $v=1$  to  $v=P_1$  are kept without aggregation on the first level  $q=1$ . Loads are aggregated on the following levels. At the second level  $q=2$ ,

there are  $P_2$  lumped cells each with a width  $2h$ . Similarly, the third level  $q=3$  has  $P_3$  lumped cells, each with a width  $4h$ . The doubling of cell width is continued to the last level  $q_{max}$  so that the aggregated cells cover all original non-aggregated loads. The number of lumped cells with the width  $2^{q-1}h$  on level  $q$  is  $P_q$ . The number  $P_q$  is chosen so that a suitable accuracy is obtained by comparing the fluid temperatures for the original and lumped-load sequences. Any choice of  $P_q$  between 5 and 20 serves the purpose. The formulas for the width of lumped cells on level  $q$ , the very last  $v$ -value, and the number of lumped cells are

$$r_q = 2^{q-1}, \quad q = 1, \dots, q_{max};$$

$$v_{max} = \sum_{q=1}^{q_{max}} P_q \cdot r_q \geq n_{max}, \quad N_{lumped\ cells} = \sum_{q=1}^{q_{max}} P_q. \quad (3.44)$$

The  $v$ -value for all the cells in each lumped cell  $p$  on level  $q$  needs to be determined. A simple expression can be used to enumerate all the  $v$ -values from 1 to  $v_{max}$ . Let  $v_{q,0}$  denote the very last  $v$ -value on level  $q-1$ , and  $v_{q,p}$  the last  $v$ -value in lumped cell  $p$  on level  $q$ , which gives

$$v_{q+1,0} = v_{q,0} + r_q \cdot P_q, \quad q = 1, \dots, q_{max} - 1, \quad v_{1,0} = 0,$$

$$v_{q,p} = v_{q,0} + r_q \cdot p, \quad p = 1, \dots, P_q, \quad q = 1, \dots, q_{max}. \quad (3.45)$$

Now,  $v(q, p, r)$  can be expressed as

$$v = v_{q,p} - r, \quad q = 1, \dots, q_{max}, \quad p = 1, \dots, P_q, \quad r = 0, \dots, r_q - 1. \quad (3.46)$$

Equation 3.5, which gives the fluid temperature at time step  $n$ , may now be written in the following way:

$$T_f(nh) = R_{ss} \cdot \sum_{q=1}^{q_{max}} \sum_{p=1}^{P_q} \sum_{r=0}^{r_q-1} Q_v^{(n)} \cdot \kappa_v, \quad (3.47)$$

$$v = v_{q,p} - r, \quad r = 0, \dots, r_q - 1.$$

In the aggregated representation of the loads, the fluid temperature is determined from the following approximation:

$$T_f(nh) \cong R_{ss} \cdot \sum_{q=1}^{q_{max}} \sum_{p=1}^{P_q} \bar{Q}_{q,p}^{(n)} \cdot \bar{\kappa}_{q,p}. \quad (3.48)$$

Here, the lumped weighting factor is equal to the sum of the corresponding original weighting factors, Equation 3.6, lower line:

$$\bar{\kappa}_{q,p} = \sum_{r=0}^{r_q-1} \kappa_v = \frac{T_{step}(v_{q,p}h) - T_{step}(v_{q,p-1}h)}{T_{step}(\infty)}. \quad (3.49)$$

In Equation 3.48, a suitable average load is used in each lumped cell  $p$  on level  $q$ :

$$Q_v^{(n)} \cong \bar{Q}_{q,p}^{(n)} \quad \text{for} \quad v = v_{q,p} - r, \quad r = 0, \dots, r_q - 1. \quad (3.50)$$

The original sequence of loads is shifted one cell position at each time step  $n$ , (Equation 3.7), which corresponds to a time displacement  $h$ . The problem is how to do this time displacement  $h$  for the aggregated cells with the width  $2h$ ,  $4h$ , etc. The immediate answer is to displace the lumped cells by the length  $h$  and conserve the energy. This gives the following set of equations to calculate the aggregated loads at step  $n$  from the values at step  $n-1$ :

$$\begin{aligned} \bar{Q}_{1,0}^{(n)} &= Q_{in}(nh), \quad q = 2, \dots q_{max} : \bar{Q}_{q,0}^{(n)} = \bar{Q}_{q-1,P_q}^{(n-1)}; \\ q = 1, \dots q_{max}, \quad p = 1, \dots P_q : \bar{Q}_{q,p}^{(n)} &= \bar{Q}_{q,p}^{(n-1)} + \frac{1}{r_q} [\bar{Q}_{q,p-1}^{(n-1)} - \bar{Q}_{q,p}^{(n-1)}]. \end{aligned} \quad (3.51)$$

The shift for the aggregated cell  $q,p$  is given on the lower line. One value from cell  $p-1$  is shifted into the cell, and one value from the cell is shifted out of the cell, as shown within the brackets. This difference divided by the width  $r_q$  of the aggregated cell gives the change of the average value in the aggregated cell in the time shift. The first line ensures that the formulas are also valid for  $p=1$ . The new heat injection at time  $n$  is put in cell  $1,0$ , and the old value in cell  $q-1,P_q$  is put into cell  $q,0$ .

## 3.4 Examples of multi-year simulations

The load aggregation scheme of the previous section and the step-response functions of Section 3.2 have been used to perform multi-year simulations of borehole systems. Both single and multi-borehole cases have been used for the simulations.

### 3.4.1 Single borehole system

The multi-year simulations of a single borehole system were performed using the synthetic load profile of Pinel<sup>[42]</sup>. The reason for using this particular load profile is that it has been used by many researchers, including Bernier et al.<sup>[15]</sup>, Lamarche and Beauchamp<sup>[33]</sup> and Lamarche<sup>[32]</sup>, when performing multi-year simulations of GSHP systems. The load profile is shown in Figure 3.14.

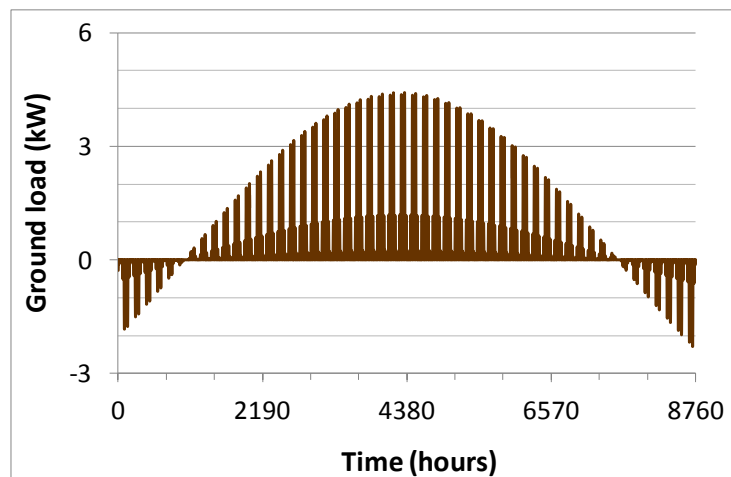


**Figure 3.14** Synthetic load profile of Pinel<sup>[42]</sup> for a single borehole

First, the fluid temperatures are determined using the non-aggregated loads. The initial ground temperature is taken as 0 °C. The sum (3.5) for the non-aggregated scheme is calculated from  $n=1$  to  $n_{max}$ . The number of operations increases as  $(n_{max})^2$ . For a 20-year simulation,  $n_{max}$  is  $20 \cdot 365 \cdot 24 = 175,200$ . The simulation time, gauged by using an Intel ® dual core 2.10 GHz processor, is approximately 88 minutes. Simulation times for other durations are given in Table 3.3. The simulated fluid temperatures for the 20th year using non-aggregated loads are shown in Figure 3.15. The temperatures lie in the range from -4 to +9 °C.

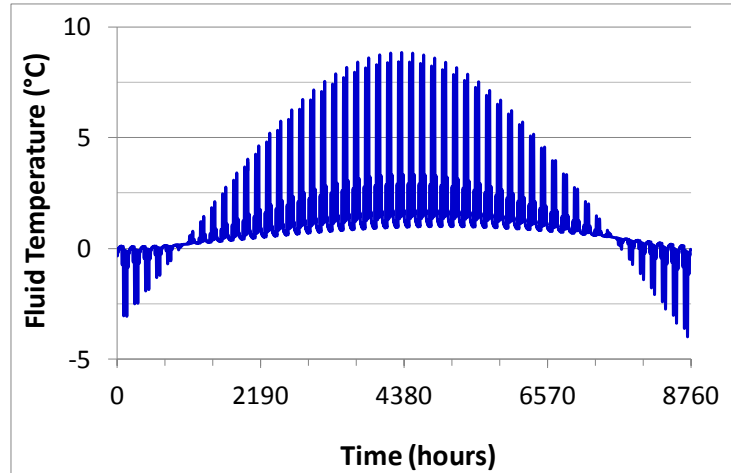


**Figure 3.15** Twentieth year fluid temperature using non-aggregated loads

Next, the fluid temperatures are determined by using the load aggregation scheme. The number of lumped cells assumed on all levels is  $P_q=5$ . The required number of load aggregation levels for the simulation is  $q_{max}=16$ . The number of aggregated cells is  $5 \cdot 16 = 80$ . The limits  $v_{q,p}$  of the aggregated cells and the lumped weighting factors for this case are given in Tables 3.1 and 3.2, respectively. The right hand limits  $v_{q,p}$  of the aggregated cells are determined from Equation 3.45. In the first line,  $q=1$ , the first 5 cells are given. In the second line, the right hand value of the doubled cells, 7 to 15, are shown. The value 5 from the first level is transferred to the next level in the  $p=0$  column. The last line indicates that 16 levels are needed to exceed 175,200 values of loads. The lumped weighting factors of Table 3.2 are calculated from Equation 3.49. The first value of 0.246 indicates that the first cell affects the extraction temperature by 25 %. The next four cells affect the extraction fluid temperatures by 7, 4, 3 and 2 %, respectively. A lumped weighting factor of 0.01 in the third cell of third level represents an influence of 1 % on the extraction fluid temperature.

**Table 3.1** Right hand limits  $v_{q,p}$  of the aggregated cells

| <b><math>q</math></b> | <b><math>p</math></b> |          |          |          |          |          |
|-----------------------|-----------------------|----------|----------|----------|----------|----------|
|                       | <b>0</b>              | <b>1</b> | <b>2</b> | <b>3</b> | <b>4</b> | <b>5</b> |
| 1                     | 0                     | 1        | 2        | 3        | 4        | 5        |
| 2                     | 5                     | 7        | 9        | 11       | 13       | 15       |
| 3                     | 15                    | 19       | 23       | 27       | 31       | 35       |
| 4                     | 35                    | 43       | 51       | 59       | 67       | 75       |
| 5                     | 75                    | 91       | 107      | 123      | 139      | 155      |
| 6                     | 155                   | 187      | 219      | 251      | 283      | 315      |
| 7                     | 315                   | 379      | 443      | 507      | 571      | 635      |
| 8                     | 635                   | 763      | 891      | 1019     | 1147     | 1275     |
| 9                     | 1275                  | 1531     | 1787     | 2043     | 2299     | 2555     |
| 10                    | 2555                  | 3067     | 3579     | 4091     | 4603     | 5115     |
| 11                    | 5115                  | 6139     | 7163     | 8187     | 9211     | 10235    |
| 12                    | 10235                 | 12283    | 14331    | 16379    | 18427    | 20475    |
| 13                    | 20475                 | 24571    | 28667    | 32763    | 36859    | 40955    |
| 14                    | 40955                 | 49147    | 57339    | 65531    | 73723    | 81915    |
| 15                    | 81915                 | 98299    | 114683   | 131067   | 147451   | 163835   |
| 16                    | 163835                | 196603   | 229371   | 262139   | 294907   | 327675   |

**Table 3.2** Lumped weighting factors  $1000 \cdot \bar{\kappa}_{q,p}$  of the aggregated cells

| <b><math>q</math></b> | <b><math>p</math></b> |          |          |          |          |
|-----------------------|-----------------------|----------|----------|----------|----------|
|                       | <b>1</b>              | <b>2</b> | <b>3</b> | <b>4</b> | <b>5</b> |
| 1                     | 245.7                 | 68.1     | 35.7     | 23.3     | 17.1     |
| 2                     | 24.4                  | 17.4     | 13.5     | 11.0     | 9.3      |
| 3                     | 15.1                  | 12.0     | 10.0     | 8.6      | 7.5      |
| 4                     | 12.6                  | 10.4     | 8.8      | 7.7      | 6.8      |
| 5                     | 11.6                  | 9.6      | 8.1      | 7.1      | 6.3      |
| 6                     | 10.9                  | 9.2      | 7.9      | 6.9      | 6.2      |
| 7                     | 10.7                  | 9.0      | 7.8      | 6.8      | 6.1      |
| 8                     | 10.5                  | 8.9      | 7.7      | 6.7      | 6.0      |
| 9                     | 10.4                  | 8.7      | 7.5      | 6.6      | 5.9      |
| 10                    | 10.2                  | 8.5      | 7.4      | 6.5      | 5.7      |
| 11                    | 9.9                   | 8.3      | 7.1      | 6.2      | 5.5      |
| 12                    | 9.4                   | 7.9      | 6.7      | 5.9      | 5.2      |
| 13                    | 8.8                   | 7.3      | 6.2      | 5.4      | 4.7      |
| 14                    | 8.0                   | 6.5      | 5.5      | 4.7      | 4.1      |
| 15                    | 6.8                   | 5.4      | 4.5      | 3.8      | 3.2      |
| 16                    | 5.2                   | 4.0      | 3.2      | 2.6      | 2.1      |

Figure 3.16 shows the extraction fluid temperatures simulated for 20 years from the load aggregation scheme. The computational time for a 20 year simulation is 25 seconds, which is approximately 200 times faster than the non-aggregated scheme. Simulation times for other durations are given in Table 3.3.

**Table 3.3** Computational times for non-aggregated and aggregated loads

| <b>Simulation time<br/>(years)</b> | <b>Computational time (seconds)</b> |                         |
|------------------------------------|-------------------------------------|-------------------------|
|                                    | <b>Non-aggregated loads</b>         | <b>Aggregated loads</b> |
| 1                                  | 14 (< 1 min)                        | 3                       |
| 3                                  | 31 (2.2 min)                        | 5                       |
| 5                                  | 330 (5.5 min)                       | 7                       |
| 10                                 | 1321 (22 min)                       | 14                      |
| 20                                 | 5289 (88 min)                       | 25                      |

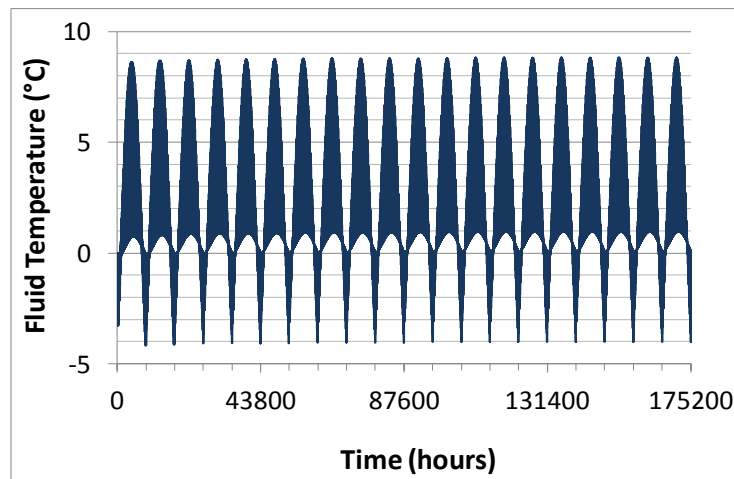


**Figure 3.16** Extraction fluid temperatures for 20 years using the aggregated loads

The errors in the extraction fluid temperatures calculated for the 20th year by using the load aggregation scheme are shown in Figure 3.17. The errors are measured with reference to the extraction fluid temperatures determined from non-aggregated loads. The maximum absolute error is 0.039 K for  $P_q=5$ . Using  $P_q=10$  and 20 reduces the maximum absolute errors to 0.018 and 0.006, respectively.

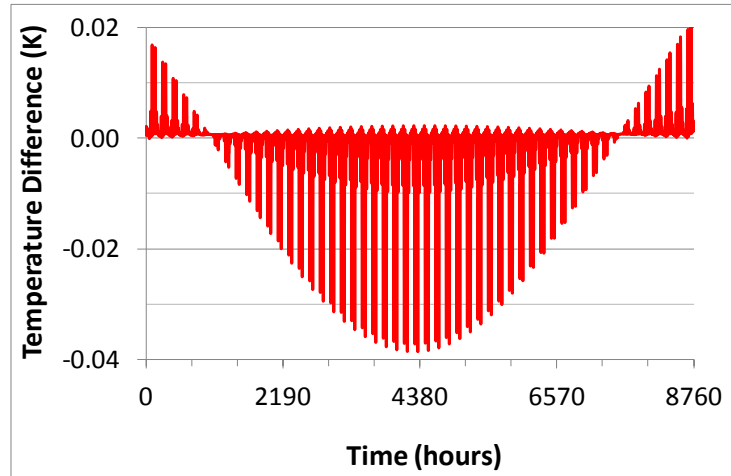


**Figure 3.17** Errors in simulated fluid temperatures for the 20th year introduced by the load aggregation scheme ( $P_q=5$ )

### 3.4.2 Multiple-borehole system

Multi-year simulations of a multiple borehole system were performed using the ground loads of Figure 3.18. The loads from an actual building in the southwest of Sweden were scaled down to suit a nine-borehole system of  $3 \times 3$  rectangular configuration. The borehole system is designed to provide minimum mean fluid temperature of  $-3^{\circ}\text{C}$  in the heating mode. Each borehole is 165 m deep and the spacing between adjacent boreholes is 5 m. The undisturbed ground temperature level of  $8^{\circ}\text{C}$  was considered.

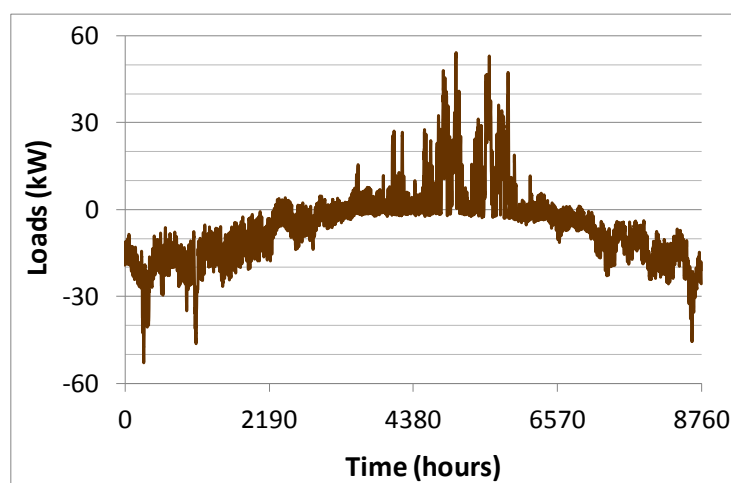


**Figure 3.18** Ground loads considered on nine boreholes in a square configuration

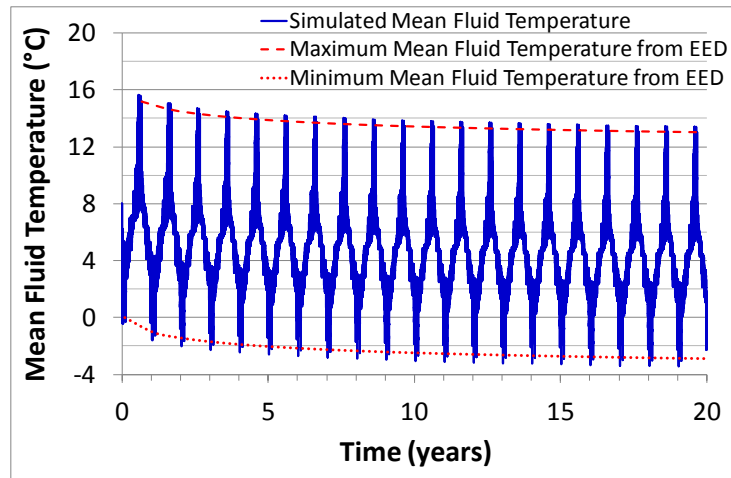
The load aggregation scheme discussed in Section 3.3 was used to determine the mean fluid temperatures. The combined step-response function based on the finite line-source solution of Equation 3.42 for nine boreholes in a square configuration was used. Five lumped cells are assumed on all levels of aggregation (i.e.,  $P_q=5$ ). In total are 80 aggregated cells on 16 levels of aggregation (i.e.  $q_{max}=16$ ). The right hand limits  $v_{q,p}$  of the aggregated cells are identical to those shown in Table 3.1. The lumped weighting factors, determined from Equation 3.49, are shown in Table 3.4. Comparison of the lumped weighting factors for this example to those determined for a single borehole (Table 3.2) yields some interesting observations. For a single borehole, the extraction fluid temperatures were greatly influenced by the most recent loads. The weighting factors fall sharply with passing time. Consequently, loads in the distant past had relatively small influence on the extraction fluid temperatures. On the other hand, for a multiple borehole system, the thermal interaction between boreholes increases over time. Hence, the weighting factors for loads in the distant past are also quite large.

**Table 3.4** Lumped weighting factors  $1000 \cdot \bar{\kappa}_{q,p}$  of the aggregated cells

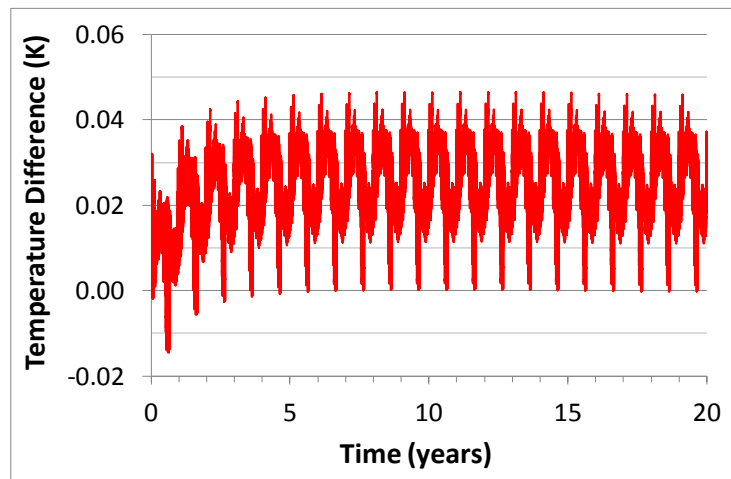
| <b><math>q</math></b> | <b><math>p</math></b> |          |          |          |          |
|-----------------------|-----------------------|----------|----------|----------|----------|
|                       | <b>1</b>              | <b>2</b> | <b>3</b> | <b>4</b> | <b>5</b> |
| 1                     | 80.4                  | 22.3     | 11.7     | 7.6      | 5.6      |
| 2                     | 8.0                   | 5.7      | 4.4      | 3.6      | 3.0      |
| 3                     | 4.9                   | 3.9      | 3.3      | 2.8      | 2.4      |
| 4                     | 4.1                   | 3.4      | 2.9      | 2.5      | 2.2      |
| 5                     | 3.8                   | 3.1      | 2.7      | 2.3      | 2.1      |
| 6                     | 3.6                   | 3.0      | 2.7      | 2.4      | 2.2      |
| 7                     | 3.9                   | 3.5      | 3.3      | 3.1      | 3.0      |
| 8                     | 5.7                   | 5.4      | 5.2      | 5.0      | 4.8      |
| 9                     | 9.2                   | 8.7      | 8.3      | 7.9      | 7.5      |
| 10                    | 14.1                  | 13.0     | 12.0     | 11.2     | 10.5     |
| 11                    | 19.1                  | 17.1     | 15.4     | 14.0     | 12.8     |
| 12                    | 22.8                  | 19.8     | 17.5     | 15.6     | 14.1     |
| 13                    | 24.6                  | 21.0     | 18.2     | 16.1     | 14.4     |
| 14                    | 24.7                  | 20.8     | 17.8     | 15.5     | 13.8     |
| 15                    | 23.4                  | 19.4     | 16.4     | 14.2     | 12.4     |
| 16                    | 20.8                  | 16.9     | 14.0     | 11.9     | 10.2     |

Figure 3.19 shows the simulated mean fluid temperatures over 20 years. The computational times for performing simulations using aggregated loads remain similar to those shown in Table 3.3. It takes approximately 26 seconds to run a 20-year simulation in this case. The annual minimum and maximum mean fluid temperatures obtained from the commercial software EED<sup>[18]</sup> are also shown as dotted lines in Figure 3.19. Some discrepancy between the two approaches is expected as (among other things) the EED software determines the monthly minimum and maximum fluid temperatures by superimposing the peak loads of

that month on the aggregated load values. However, the difference between the two approaches is relatively small. The errors in simulated fluid temperatures with reference to the non-aggregated loads are shown in Figure 3.20 for the 20-year period. The maximum difference between the fluid temperatures calculated from the aggregated scheme ( $P_q=5$ ) and non-aggregated loads for the 20-year period is only 0.046 K.



**Figure 3.19** Extraction fluid temperatures for 20 years using the aggregated loads



**Figure 3.20** Errors in simulated fluid temperatures for 20 years introduced by the load aggregation scheme ( $P_q=5$ )

The extraction fluid temperatures for the 20th year and the errors in reference to the non-aggregated scheme are shown in Figures 3.21 and 3.22, respectively.

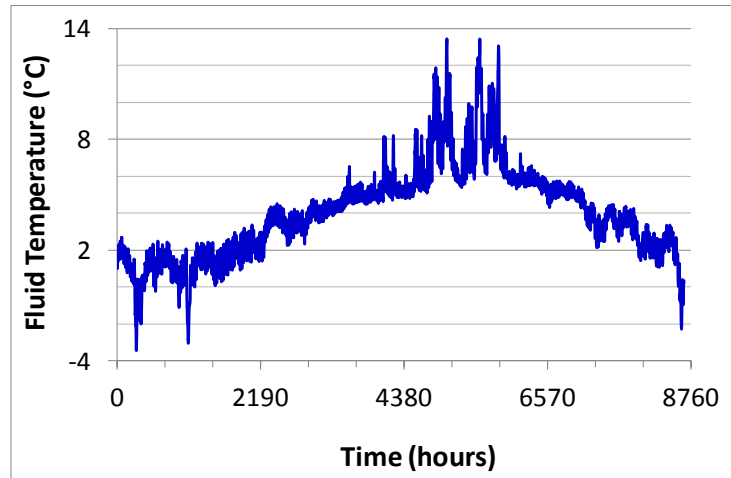


**Figure 3.21** Twentieth year fluid temperature using aggregated loads

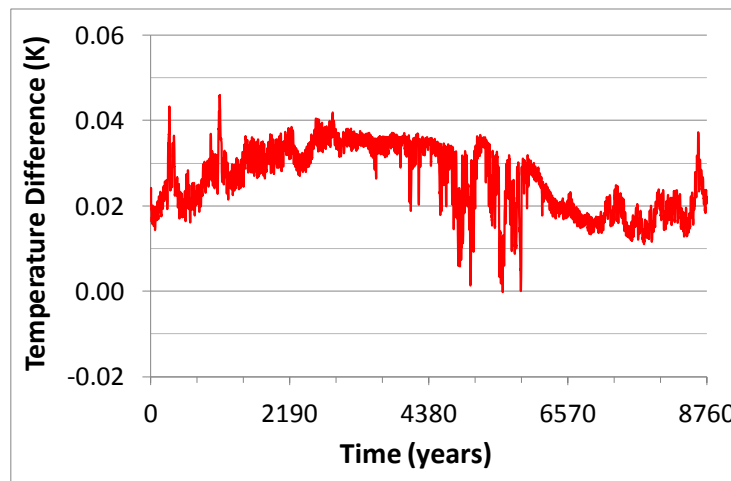


**Figure 3.22** Errors in simulated fluid temperatures for the 20th year introduced by the load aggregation scheme ( $P_q=5$ )

Figure 3.23 shows loads for peak heating and cooling days. It is quite interesting to follow the development of fluid temperatures for these days. On the peak heating day, the heating load gradually increases from approximately 27 kW at the beginning of the day to over 53 kW by the end of the day. The fluid temperatures follow the heating loads closely. They decrease from a positive value at the beginning of the day to below -3 °C by the end of the day. On the peak cooling day, the cooling load is approximately constant at 22-23 kW for the first six hours of the day. It then starts increasing and reaches a value of approximately 53 kW at mid day. The cooling load remains fairly constant for the next eight hours before it starts decreasing in the late evening. The simulated fluid temperature is lower at the start of the day. Following the pattern of the cooling loads, the extraction fluid temperature increases during the day before decreasing

again in the late afternoon. In both cases, the fluid temperatures from the borehole heat exchanger closely follow the heating and cooling loads on the system.

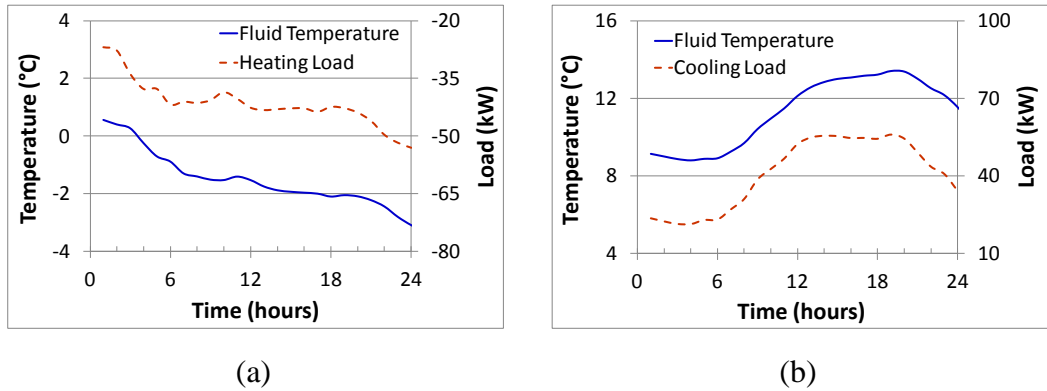


**Figure 3.23** Extraction fluid temperatures for peak heating and cooling days

### 3.5 Conclusions

Energy simulations of ground source heat pump systems are critical for the design and optimal operation of these systems. However, it is very time consuming to perform hourly simulations of borehole systems over multiple years. The extraction fluid temperature depends on a long sequence, backwards in time, of heat extraction and injection rates. This chapter presented a load aggregation scheme to perform multi-year simulations of borehole systems. The starting point is the step-response function for the considered borehole system and the corresponding long sequence of cells, each with a load and a weighting factor. The step-response function was computed using a combination of the short-term analytical solution of Chapter 2 and a finite line-source solution. The analytical solution was used for times up to 100 hours. The finite line-source solution was used afterwards. Multi-year simulations of single and multiple borehole systems were performed using aggregated loads and step-response functions. The load aggregation was performed on different levels. At the first level, the original weighting factors were kept. At levels 2, 4, 8, etc., weighting factors were lumped together. The accuracy of the scheme depends on the number of lumped cells on each aggregation level. The number of cells to be lumped can be chosen freely to obtain the desired accuracy level. A choice of 5 lumped cells on each of 16 aggregation levels required for a 20-year simulation gives a maximum absolute error of less than 0.05 K. Approximately 80 aggregated loads are used, and the new scheme was found to be 200 times faster than the non-aggregated case.



## 4 Thermal response testing and analysis

It is now a standard practice to perform a thermal response test (TRT) when designing medium- to large-sized borehole systems. Thermal response tests are conducted on pilot boreholes to determine thermal properties including ground conductivity, borehole resistance and undisturbed ground temperature. These properties are used in the design of borehole systems as inputs in manual calculations or design software to determine the size and configuration of the borehole heat exchanger.

The idea of using TRT to measure ground thermal properties was first presented by Mogensen<sup>[40]</sup>. Gehlin<sup>[23]</sup> introduced a now commonly used testing and evaluation procedure. Other noteworthy evaluation methods were developed by Austin et al.<sup>[8]</sup> and Shonder and Beck<sup>[44]</sup>. Beier and Smith<sup>[13]</sup> and Beier<sup>[10]</sup> proposed methods to evaluate tests interrupted by a power failure. Distributed thermal response tests were used by Acuña<sup>[2]</sup> to determine the local variations of ground conductivity and borehole resistance along the borehole depth. Kavanaugh et al.<sup>[31]</sup> investigated the effects of test duration, power quality and borehole retesting using experimental studies. Witte et al.<sup>[49]</sup> analyzed the impact of groundwater flow on the thermal response of a borehole heat exchanger. Gehlin<sup>[23]</sup> reported on the influence of natural convection and thermosiphon effects on testing of groundwater-filled boreholes. Gustafsson and Westerlund<sup>[26]</sup> suggested multiple injection rates to investigate the presence and influence of natural convection and advection on groundwater-filled boreholes.

Despite widespread interest and research on thermal response testing, many areas remain that call for more study. There is a dearth of research on issues such as test accuracy, the sensitivity of borehole system design to uncertainties in TRT results, the role of natural convection in groundwater-filled boreholes, the evaluation of multi-injection rate tests, and the required recovery times after a TRT. This chapter deals with some of the uncertainties and unresolved issues in testing of borehole systems. The chapter first reports on the development of a new GSHP test facility and its TRT setup. Testing and evaluation of test facility boreholes is presented next. Case studies are then used to perform sensitivity and uncertainty analysis of TRT results. Finally, the analytical solution derived in Chapter 2 is used to develop an evaluation method for multi-injection rate tests on groundwater filled boreholes and to determine the waiting times needed before performing a retest.

### 4.1 Test facility

A newly developed GSHP test facility<sup>[30]</sup> was used to conduct most of the TRTs reported in this chapter. The GSHP system of the test facility consists of a nine-borehole system drilled in a 3x3 rectangular configuration. All the boreholes are groundwater-filled and have single U-tubes as ground loop heat exchangers. The distance between adjacent boreholes is approximately 4 m and each borehole has an active depth of approximately 80 meters. The spacing between the two legs of the U-tube and between the U-tube legs and the borehole boundary is not controlled. The horizontal cross-section of an individual borehole and the layout of the whole borehole system are shown in Figure 4.1. Additional details of the borehole field and its elements are given in Table 4.1.

**Table 4.1** Details of the borehole system

| Element                   | Specification    |
|---------------------------|------------------|
| Borehole                  |                  |
| Effective borehole depth  | 80 m             |
| Borehole diameter         | 110 mm           |
| Borehole filling material | Groundwater      |
| Surrounding ground type   | Bedrock          |
| Heat exchanger            |                  |
| Type                      | Single U-tube    |
| Material                  | Polyethylene     |
| Pipe outer diameter       | 40 mm            |
| Pipe thickness            | 2.3 mm           |
| Thermal conductivity      | 0.42 W/(m·K)     |
| Shank spacing             | Not controlled   |
| Circulating fluid         |                  |
| Type                      | Ethanol (29.5 %) |
| Thermal conductivity      | 0.401 W/(m·K)    |
| Freezing point            | -20 °C           |
| Specific heat capacity    | 4180 J/(kg·K)    |

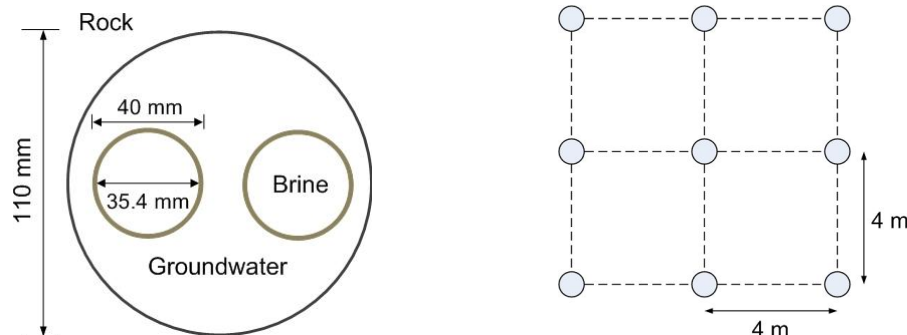


**Figure 4.1** Geometry and layout of the test-facility boreholes

The experimental setup of the test facility to conduct TRTs is shown in Figure 4.2. The setup includes an electric heater, nine circulation pumps, and temperature and flow sensors. The installed electric heater is of variable capacity and can operate at various power levels between 2.5 and 15 kW. All nine boreholes have dedicated variable speed pumps and flow control valves to monitor and control the flow of circulating fluid in individual boreholes. The circulation pumps used

in the TRT setup are designed specifically for GSHP system applications. Each pump has a nominal motor power of 100 W. The pumps can be operated between 1400-3900 rpm. Depending on the pump speed, the power and current inputs to the pump vary between 8-130 W and 0.07-0.95 A, respectively. These inputs are significantly smaller than those typical of ordinary circulation pumps. A state-of-the-art data acquisition and storage system is used for recording TRT measurements. Temperature measurements in the system are made using electronic immersion temperature transmitters. Temperature measurements of the circulating fluid are made in two instances: first, when the fluid enters or leaves the laboratory building; and second, before and after the electric heater. The flow rate is also measured twice: first, by using an installed vortex flow meter; and second, over the individual borehole valves. The input power to the electric heater is measured by means of a high-accuracy meter that also provides the possibility of waveform analysis. The accuracy of the power meter is 0.15 % of the reading plus 0.025 % of the full scale, resulting in a total accuracy of < 1 %. Other measurements that may be taken include ambient air temperature and indoor air temperature of the test facility. All the data can be recorded for any interval over 10 seconds.

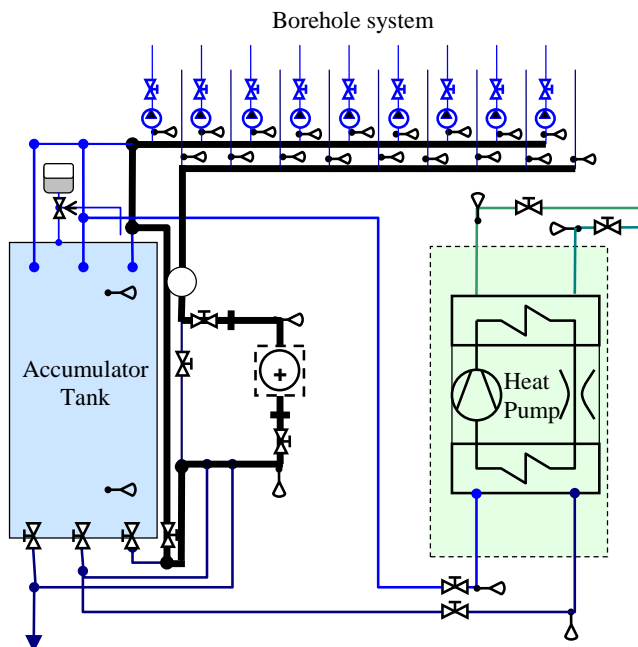


**Figure 4.2** Test facility's TRT setup

## 4.2 Response testing and evaluation of the test facility boreholes

*This section is based on Paper IV.*

The laboratory borehole system provides a unique opportunity to study thermal properties, including undisturbed ground temperature, ground thermal conductivity and borehole thermal resistance of nine boreholes in close proximity. Issues such as repeatability and reproducibility of TRTs can be comprehensively studied. Such investigations, which show the effects of the random test errors and

local inhomogeneities on TRT results, have rarely been conducted on an academic level in controlled laboratory conditions for a borehole field of this size.

The TRTs of the nine laboratory boreholes were conducted over a period of four months. Before conducting the tests, undisturbed ground temperatures were measured for all nine boreholes. Following the undisturbed ground temperature measurements, TRTs were conducted in the heat injection mode. Tests were conducted for different times between 48 and 260 hours. Similar heat injection and flow rates were used for all tests. The power level used for the tests was approximately 4.5 kW. The chosen power level resulted in a heat injection rate of approximately 55 W/m, which is in accordance with the ASHRAE recommendations<sup>[6]</sup>. The flow from the circulation pumps was kept at more than 1.4 m<sup>3</sup>/h to ensure turbulent flow in the ground loop. Readings of the circulating fluid temperatures, power input, flow and ambient temperature were taken at regular intervals of 3 to 5 minutes. After a test, measurements obtained from the test were analyzed, and the ground thermal conductivity and borehole thermal resistance were estimated.

The undisturbed ground temperature for each borehole was determined using two different approaches. In the first approach, the fluid was circulated a number of times through the undisturbed borehole. The inlet and outlet fluid temperatures were recorded at intervals of 10 seconds. The variations in circulating fluid temperature diminish after approximately 30 minutes. The undisturbed ground temperature is then approximated from the stabilized fluid temperature. A problem with this approach is that, for longer times, the undisturbed ground temperatures are affected by the heat gains from the circulation pump. However, use of pumps custom made for borehole applications avoided this problem. The highly efficient pumps add only a few watts to the circulating fluid. The measurements of the undisturbed ground temperature calculated by this approach are shown in Table 4.2. The measurements vary between 8.1 and 9.2 °C. The variations in the undisturbed ground temperature measurements are due to different initial temperatures of the fluid present in the circulation loop outside the borehole.

**Table 4.2** Undisturbed ground temperature from flow circulation approach

| Borehole | Undisturbed ground temperature (°C) |
|----------|-------------------------------------|
| 1        | 9.1                                 |
| 2        | 8.7                                 |
| 3        | 8.9                                 |
| 4        | 8.5                                 |
| 5        | 8.4                                 |
| 6        | 8.2                                 |
| 7        | 8.1                                 |
| 8        | 8.3                                 |
| 9        | 9.2                                 |

The second approach used to measure the undisturbed ground temperature was to monitor the start-up exit fluid temperatures from the U-tube. Figure 4.3 shows the temperatures of the exit fluid from the nine boreholes. The decline in temperatures from the start-up to the first set of troughs is because of the fluid present in the return horizontal piping from the boreholes to the test facility building. The fluid had remained in the piping for several weeks before the tests and hence was in equilibrium with the corresponding ambient temperatures. After the first set of troughs, the fluid from the U-tube flows past the temperature sensor. The flow from the U-tube continues until the start of the second set of troughs. The temperature of the fluid from the U-tube, highlighted in Figure 4.3, remains fairly constant at approximately 8.2-8.3 °C for all boreholes. Next, the fluid present in the supply horizontal piping to the boreholes flows past the temperature sensor. This is represented by the second set of troughs in the figure. At this time, the fluid has completed the first round of circulation. During the next rounds, the variations diminish and the fluid temperature stabilizes. Figure 4.3 also indicates that after 20-30 minutes of circulation, the stabilized fluid temperature is influenced by the initial temperatures of the fluid present in the circulation loop. The undisturbed ground temperatures, calculated from the start-up exit fluid temperature approach, were used for further analysis.

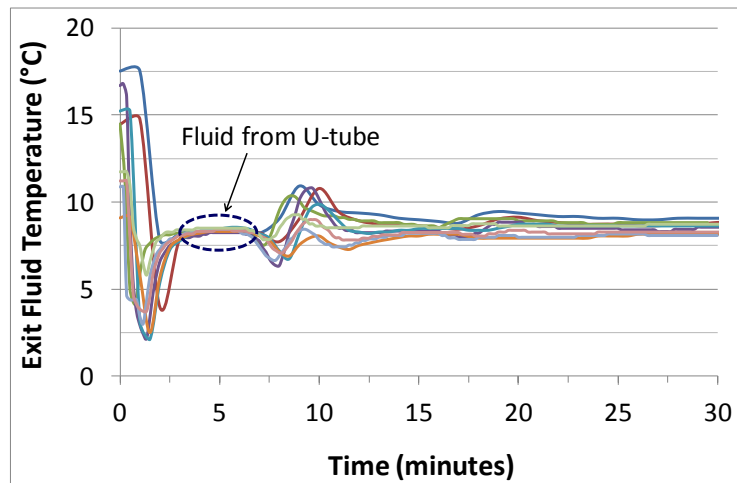


**Figure 4.3** Undisturbed ground temperature from start-up exit fluid temperatures

The power levels used for the TRTs of the boreholes and the resulting mean fluid temperatures are shown in Figures 4.4 and 4.5, respectively. The ground conductivity and borehole thermal resistance estimations for the tests were estimated using the line-source approximation methods of Gehlin<sup>[23]</sup> and Beier and Smith<sup>[11]</sup>, respectively. The results of the TRTs of the boreholes are given in Table 4.3. The ground thermal conductivity estimations for the nine boreholes vary between the extreme values of 2.81 and 3.2 W/(m·K). The ground conductivity estimations have a mean value of 3.01 W/(m·K). The whole range of ground conductivity estimations of the nine boreholes can be represented and expressed as  $3.01 \text{ W}/(\text{m}\cdot\text{K}) \pm 7\%$ . The estimations of borehole thermal resistance for the nine boreholes vary between the extreme values of 0.049 and 0.074 (m·K)/W. The borehole resistance estimations exhibit larger variations. The borehole resistance values of the nine boreholes lay in a range of  $0.062 \text{ (m}\cdot\text{K})/\text{W} \pm 20\%$ .

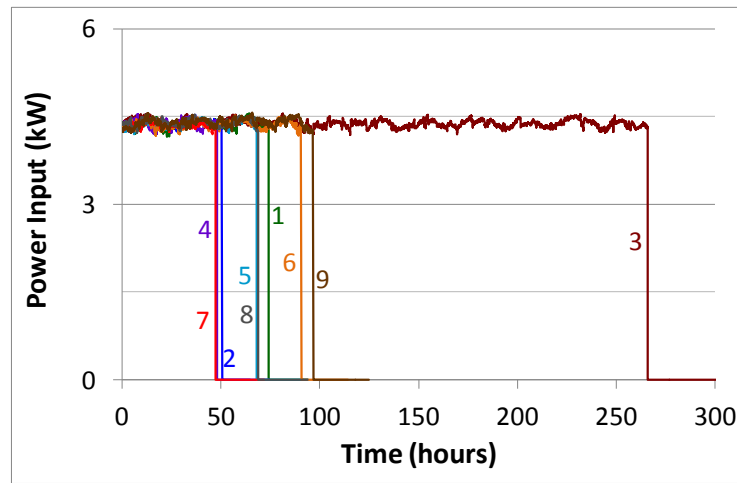


**Figure 4.4** Power inputs for TRTs of nine boreholes

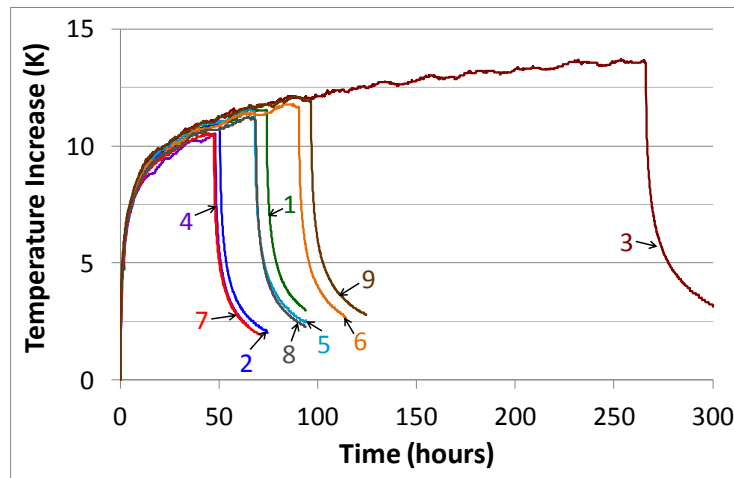


**Figure 4.5** Mean fluid temperatures for TRTs of nine boreholes

**Table 4.3** Ground conductivity and borehole resistance estimations for the test facility boreholes

| Borehole | Duration (hours) | Heat injection rate (W/m) | Ground conductivity (W/(m·K)) | Borehole resistance ((m·K)/W) |
|----------|------------------|---------------------------|-------------------------------|-------------------------------|
| 1        | 75               | 54.7                      | 2.88                          | 0.059                         |
| 2        | 54               | 54.9                      | 3.06                          | 0.064                         |
| 3        | 267              | 56.2                      | 3.04                          | 0.074                         |
| 4        | 48               | 54.6                      | 2.81                          | 0.049                         |
| 5        | 68               | 54.9                      | 2.98                          | 0.064                         |
| 6        | 91               | 53.2                      | 2.89                          | 0.063                         |
| 7        | 48               | 54.5                      | 3.19                          | 0.064                         |
| 8        | 69               | 55.0                      | 3.20                          | 0.065                         |
| 9        | 98               | 55.0                      | 3.12                          | 0.069                         |

The results of thermal response tests on nine nearby boreholes suggest that the ground conductivity and borehole thermal resistance values, determined from a carefully conducted TRT, can have uncertainties on the order of 7 and 20 %, respectively. These uncertainties in the TRT results are induced from the experimental setup, the evaluation method, and the input parameters to the evaluation method as well as possible inhomogeneities in the bedrock properties. A sensitivity analysis was carried out to determine the effects of the different uncertainties shown in Table 4.4 on the TRT results. The analysis indicates that the considered uncertainties can result in ground conductivity and borehole resistance estimations varying up to 10 and 40 %, respectively. The variations in ground thermal conductivity and borehole thermal resistance estimations of nine nearby boreholes are well within the range determined from the sensitivity analysis shown in Table 4.4.

**Table 4.4** Sensitivity of ground thermal conductivity and borehole thermal resistance estimations of test facility's boreholes

| Factors  | Sensitivity of ground conductivity estimations (%) | Sensitivity of borehole resistance estimations (%) |
|--|--|--|
| Test duration between 50 and 100 hours                               | ± 4 %  | ± 7 %  |
| Power fluctuations of ± 1 %  | ± 1 %  | ± 2 %  |
| Temperature measurement uncertainty of ± 0.2 K                       | < ±1 %   | < ±1 %   |
| Uncertainty of ± 0.2 K in undisturbed ground temperature measurement | -  | ± 8 %  |
| Uncertainty of ± 10 % in the volumetric heat capacity                | -  | ± 6 %  |
| Borehole geometry  |  |  |
| ± 1 % uncertainty in borehole depth                                  | ± 1 %  | < ±1 %   |
| ± 3 % uncertainty in borehole radius                                 | -  | ± 4 %  |
| Estimation method  | ± 2.5 %  | ± 10 %   |
| Total sensitivity  | ~ ± 10 %   | ~ ± 40 %   |

### 4.3 Sensitivity of borehole system design to uncertainties in TRT results

*This section is based on Paper III.*

The effect of the variations in ground conductivity and borehole resistance estimations of the test facility boreholes on the design of borehole systems have been analyzed using case studies. For the case studies, a hypothetical office building<sup>[24]</sup>, based on three floors of an actual office building in Tulsa, Oklahoma, has been used. The building has a square footprint of 49 m x 49 m. Approximately 60 % of the building facade is covered by double-pane glass windows. The building has high occupancy (1 person per 5 m<sup>2</sup>) and high lighting and equipment heat gains (combined 23.1 W/m<sup>2</sup>) with office-appropriate schedules. The hourly heating and cooling loads of this office building have been determined for different climate conditions of Tulsa, Oklahoma (warm-humid) and Burlington, Vermont (cold-humid) using building energy simulation software. The annual hourly demands for the Tulsa and Burlington buildings are shown in Figures 4.6 and 4.7, respectively.

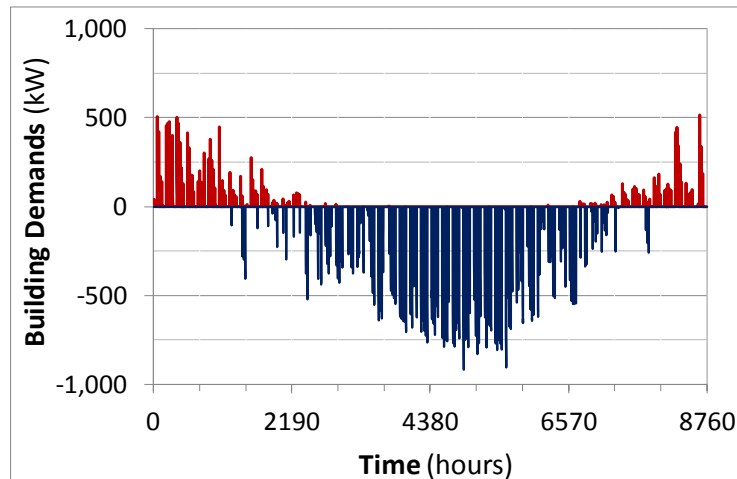


**Figure 4.6** Annual heating and cooling demands for the Tulsa case

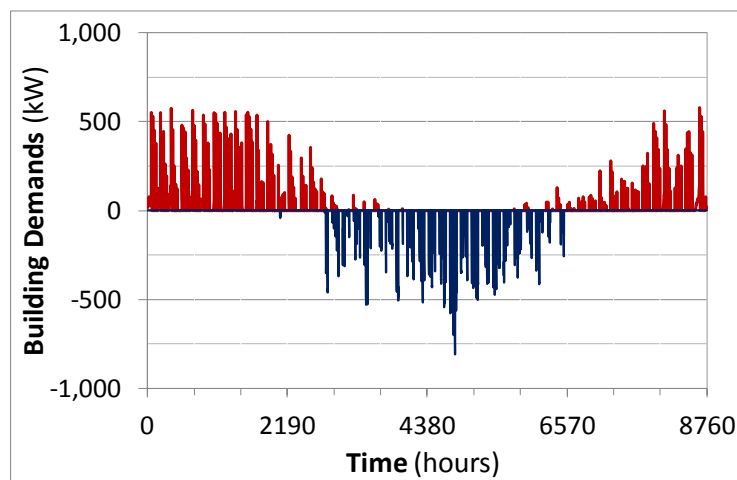


**Figure 4.7** Annual heating and cooling demands for the Burlington case

**Table 4.5** Monthly heating and cooling demands of the case study buildings

| Month     | Tulsa            |                  | Burlington       |                  |
|-----------|------------------|------------------|------------------|------------------|
|           | Heating<br>(MWh) | Cooling<br>(MWh) | Heating<br>(MWh) | Cooling<br>(MWh) |
| January   | 16.3             | -                | 36.4             | -                |
| February  | 5.0              | 1.8              | 30.4             | -                |
| March     | 1.6              | 9.7              | 18.3             | 0.1              |
| April     | 0.4              | 21.4             | 4.5              | 5.7              |
| May       | -                | 54.3             | 0.5              | 23.4             |
| June      | -                | 103.5            | -                | 37.0             |
| July      | -                | 127.9            | -                | 63.0             |
| August    | -                | 128.2            | -                | 54.5             |
| September | -                | 54.1             | 0.4              | 18.7             |
| October   | 0.3              | 31.0             | 1.8              | -                |
| November  | 1.7              | 4.0              | 7.6              | -                |
| December  | 6.9              | -                | 23.4             | -                |
| Year      | 32               | 536              | 123              | 202              |

The commercially available software, Earth Energy Designer (EED)<sup>[18]</sup>, was used to design the borehole systems for both cases. For the Tulsa case, the building has predominant cooling requirements of 536 MWh and heating requirements of just 32 MWh, as shown in Table 4.5. Therefore, the borehole system of the Tulsa building is designed to maximize the heat transfer between the ground heat exchanger and the surrounding ground. The limiting factors considered for the Tulsa borehole system include maximum area utilization of 125 m x 50 m, borehole depth of approximately 100 m and minimum and maximum fluid temperatures of -5 and 35 °C to the heat pump(s) in heating and cooling modes, respectively. A field of 225 boreholes in a rectangular configuration of 9 x 25 was chosen for the Tulsa case. The borehole spacing between adjacent boreholes is 5 m. The layout of the borehole field is shown in Figure 4.8.

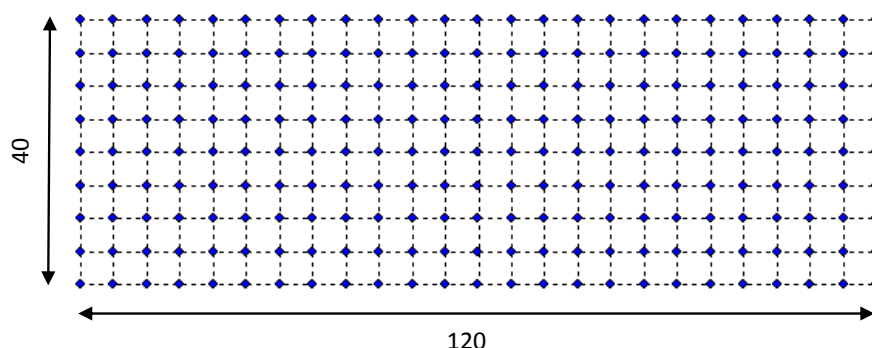


**Figure 4.8** Layout of the borehole field considered for the Tulsa case

The simulated heating and cooling demands of the Burlington building, as shown in Table 4.5, are 123 and 202 MWh, respectively. The heating and cooling demands are fairly balanced and hence the chosen borehole field should exploit the seasonal heat storage ability of the ground. The borehole field in the Burlington case was also designed to provide a minimum fluid temperature of -5 °C in heating mode and a maximum fluid temperature of 35 °C in cooling mode to the heat pump(s). Other restrictions included a maximum borehole field area of 40 m x 50 m and individual borehole depth of approximately 100 m. The layout of the borehole field chosen for the Burlington case is shown in Figure 4.9. There are 70 boreholes in a 7 x 10 rectangular configuration. The spacing between the boreholes of the chosen field is 5 m.

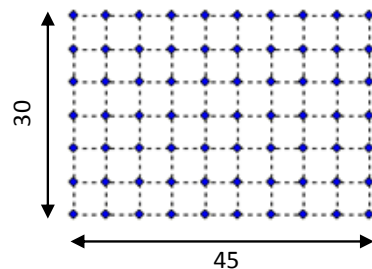


**Figure 4.9** Layout of the borehole field considered for the Burlington case

The two case studies of the Tulsa and the Burlington buildings were used to perform a sensitivity analysis of random variations in the TRT results on the design of a borehole system. This analysis was done by calculating the required length of the borehole field, for both Tulsa and Burlington cases, using ground thermal conductivity and borehole thermal resistance values estimated for each of the nine test facility boreholes. The results of the sensitivity analysis are shown in Table 4.6. In the case of the Tulsa building, the random uncertainties in the TRT results vary the total borehole length between the extremes of 20,870 and 22,615 m. The difference between the smallest and largest lengths is 1,745 m, which is approximately equivalent to 17 boreholes out of 225 boreholes. For the Burlington case, 6860 and 7,500 m are, respectively, the smallest and largest required borehole lengths. The 640 m difference between these two lengths corresponds to approximately 6 out of 70 boreholes. The random uncertainties between TRTs affect the total length requirements of Tulsa and Burlington fields by 8-9 %. Thus, a safety factor on the order of 10 % should be considered when designing borehole systems based on thermal conductivity and the borehole resistance estimations from a single careful 50+ hour test conducted in accordance with ASHRAE recommendations<sup>[6]</sup>.

**Table 4.6** Effects of random variations in TRT results of adjacent boreholes on the size of the borehole fields for the Tulsa and Burlington cases

| TRT | Tulsa            |                               | Burlington       |                               |
|-----|------------------|-------------------------------|------------------|-------------------------------|
|     | Total length (m) | Individual borehole depth (m) | Total length (m) | Individual borehole depth (m) |
| 1   | 22,410           | 99.6                          | 7,120            | 101.7                         |
| 2   | 21,600           | 96.0                          | 7,120            | 101.7                         |
| 3   | 22,500           | 100.0                         | 7,500            | 107.1                         |
| 4   | 22,165           | 98.5                          | 6,860            | 98.0                          |
| 5   | 22,140           | 98.4                          | 7,195            | 102.8                         |
| 6   | 22,615           | 100.5                         | 7,260            | 103.7                         |
| 7   | 20,870           | 92.7                          | 6,955            | 99.3                          |
| 8   | 20,890           | 92.8                          | 6,980            | 99.7                          |
| 9   | 21,595           | 96.0                          | 7,235            | 103.4                         |

#### 4.4 Convection in groundwater-filled boreholes

*This section is based on Paper III and one of the additional publications (Paper 8 on Page viii).*

Heat transport in groundwater-filled boreholes is driven by natural convection and advection. During a TRT, the magnitude of natural convection in groundwater-filled boreholes depends on the heat-injection rate used for the test. Gustafsson and Westerlund<sup>[26]</sup> showed that for groundwater-filled boreholes located in solid, unfractured bedrock, the estimated values of borehole thermal resistance decrease with increasing injection rates, while the ground thermal conductivity estimates remain unchanged. In contrast, for groundwater-filled boreholes located in fractured bedrock, a larger heat injection results in higher ground thermal conductivity estimations, whereas the borehole thermal resistance values remain unchanged. This difference is because a larger heat injection rate increases the convective heat transport in a solid bedrock borehole which, consequently, decreases the borehole thermal resistance. On the other hand, in the case of a groundwater-filled borehole in fractured bedrock, a larger heat injection rate increases the convective heat flow through the surrounding rock, which results in a higher estimate of the ground thermal conductivity.

This section reports on the effects of natural convection in groundwater-filled boreholes on the TRT results, which were studied using a series of investigations. Multiple tests have been conducted on borehole 9 of the test facility. The tests were conducted using different heat injection rates between 25 and 140 W/m. The ground conductivity and borehole resistance estimations obtained for these tests are shown in Figure 4.10. For tests on borehole 9, larger injection rates result in lower borehole thermal resistance values, whereas ground thermal conductivity values remain nearly constant.

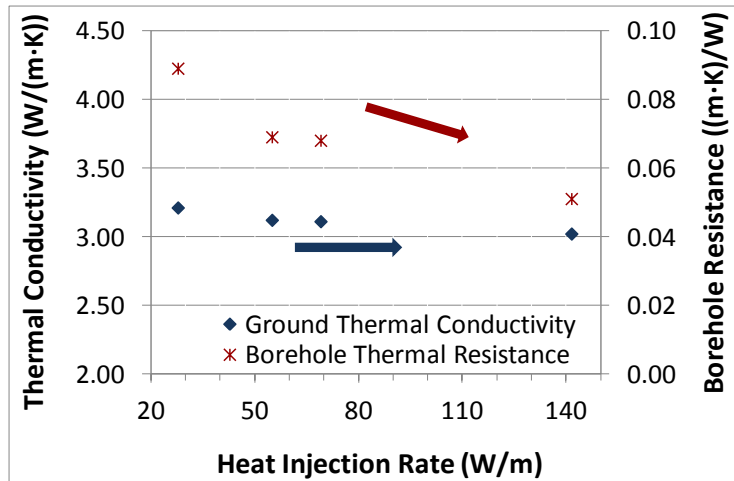


**Figure 4.10** Ground conductivity and borehole resistance values for TRTs with different heat injection rates on borehole 9

Similar tests were also conducted on borehole 7 of the test facility. The ground conductivity and borehole resistance estimations for TRTs on borehole 7 are shown in Figure 4.11. For borehole 7, ground conductivity values increase at high injection rates, whereas borehole thermal resistance remains nearly constant.

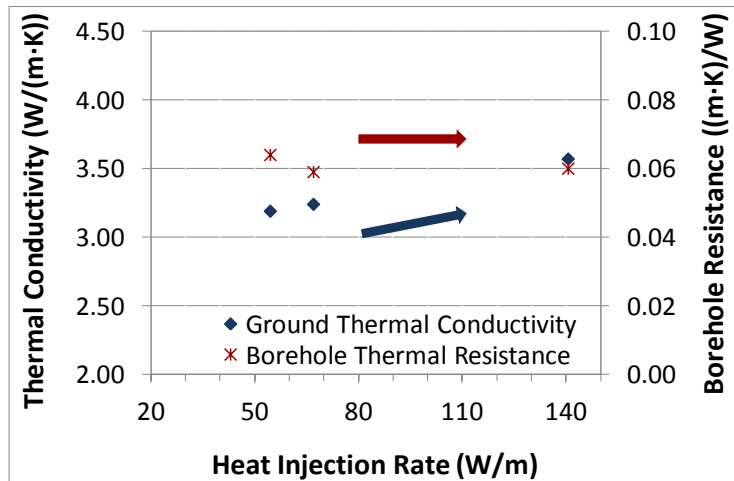


**Figure 4.11** Ground conductivity and borehole resistance values for TRTs with different heat injection rates for borehole 7

The results from TRTs conducted on borehole 7 and 9 of the test facility are in line with the observations of Gustafsson and Westerlund<sup>[26]</sup> of fractured and unfractured boreholes, respectively. However, what is of particular interest is that the two boreholes from the same field appear to have different degrees of fracturing in the surrounding bedrock. The results suggest that borehole 9 has fractured bedrock, whereas borehole 7 appears to be in solid, unfractured bedrock. However, despite the seemingly different patterns of ground conductivity and borehole resistance estimations for boreholes 7 and 9, tests conducted with larger injection rates on both boreholes tend to suggest shorter length requirements of

borehole heat exchangers. For the case studies of Tulsa and Burlington discussed in Section 4.3, the required lengths of borehole heat exchangers determined from the tests conducted with 140 W/m on boreholes 7 and 9 are approximately 10 % shorter than those determined from tests conducted with 55 W/m for both boreholes. This difference is due to the higher convective heat transport in the borehole, which improves the thermal contact between the U-tube and the surrounding ground, and consequently, shorter lengths of the borehole heat exchanger are suggested for tests conducted with larger injection rates.

The effects of convection on TRT results of groundwater-filled boreholes have been further investigated in a research collaboration<sup>[36]</sup> with the Department of Geology and Mineral Resources Engineering at Norwegian University of Science and Technology. Two multi-injection rate tests were conducted on a 150 m deep groundwater-filled borehole located in Lade, Norway. Before conducting the TRTs, the borehole was tested for hydraulic active fractures. The test for hydraulic fractures was performed by lowering a propeller in the borehole. The groundwater was pumped at a flow rate of 0.78 m<sup>3</sup>/hour using a pump installed at a depth of 20 m. The active fractures and the flow through them were determined using the rotational speed of the propeller. Figure 4.12a shows the reduction in propeller speed at the depth of approximately 34 m, indicating the presence of a notable fracture. The televIEWer image<sup>[21]</sup> shown in Figure 4.12b also confirms the presence of the fracture.

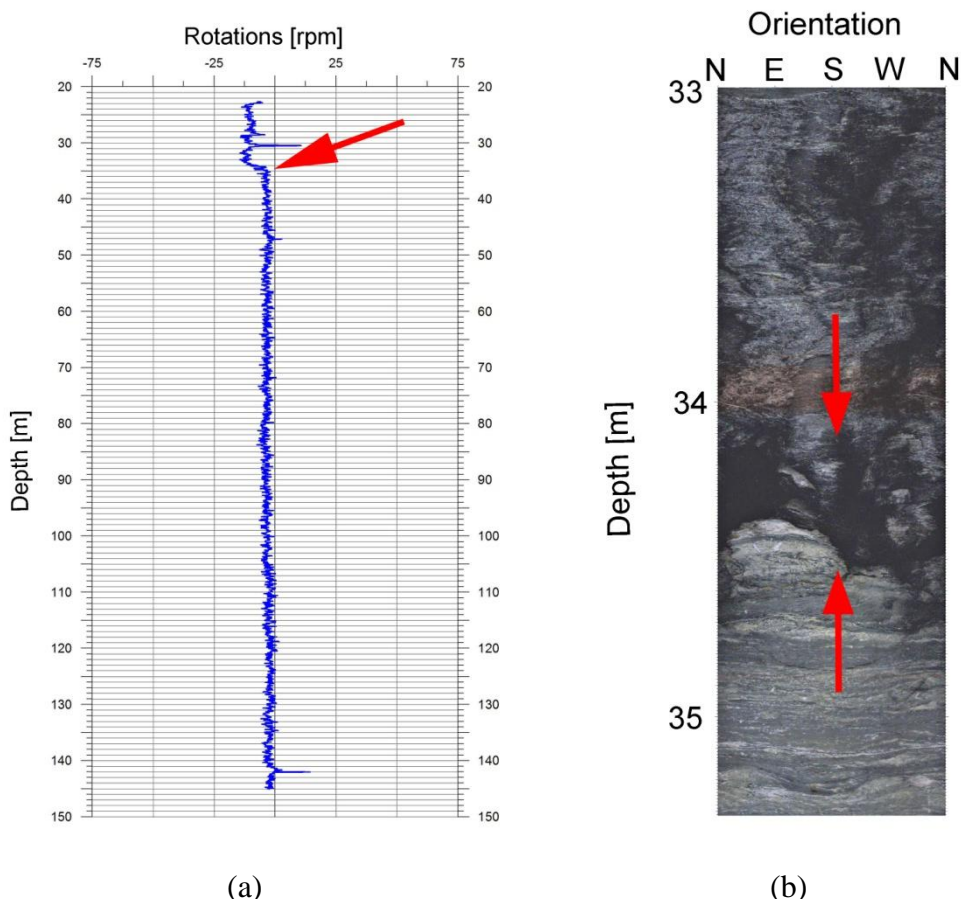


**Figure 4.12** An active fracture at 34 m indicated by a) flow measurement test and b) TelevIEWer image (Source: Elvebakk<sup>[21]</sup>)

Following the pumping test, two multi-injection rate TRTs were conducted on the borehole. Both tests were conducted using four injection rates each. The first test was conducted without any pumping of groundwater. For this test, the convective heat flow expected through the fracture at 34 m depth is nominal. Video recordings also indicated minimal groundwater movement in the borehole before the test. However, some buoyancy-driven convective movement was detected in the borehole during the test. The injection rates used for the test and the resulting mean fluid temperatures are shown in Figure 4.13.

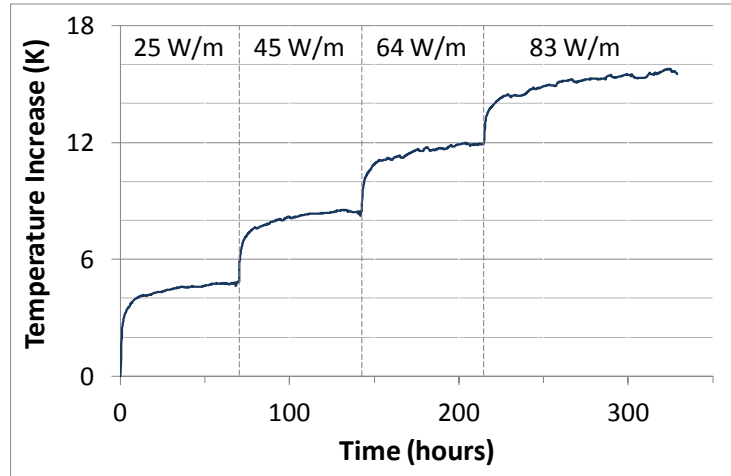


**Figure 4.13** Injection rates and mean fluid temperature increase for TRT without pumping of groundwater

A second test using groundwater pumping was later performed on the same borehole. A submersible water pump installed at the bottom of the borehole was used to create artificial convection in the borehole by discharging water at the top of the borehole. Video recordings suggest that the forced convective flow driven by the pump in the borehole is much greater than the buoyancy-driven convective flow with no pumping. The heat injection rates and the mean fluid temperatures for this test are shown in Figure 4.14.

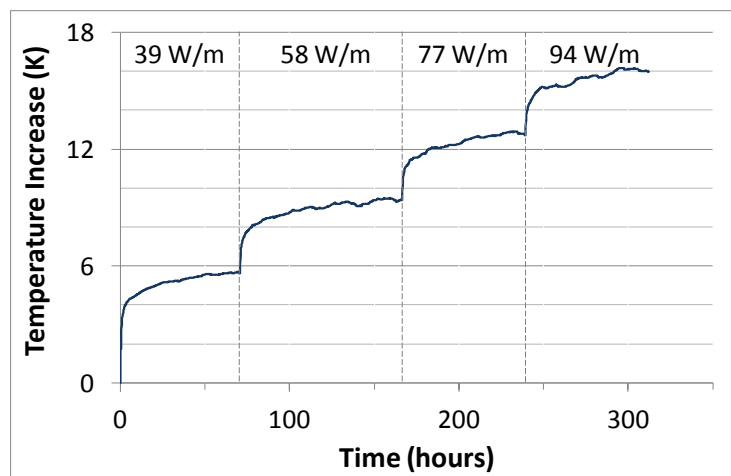


**Figure 4.14** Injection rates and mean fluid temperature increase for TRT with pumping of groundwater

The effects of convection on the design of a borehole field were studied for a single borehole system. The choice of single borehole simplifies the analysis because thermal interference from neighbouring boreholes is avoided. The annual hourly heating loads shown in Figure 4.15, simulated by Spitler et al.<sup>[46]</sup> for a modern two-story single family house in Sweden, are used as borehole loads.

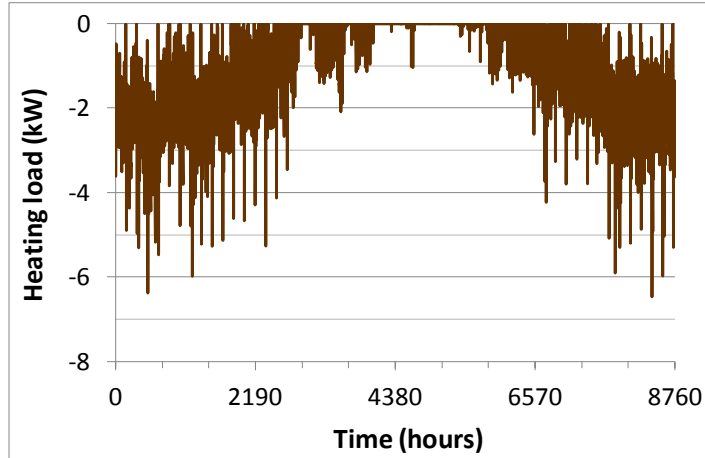


**Figure 4.15** Annual hourly heating loads on the borehole

The required length of the borehole heat exchanger was calculated using the ground conductivity and borehole resistance estimations for every individual injection rate of two tests of Figures 4.13 and 4.14. The effects of increasing injection rates on the required borehole lengths for both tests are shown in Figure 4.16. In the first test, without artificial pumping of groundwater, higher injection rates tended to give shorter borehole lengths. The borehole length calculated from the thermal conductivity and borehole resistance values for the injection rate of 25 W/m is approximately 140 m, which reduces to approximately 115 m for an injection rate of 83 W/m. These results are generally similar to those for the Tulsa and Burlington cases.

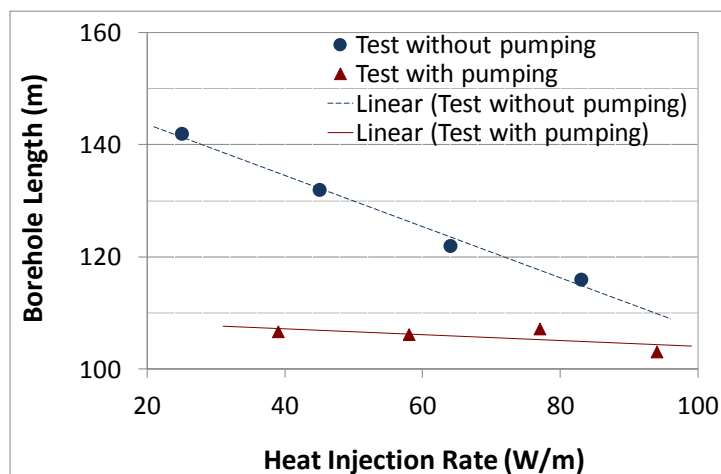


**Figure 4.16** Simulated borehole lengths for a test case using multi-injection rate TRTs with and without pumping of groundwater

On the other hand, the borehole lengths calculated from the results of the second TRT, which was conducted with pumping of groundwater, remain almost equal for all injection rates. As seen in Figure 4.16, the average value of borehole length for this test with artificial convection is 106 m. A comparison of the results of the two tests, conducted with and without pumping of groundwater, for lower injection rates provides an estimate of maximum uncertainty from convection in the borehole heat exchanger. Although more research is needed, the initial results reported here suggest that uncertainties on the order of 25 % in the borehole length can be caused by convective heat transport in the fractured boreholes.

## 4.5 Recovery times after a TRT

*This section is based on Paper VI.*

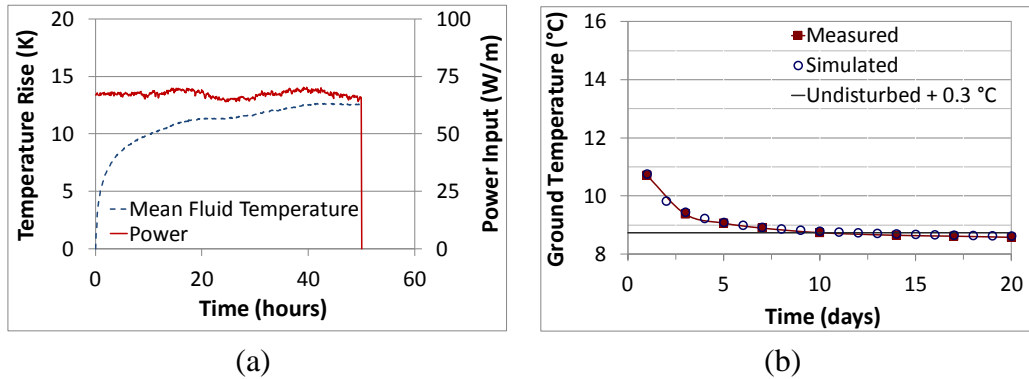
Thermal response tests are sometimes affected by problems that can create detrimental effects on the estimations of ground thermal conductivity and borehole thermal resistance. These issues include problems such as power outage, equipment failure and fluid leakage, among other unexpected circumstances. If the problem cannot be resolved quickly, or if it is caused by equipment malfunction or a data logging failure, conducting a retest might be indispensable. The retesting of boreholes is also needed in the research setting to perform experimental parametric analysis and to investigate the repeatability and reproducibility of the thermal response test results.

For a retest to be conducted, the loop temperature must be allowed to return to within 0.1-0.3 K of the undisturbed loop temperature<sup>[31]</sup>. The existing guidelines<sup>[6]</sup> suggest a recovery time of minimum 10-14 days for the loop temperature to return to the desired temperature level after a typical TRT. A significant issue is that the effects of factors such as ground formation, heat injection rates, and test duration on borehole recovery times are not fully addressed by the existing guidelines. In order to supplement the current guidelines, a systematic series of tests was conducted to determine the recovery times following TRTs conducted with various heat injection rates and conducted for different time durations.

Before conducting a TRT, the undisturbed loop temperature of the borehole was determined. Following a test, the development of ground temperatures over time was measured regularly. The measurements were taken every 2 to 5 days for two weeks after the test was initially conducted and every 7 to 10 days thereafter. The measurements continued until the loop temperature returned to approximately 0.1 K of its initial undisturbed value. Next, the short-term response solution of Chapter 2 was used to validate the experimentally measured recovery times. The solution was used to simulate ground temperatures after a TRT by superposition of the temperature response with the heat injection rates used in the tests. The recovery times were determined using actual injection rates during the test followed by a zero injection after the test.

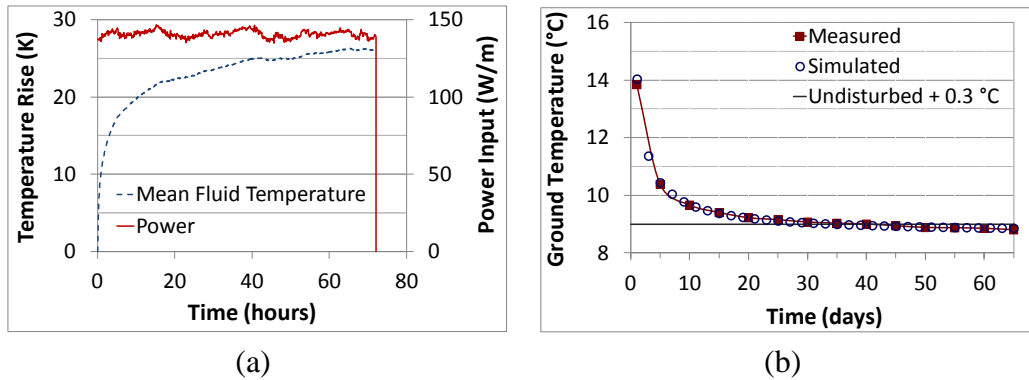
Figure 4.17a shows the details of a TRT conducted in compliance with ASHRAE guidelines<sup>[6]</sup>. The test was conducted for approximately 48 hours with a mean injection rate of 67 W/m. Figure 4.17b presents the experimentally measured and simulated recovery times after the TRT. The experimentally measured recovery time for the loop temperature to return to 0.3 K of its initial undisturbed value was

approximately 10 days. Simulated results suggest a recovery time of approximately 11 days.



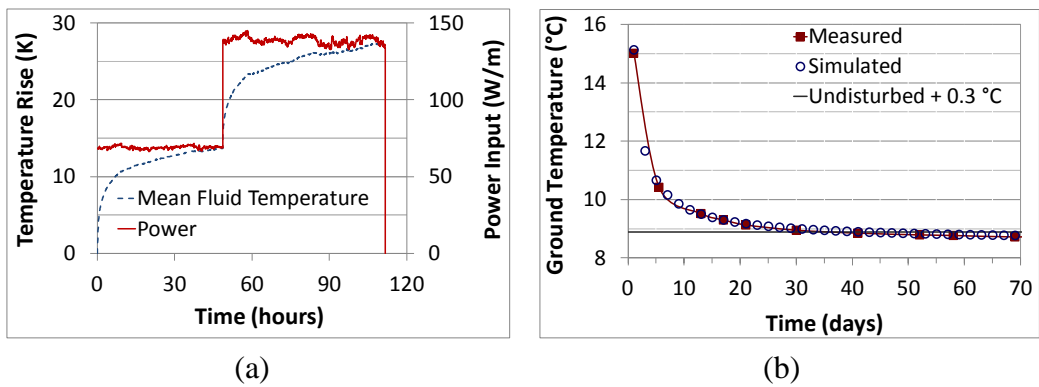
**Figure 4.17** Recovery times (4.17b) for a TRT (4.17a) conducted in accordance with ASHRAE guidelines<sup>[6]</sup>

Figure 4.18b shows recovery time after a 72-hour TRT conducted with a higher injection rate of 140 W/m (Figure 4.18a). The experimentally measured recovery time for this test was between 35-40 days. The simulation results indicate a recovery time of approximately 36 days.



**Figure 4.18** Recovery times (4.18b) for a TRT (4.18a) conducted with a high injection rate

Figure 4.19b presents recovery times following a TRT conducted with multiple injection rates. The test, shown in Figure 4.19a, was conducted using an injection rate of 70 W/m for the first 48 hours followed by a higher injection rate of 140 W/m for the next 64 hours. Experimental measurements suggested a recovery time of approximately 40 days. Simulated recovery time for this test is 43 days.



**Figure 4.19** Recovery times (4.19b) for a TRT (4.19a) conducted with multiple injection rates

The recovery times, which were determined experimentally and simulated using the mathematical model, are in close agreement in all cases. The mathematical model can now be used to extend the results by simulating recovery times for various testing conditions. Table 4.7 gives the recovery times for various combinations of ground formation, heat injection rate and test duration. Recovery times for longer tests and for tests conducted with higher injection rates are also available in Paper VI.

**Table 4.7** Recovery times (in days) for various test conditions

| Formation   | Heat injection rate (W/m) | Recovery times (days) after a TRT of duration |          |          |
|---|---------------------------|---|----------|----------|
|   |                           | 10 hours                                      | 25 hours | 50 hours |
| Soil, dry<br>[ $\lambda = 1.0 \text{ W}/(\text{m}\cdot\text{K})$ ]                          | 25                        | 3   | 7        | 13       |
|   | 50                        | 6   | 14       | 27       |
|   | 75                        | 9   | 21       | 41       |
| Clay, moist<br>[ $\lambda = 1.6 \text{ W}/(\text{m}\cdot\text{K})$ ]                        | 25                        | 2   | 4        | 8        |
|   | 50                        | 4   | 9        | 17       |
|   | 75                        | 5   | 13       | 25       |
| Rock, average /<br>Sand, saturated<br>[ $\lambda = 2.4 \text{ W}/(\text{m}\cdot\text{K})$ ] | 25                        | 1   | 3        | 5        |
|   | 50                        | 3   | 6        | 11       |
|   | 75                        | 4   | 9        | 17       |
| Rock, dense<br>[ $\lambda = 3.4 \text{ W}/(\text{m}\cdot\text{K})$ ]                        | 25                        | 1   | 2        | 4        |
|   | 50                        | 2   | 4        | 8        |
|   | 75                        | 3   | 6        | 12       |

Table 4.7 shows that the recovery times after a TRT are strongly related to the test duration, the heat injection rate and the ground formation. For a specific ground formation and a fixed injection rate, increasing the test duration twofold doubles the recovery times. Similarly, for a particular test duration, the recovery times increase proportionally with an increase in the injection rates. The recovery times for medium and low conductivity formations are two to four times longer than for high conductivity formations. The existing recommendations for recovery times should be revised to incorporate these findings.

## 4.6 New TRT evaluation method

*This section is based on Paper VII.*

The evaluation of TRTs conducted on groundwater-filled boreholes poses challenges that are different than those conducted on grouted boreholes. A larger injection rate in a groundwater-filled borehole enhances convective heat transfer in the borehole, which subsequently affects the estimations of ground thermal conductivity and borehole thermal resistance. The effects of injection rates on ground conductivity and borehole resistance estimations of groundwater-filled boreholes can be examined using tests with multiple injection rates. Most existing evaluation methods are not designed to analyze tests in which ground conductivity and borehole resistance estimations vary in time with changing heat injection rates.

A new method to evaluate TRTs on grouted and water-filled boreholes was developed. The new method for evaluating TRTs uses the short-term response solution derived in Chapter 2 with a parameter estimation technique. The inputs to the method include the following: the heat injection rate; the borehole geometry, including the borehole depth and the inner and outer diameters of the U-tube; the thermal conductivities of the pipe, grout and ground; and the volumetric heat capacities of the grout and ground. The equivalent diameter of the pipe, the thermal capacities, and the resistances of the circulating fluid and the U-tube are determined from the input values. The ground and grout conductivities are assumed to be unknowns and their initial values are guessed.

The method first simulates the fluid temperature from Equations 2.36 and 2.37 using guessed and input parameters. The simulated fluid temperature is then compared with the experimentally measured fluid temperature. Next, the initial guess values are iteratively refined to minimize the sum of squared errors between the experimental and simulated fluid temperatures. The optimized guess values that provide the minimum squared error are taken as the final conductivity estimations. The borehole thermal resistance is estimated next. An effective value of steady-state borehole resistance is estimated by taking the ratio of the temperature difference of the circulating fluid and the borehole wall to the specific heat-injection rate. The borehole wall temperature is estimated from Equations 3.28 and 3.29 using the previously estimated ground thermal conductivity value as an input.

The proposed evaluation method is accurate even for short times because it is based on a short-term analytical solution, which considers the thermal capacities, thermal resistances, and thermal properties of all borehole elements. Hence, unlike

other analytical solution-based evaluation methods, there is no need to discard any initial data when evaluating a TRT. Thus, the duration of the test can be reduced to a certain extent. Another advantage of the proposed method is that it can be used to evaluate tests conducted with both single and multiple injection rates. It has been implemented in such a way that the grout conductivity and the borehole resistance values can be estimated for any given time range. This implies that ground conductivity and borehole resistance values can be estimated for a specific injection rate when evaluating multiple injection rate tests on groundwater-filled boreholes.

The thermal response tests reported in the last section were used for testing of the proposed evaluation method. Thermal response tests shown in Figures 4.17a, 4.18a and 4.19a were all evaluated. The validation was performed against existing evaluation methods, including the direct line-source method<sup>[23]</sup>, line-source method with parameter estimation approach, Geothermal Properties Measurement (GPM) program based on Shonder and Beck's method<sup>[44]</sup>, and Austin et al.'s<sup>[8]</sup> Vertical Borehole Analysis and Parameter Estimation program. For details of these methods and for further description of the new method, readers are referred to Paper VII.

Table 4.8 shows thermal conductivity and borehole resistance estimations for TRT of Figure 4.17a. The evaluation of the first test, conducted over 48 hours with an injection rate of approximately 68 W/m, gives similar results for all evaluation methods. The ground conductivity estimations from the existing methods vary between 2.99 and 3.24 W/(m·K). The estimations of borehole resistance lie between 0.059 and 0.063 (m·K)/W. The new method estimates ground conductivity and borehole resistance values of 3.02 W/(m·K) and 0.053 (m·K)/W, respectively. Figure 4.20 shows the fit of the models to the experimentally measured temperatures.

**Table 4.8** Ground conductivity and borehole resistance estimations for TRT of Figure 4.17a

| Evaluation method                  | Ground conductivity (W/(m·K)) | Borehole resistance ((m·K)/W) |
|------------------------------------|-------------------------------|-------------------------------|
| Line-source (direct)               | 3.24                          | 0.059                         |
| Line-source (parameter estimation) | 3.13                          | 0.060                         |
| GPM (Shonder and Beck)             | 2.99                          | 0.063                         |
| Austin et al.                      | 3.09                          | -                             |
| New method                         | 3.02                          | 0.053                         |

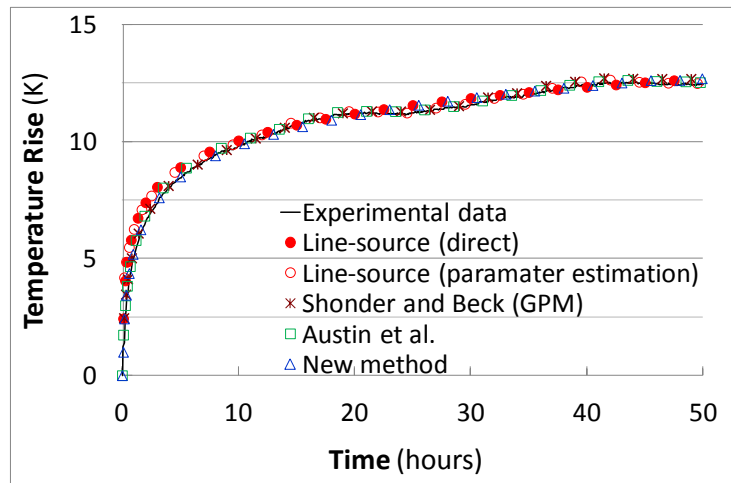


**Figure 4.20** Model fits to experimentally measured fluid temperature for TRT of Figure 4.17a

For the TRT of Figure 4.18a, the ground conductivity and borehole resistance estimations from different methods are shown in Table 4.9. The test was conducted for 72 hours using an injection rate of 140 W/m. The ground conductivity estimations from the existing methods are between 3.24 and 3.57 W/(m·K). The borehole resistance estimations are in the range of 0.058 to 0.060 (m·K)/W. The new method estimates ground conductivity and borehole resistance values of 3.36 W/(m·K) and 0.054 (m·K)/W, respectively. The fit of the models to the experimentally measured temperatures is shown in Figure 4.21.

**Table 4.9** Ground conductivity and borehole resistance estimations for TRT of Figure 4.18a

| Evaluation method                  | Ground conductivity (W/(m·K)) | Borehole resistance ((m·K)/W) |
|------------------------------------|-------------------------------|-------------------------------|
| Line-source (direct)               | 3.57                          | 0.060                         |
| Line-source (parameter estimation) | 3.41                          | 0.060                         |
| GPM (Shonder and Beck)             | 3.24                          | 0.058                         |
| Austin et al.                      | 3.42                          | -                             |
| New method                         | 3.36                          | 0.054                         |

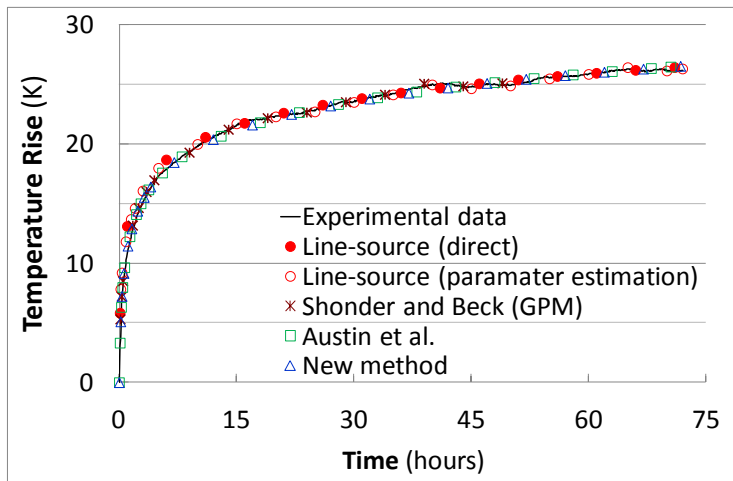


**Figure 4.21** Model fits to experimentally measured fluid temperature for TRT of Figure 4.18a

The thermal response test illustrated in Figure 4.19a was conducted with stepwise increasing injection rates of 68 and 140 W/m for 52 and 67 hours, respectively. This test cannot be evaluated using the direct line-source method and the GPM program. The direct line-source method can evaluate only tests with constant injection rates. The GPM program has also similar limitations. These methods can evaluate only the first injection rate part of the test with multiple injection rates. On the other hand, although the line-source-based parameter estimation method can be implemented to evaluate this test with two injection rates, the data corresponding to the first 10-15 hours of each injection rate must be discarded. The test can be evaluated using the computer program<sup>[8]</sup> based on the method of Austin et al. However, this program does not provide a direct estimation of borehole resistance and only estimates ground conductivity values. The ground conductivity and borehole resistance values for the two injection rates of the test, as estimated by the existing methods, are given in Table 4.10.

The new method estimates the ground conductivity and borehole resistance estimations of 3.10 W/(m·K) and 0.060 (m·K)/W, respectively, for the first injection rate. These values are similar to the ground conductivity and borehole resistance values estimated from other methods for the first injection rate. The estimated values are also comparable to those estimated for TRT of Figure 4.17a, which was also conducted with the same injection rate. The ground conductivity and borehole resistance estimations from the new method for the second injection rate are 3.48 W/(m·K) and 0.055 (m·K)/W, respectively. As discussed previously, the direct line-source method and the GPM program cannot evaluate the second injection rate of this test. The results from the Austin et al. and line-source-based parameter estimation methods are comparable to results from new method. The results of the new method for the second injection rate of TRT shown in Figure 4.19a and the TRT of Figure 4.18a, which were conducted with similar injection rates, are also similar.

**Table 4.10** Ground thermal conductivity and borehole resistance estimations for TRT of Figure 4.19a

| Evaluation method                  | Ground conductivity (W/(m·K)) | Borehole resistance ((m·K)/W) |
|------------------------------------|-------------------------------|-------------------------------|
| Line-source (direct)               |                               |                               |
| 1st injection rate                 | 3.08                          | 0.060                         |
| 2nd injection rate                 | -                             | -                             |
| Line-source (parameter estimation) |                               |                               |
| 1st injection rate                 | 3.07                          | 0.059                         |
| 2nd injection rate                 | 3.68                          | 0.060                         |
| GPM (Shonher and Beck)             |                               |                               |
| 1st injection rate                 | 3.01                          | 0.062                         |
| 2nd injection rate                 | -                             | -                             |
| Austin et al.                      |                               |                               |
| 1st injection rate                 | 3.15                          | -                             |
| 2nd injection rate                 | 3.61                          | -                             |
| New method                         |                               |                               |
| 1st injection rate                 | 3.10                          | 0.060                         |
| 2nd injection rate                 | 3.48                          | 0.055                         |

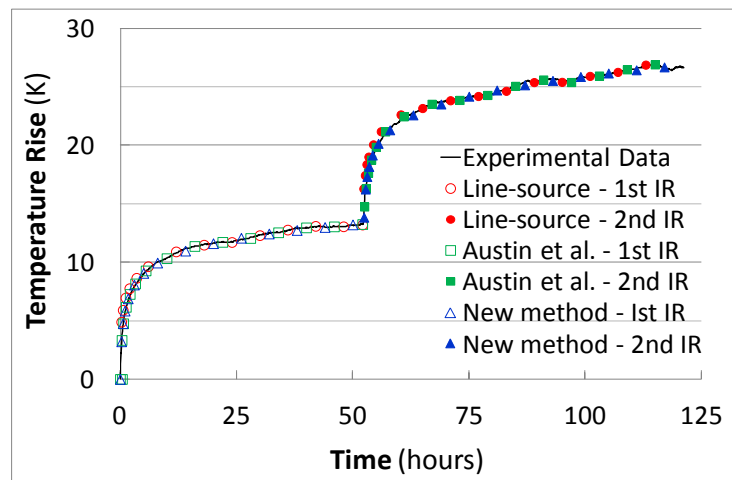


**Figure 4.22** Model fits to experimentally measured fluid temperature for TRT of Figure 4.19a

## **4.7 Conclusions**

Thermal response tests conducted on nine adjacent boreholes were reported. It was shown that the fluid exiting the U-tube at start-up provides consistent and more accurate measurement of the undisturbed ground temperature. The ground conductivity and borehole resistance estimations for the nine boreholes exhibit considerable variations. The variations in the estimated parameters were analyzed using two case studies. The random variations in the estimated parameters tend to change the borehole length requirements of the case study buildings up to 10 %.

The role of convective heat transfer in groundwater-filled boreholes was investigated. The results of TRTs performed on groundwater-filled boreholes using a larger injection rate tend to suggest borehole heat exchangers with considerably shorter lengths than would result from a lower injection rate.

The recovery times needed after a TRT were simulated for various test conditions by using the analytical model derived in Chapter 2. The simulated recovery times were validated against experimental data. It was observed that the required recovery times are strongly related to the test duration, the heat input to the borehole and the ground formation surrounding the borehole.

A new method for evaluating multi-injection rate tests on groundwater-filled boreholes was developed, tested and validated. The proposed method is also based on the analytical solution given in Chapter 2. The method estimates ground conductivity and borehole resistance values for all levels of a multi-injection rate test with good accuracy.

## 5 Concluding remarks

In the structure of this thesis, each chapter is self contained, having its own introduction, results, discussion and conclusions. Specific conclusions have been drawn and reported at the end of Chapters 2 to 4. This chapter provides a summary of the major conclusions of each chapter in the context of the overall research objectives.

### 5.1 Summary and conclusions

The research objectives of this work included the development of analytical methods for modelling and simulation of borehole heat transfer in GSHP systems in addition to a contribution to scholarly knowledge on thermal response testing of borehole systems. Chapters 2 and 3 of this thesis deal with the analytical modelling and simulations of borehole heat transfer, whereas Chapter 4 focuses on testing of boreholes.

Chapter 2 presents an analytical solution to model the radial heat transfer problem in borehole systems. The solution is valid for short time scales because it accounts for the thermal properties of all borehole elements, including the circulating fluid and the pipe, the grout, and the surrounding ground. The solution derives from modelling of the heat transfer in a borehole and the related boundary conditions in the Laplace domain. A thermal network is used to represent the Laplace transform equations. The inversion of Laplace to time domain is carried out analytically using very concise formulas. The analytical solution was validated against semi-analytical and numerical solutions and experimental data. The validation results indicate that the analytical solution can accurately predict the dynamic thermal response of a borehole.

Chapter 3 of this thesis presents an analytical approach to performing dynamic, multi-year simulations of borehole heat transfer. The analytical solution of Chapter 2 was used together with a finite line-source solution to develop step-response functions valid from very short (minutes) to very long (years, or longer) periods. The analytical solution was used for periods up to 100 hours. The finite line-source solution, which was reduced to one integral only, was used for periods longer than 100 hours. The step-response functions were developed for both single and multiple borehole systems. For small- to medium-sized borehole systems, comparison of analytically-developed response functions to numerically-obtained response functions showed very good agreement up to 20 to 25 years. The step-response functions were then used to perform multi-year simulations of borehole systems for prescribed heating and cooling loads. Simulations performed using non-aggregated loads require a lot of computational time. The time required to perform a 20-year simulation using annual hourly loads is approximately two hours. A load aggregation scheme was presented to reduce computational time requirements with little penalty in terms of simulation accuracy. The aggregation is performed on different levels. The first level corresponds to most recent loads, which are not aggregated. At the next level, two load values are lumped together in each aggregated cell. Similarly, on level 3, four load values were lumped together in each aggregated cell. The doubling continued to the very last level. The number of aggregated cells on each level was chosen freely. For the two cases discussed in Chapter 3, a 20-year simulation performed with five lumped cells on

each of the 16 aggregation levels, had an absolute error of less than 0.05 K compared with the non-aggregated scheme. The aggregation scheme is over 200 times faster than the non-aggregated case and reduces the computational time requirements to greater than 99 %.

Chapter 4 of this thesis brings together research findings on various aspects of thermal response testing. Firstly, results of TRTs conducted on nine adjacent boreholes were presented. The ground thermal conductivity and borehole thermal resistance values for the nine boreholes showed moderate variations. The ground conductivity estimations vary within a 7 % range on either side of the mean value. The borehole resistance estimations have approximately 20 % variations around a central value. Secondly, the effects of the variations in ground conductivity and borehole resistance values on the design of the borehole field were analyzed using case studies. It was shown that the random uncertainties in TRT results can affect the length requirements of borehole heat exchangers by approximately 10 %. Next, the effect of convective heat transfer on thermal response testing was determined in a series of tests. The initial results suggest that the length requirements of a single borehole heat exchanger can be affected up to 25 % because of the convective heat transfer inside the borehole. The recovery time requirements of a borehole system after a TRT were determined next. The analytical model of Chapter 2 was used to estimate the recovery time for various sets of ground formations, heat injection rates and test durations. The recovery times determined from the analytical solution were validated using a series of TRTs. It was shown that the recovery times are strongly related to the test duration and to the heat injection rates used for the TRT. Recommendations on revising recovery times for low to medium conductivity formations were made. Lastly, development and validation of a TRT evaluation method were presented. The method is based on the analytical solution in Chapter 2 and can be used to evaluate tests on both grouted and groundwater-filled boreholes. The method was shown to work well in cases where most existing methods cannot be used. For example, for a multi-injection rate test on a groundwater-filled borehole, the proposed method correctly estimates ground conductivity and borehole resistance values for each injection rate of the test.

## 5.2 Future work

The following recommendations are made for extending the present work and for future research.

- The analytical solution presented in Chapter 1 of this thesis is for the radial heat transfer in the borehole and the surrounding ground. The development of an analytical solution to the two-dimensional heat transfer problem in the borehole is suggested as a next step. Such a solution will eliminate the requirement of the U-tube to be approximated as an equivalent diameter pipe and will further improve the accuracy of modelling and simulations of borehole heat transfer.
- The choice of the equivalent-diameter, to approximate the two legs of the U-tube as a single pipe, affects the outcome of the analytical solution of Chapter 2. Although some research has been done, issues remain on the choice of the most suitable equivalent-diameter approximation,

particularly for groundwater-filled boreholes. A computational fluid dynamic (CFD) analysis to develop and/or validate the equivalent diameter approximations for different U-tube shank spacings is suggested for both groundwater-filled and grouted boreholes.

- Another recommendation regarding the analytical solution derived in Chapter 2 is to develop simpler approximation formulas for the solution. The approximation formulas will reduce the computational time required for solving the Laplace transform and hence will lead to rapid simulations of borehole heat transfer and faster evaluation of TRTs.
- The load aggregation scheme and the step-response functions, presented in Chapter 3 of this thesis, should be combined with heat pump and other subsystem models to perform dynamic modelling and simulations of the complete GSHP system, which can be done by implementing the load aggregation scheme and the step-response functions in building energy simulation software. Alternatively, a stand-alone computer program can be developed using the load aggregation scheme and the step-response functions integrated with a simulation model for the transient response of the heat pump.
- The step-response functions of Chapter 3 use the finite line-source solution for long-term response. The long-term response of a multiple borehole system depends on an exponential function, which in turn is based on the size and the configuration of the borehole field. The complexity of the exponential function increases with the asymmetry of the configuration and the number of boreholes. A computational tool to automatically generate the exponential function and/or the finite line-source response of a multiple borehole system should be developed. Additionally, development of a database of step-response functions for different geometries and configurations of borehole fields is suggested.
- The role of convection in groundwater-filled boreholes was discussed in Section 4.4 of this thesis. Future work in this regard should include the development of a convective heat transfer coefficient correlation for the annulus region of groundwater-filled boreholes. Such a correlation would simplify the estimation of borehole resistance for groundwater-filled boreholes with natural convection in their annulus regions.
- In Section 4.5, the recommended waiting times required before performing a retest were presented in a tabular form for different sets of ground conductivity values, heat injection rates and duration of the previous test. The development of a mathematical expression to directly calculate the required recovery times using ground conductivity, heat input, and previous test duration values as inputs is recommended.



## References

1. Abramowitz, M, Stegun, I, 1964. Handbook of mathematical functions. (Dover Publications.) New York.
2. Acuña, J, 2010. Improvements of U-pipe borehole heat exchangers. Licentiate Thesis, (KTH Royal Institute of Technology.) Sweden.
3. Al-Khoury, R, Bonnier, P G, 2006. Efficient finite element formulation for geothermal heating systems (Part II: transient). International Journal for Numerical Methods in Engineering, vol. 67, no. 5, pp. 725-745.
4. Al-Khoury, R, Bonnier, P G, Brinkgreve, B J, 2005. Efficient finite element formulation for geothermal heating systems (Part I: steady state). International Journal for Numerical Methods in Engineering, vol. 63, no. 7, pp. 988-1013.
5. Andersson, O, 2009. Ground source heating and cooling in Sweden. IEA Heat Pump Newsletter, vol. 27, no. 2, pp. 19-22.
6. ASHRAE, 2007. HVAC Applications. (American Society of Heating, Refrigerating and Air-Conditioning Engineers.) Atlanta, USA.
7. Austin, W, 1998. Development of an in-situ system for measuring ground thermal properties. M.Sc. Thesis, (Oklahoma State University.) USA.
8. Austin, W, Yavuzturk, C, Spitler, J, 2000. Development of an in-situ system for measuring ground thermal properties. ASHRAE Transactions, vol. 106(1), pp. 365-379.
9. Bandyopadhyay, G, Gosnold, W, Mann, M, 2008. Analytical and semi-analytical solutions for short-time transient response of ground heat exchangers. Energy and Buildings, vol. 40, no. 10, pp. 1816-1824.
10. Beier, R A, 2008. Equivalent time for interrupted tests on borehole heat exchangers. HVAC&R Research, vol. 14, no. 3, pp. 489-505.
11. Beier, R A, Smith, M D, 2002. Borehole thermal resistance from line-source model of in-situ tests. ASHRAE Transactions, vol. 108 (2), pp. 212-219.
12. Beier, R A, Smith, M D, 2003. Minimum duration of in-situ tests on vertical boreholes. ASHRAE Transactions, vol. 109 (2), pp. 475-486.
13. Beier, R A, Smith, M D, 2005. Analyzing interrupted in-situ tests on vertical boreholes. ASHRAE Transactions, vol. 111 (1), pp. 702-713.
14. Beier, R A, Smith, M D, Spitler, J D, 2011. Reference data sets for vertical borehole ground heat exchanger models and thermal response test analysis. Geothermics, vol. 40, no. 1, pp. 79-85.

15. Bernier, H, Kummert, M, Bertagnolio, S, 2007. Development and application of test cases for comparing vertical ground heat exchanger models. Proceedings of 10th International IBPSA Conference, Beijing, China.
16. Bernier, M A, Labib, R, Pinel, P, Paillot, R, 2004. A multiple load aggregation algorithm for annual hourly simulations of GCHP systems. HVAC&R Research, vol. 10, no. 4, pp. 471-487.
17. Blackwell, J H, 1954. A transient-flow method for determination of thermal constants of insulating materials in bulk (Part I-Theory). Journal of Applied Physics, vol. 25, no. 2, pp. 137-144.
18. Blomberg, T, Claesson, J, Eskilson, P, Hellström, G, Sanner, B, 2008. EED 3.0 - Earth Energy Designer, User Manual. (Blocon.) Sweden.
19. Carslaw, H S, Jaeger, J C, 1947. Conduction of heat in solid. (Oxford University Press.) Oxford.
20. Claesson, J, 2011. Radial heat flow for a pipe in a borehole in ground using Laplace solutions - Mathematical background report. (Chalmers University of Technology.) Sweden.
21. Elvebakk, H, 2003. Televiewer image. (Unpublished.).
22. Eskilson, P, 1987. Thermal analysis of heat extraction boreholes. Department of Mathematical Physics, PhD Thesis, (Lund University.) Sweden.
23. Gehlin, S, 2002. Thermal response test - Method development and evaluation. PhD Thesis, (Luleå University of Technology.) Sweden.
24. Gentry, J, 2007. Simulation and validation of hybrid ground source and water-loop heat pump systems. M.Sc. Thesis, (Oklahoma State University.) USA.
25. Gu, Y, O'Neal, D L, 1995. Analytical solution to transient heat conduction in a composite region with a cylindrical heat source. Journal of Solar Energy Engineering, Transactions of the ASME, vol. 117, no. 3, pp. 242-248.
26. Gustafsson, A M, Westerlund, L, 2010. Multi-injection rate thermal response test in groundwater filled borehole heat exchanger. Renewable Energy, vol. 35, no. 5, pp. 1061-1070.
27. He, M, Rees, S, Shao, L, 2010. Simulation of a domestic ground source heat pump system using a three-dimensional numerical borehole heat exchanger model. Journal of Building Performance Simulation, vol. 4, no. 2, pp. 141-155.

28. Ingersoll, L R, Zobel, O J, Ingersoll, A C, 1954. Heat conduction with engineering, geological and other applications. (McGraw-Hill.) New York.
29. Javed, S, 2010. Design of ground source heat pump systems - Thermal modelling and evaluation of boreholes. Licentiate Thesis, (Chalmers University of Technology.) Sweden.
30. Javed, S, Fahlén, P, 2010. Development and planned operation of a ground source heat pump test facility. IEA Heat Pump Center Newsletter, vol. 28, no. 1, pp. 32-35.
31. Kavanaugh, S, Xie, L, Martin, C, 2001. Investigation of methods for determining soil and rock formation thermal properties from short-term field tests. (American Society of Heating, Refrigerating and Air-Conditioning Engineers.) Atlanta, USA.
32. Lamarche, L, 2009. A fast algorithm for the hourly simulations of ground-source heat pumps using arbitrary response factors. Renewable Energy, vol. 34, no. 10, pp. 2252-2258.
33. Lamarche, L, Beauchamp, B, 2007. A fast algorithm for the simulation of GCHP systems. ASHRAE Transactions, vol. 113 no. 1, pp. 470-476.
34. Lamarche, L, Beauchamp, B, 2007. A new contribution to the finite line-source model for geothermal boreholes. Energy and Buildings, vol. 39, no. 2, pp. 188-198.
35. Lamarche, L, Beauchamp, B, 2007. New solutions for the short-time analysis of geothermal vertical boreholes. International Journal of Heat and Mass Transfer, vol. 50, no. 7-8, pp. 1408-1419.
36. Liebel, H, Javed, S, Vistnes, G, (Unpublished). Multi-injection rate thermal response test with forced convection in a groundwaterfilled borehole in hard rock. Submitted to Renewable Energy.
37. Liu, X, 2005. Development and experimntal validation of simulation of hydronic snow melting systems for bridges. PhD Thesis, (Oklahoma State University ) USA.
38. Lund, J W, Freeston, D H, Boyd, T L, 2011. Direct utilization of geothermal energy 2010 worldwide review. Geothermics, vol. 40, no. 3, pp. 159-180.
39. Marcotte, D, Pasquier, P, 2008. Fast fluid and ground temperature computation for geothermal ground-loop heat exchanger systems. Geothermics, vol. 37, no. 6, pp. 651-665.
40. Mogensen, P, 1983. Fluid to duct wall heat transfer in duct system heat storages. Proceedings of International Conference on Subsurface Heat Storage in Theory and Practice, Sweden.

41. Muraya, N K, 1994. Numerical modeling of the transient thermal interference of vertical U-tube heat exchangers. PhD Thesis, (Texas A&M University.) USA.
42. Pinel, P, 2003. Amélioration, validation et implantation d'un algorithme de calcul pour évaluer le transfert thermique dans les puits verticaux de systèmes de pompes à chaleur géothermiques. M.Sc. Thesis, (École Polytechnique de Montréal.) Canada.
43. Shonder, J, Beck, J, 2000. A new method to determine the thermal properties of soil formations from in situ field tests. (Oak Ridge Laboratory.) Tennessee, USA.
44. Shonder, J A, Beck, J V, 1999. Determining effective soil formation properties from field data using a parameter estimations technique. ASHRAE Transactions vol. 105 (1), pp. 458–466.
45. Spitler, J, 2010. Validation Data. Javed, S. (Personal Communication.).
46. Spitler, J, Xing, L, Cullin, J, Fisher, D, Shonder, J, 2010. Residential ground source heat pump systems utilizing foundation heat exchangers. Proceedings of 10th REHVA World Congress (Clima 2010), Antalya, Turkey.
47. Spitler, J D, 2000. GLHEPRO - A design tool for commercial building ground loop heat exchangers. Proceedings of 4th International Heat Pumps in Cold Climates Conference, Québec, Canada.
48. Stehfest, H, 1970. Remark on algorithm 368: Numerical inversion of Laplace transforms. Commun. ACM, vol. 13, no. 10, pp. 624.
49. Witte, H J L, van Gelder, A J, 2006. Geothermal response test using controlled multi-power level heating and cooling pulses (MPL-HCP): quantifying ground water effects on heat transport around a borehole heat exchanger. Proceedings of 10th International Conference on Thermal Energy Storage (Ecostock), New Jersey, USA.
50. Xu, X, Spitler, J D, 2006. Modeling of vertical ground loop heat exchangers with variable convective resistance and thermal mass of the fluid. Proceedings of 10th International Conference on Thermal Energy Storage (Ecostock), New Jersey, USA.
51. Yavuzturk, C, 1999. Modelling of vertical ground loop heat exchangers for ground source heat pump systems. PhD Thesis, (Oklahoma State University.) USA.
52. Yavuzturk, C, Spitler, J D, 1999. Short time step response factor model for vertical ground loop heat exchangers. ASHRAE Transactions, vol. 105 (2), pp. 475-485.

53. Young, T R, 2004. Development, verification, and design analysis of the borehole fluid thermal mass model for approximating short term borehole thermal response. M.Sc. Thesis, (Oklahoma State University.) USA.
54. Zeng, H Y, Diao, N R, Fang, Z H, 2003. Heat transfer analysis of boreholes in vertical ground heat exchangers. International Journal of Heat and Mass Transfer, vol. 46, no. 23, pp. 4467-4481.

